MIAMI UNIVERSITY
The Graduate School

Certificate for Approving the Dissertation

We hereby approve the Dissertation

of

Robert John Skoumal

Candidate for the Degree

DOCTOR OF PHILOSOPHY

_____
Michael Brudzinski, Director

_____
Brian Currie, Reader

_____
Jens Mueller, Reader

_____
Jonathan Levy, Graduate School Representative

_____
Jacob Walter, External Representative

ABSTRACT

CHARACTERIZING INDUCED AND NATURAL EARTHQUAKE SWARMS USING CORRELATION ALGORITHMS

by

Robert J. Skoumal

Relationships between earthquakes are observed by the clustering of seismic events in space and time. This clustering commonly occurs as mainshock-aftershock sequences, which are generally interpreted to contain the initial rupture of a fault (the mainshock) and a decaying cascade of smaller ruptures on or very near to the initial rupture plane (aftershocks). Clustering of earthquakes in space and time can also occur as earthquake swarms, which are empirically defined as an increase in seismicity rate above the background rate without a clear triggering mainshock earthquake. Earthquake swarms are often associated with volcanic regions and are studied because of their relationship to eruptions. Earthquake swarms have also been correlated with subduction zone slow slip events, including a case that led into the 2011 Tohoku earthquake. Earthquake swarms are also well associated with many induced ("human influenced") earthquake sequences. Understanding the mechanisms that lead to earthquake swarms and the rapid detection of these events are key factor in reducing the hazard posed by these events. Here, we present four chapters that seek to detect and better characterize earthquake swarms with an emphasis on induced seismicity. We develop an efficient template matching algorithm that can be used to improve an earthquake catalog completeness by more than an order of magnitude and apply it throughout the state of Ohio. We also develop a new method, referred to as a Repeating Signal Detector (RSD), that uses agglomerative clustering to group signals of interest according to their temporal and frequency domain characteristics. Resulting signal families can be stacked, improving the signal-to-noise ratio of the recorded signals, and then the signal stack can the used in template matching. We apply the technique to detect earthquake swarms in volcanic, subduction, and induced seismicity settings throughout North America. In each case, RSD duplicates or improves upon existing catalogs in rapid, computationally-efficient manner. As more observations typically lead to improved interpretations, techniques like optimized template matching and RSD are important tools for the future understanding of earthquake swarms in a variety of settings.

CHARACTERIZING INDUCED AND NATURAL EARTHQUAKE SWARMS USING CORRELATION ALGORITHMS

A DISSERTATION

Presented to the Faculty of

Miami University in partial

fulfillment of the requirements

for the degree of

Doctor of Philosophy

Department of Geology and Environmental Earth Science

by

Robert J. Skoumal

The Graduate School
Miami University
Oxford, Ohio

2016

Dissertation Director: Michael R. Brudzinski

Table of Contents

List of Tables

List of Figures

INTRODUCTION

Relationships between earthquakes are observed by the clustering of seismic events in space and time. This clustering commonly occurs as mainshock-aftershock sequences, which are generally interpreted to contain the initial rupture of a fault (the mainshock) and a decaying cascade of smaller ruptures on or very near to the initial rupture plane (aftershocks) (Lay & Wallace, 1995). Clustering of earthquakes in space and time can also occur as earthquake swarms, which are empirically defined as an increase in seismicity rate above the background rate without a clear triggering mainshock earthquake (Mogi, 1963). Earthquake swarms are often associated with volcanic regions and are studied because of their relationship to eruptions (McNutt, 1996). Earthquake swarms have also been correlated with subduction zone slow slip events (Hirose et al., 2014), including a case that led into the 2011 Tohoku earthquake (Kato et al., 2012). Earthquake swarms are also well associated with many induced ("human influenced") earthquake sequences (e.g., Horton, 2012). Understanding the mechanisms that lead to earthquake swarms and the rapid detection of these events are key factor in reducing the hazard posed by these events. Here, we present four chapters that seek to detect and better characterize earthquake swarms with an emphasis on induced seismicity.

In Chapter 1, we present the use of an optimized multi-station template matching algorithm and identify a previously unknown induced sequence resulting from hydraulic fracturing with $M \leq 3$ in Poland Township, Ohio, during the month of March 2014. To date, this remains one of the largest magnitude earthquakes recognized as induced by hydraulic fracturing in the United States. Due to close temporal and spatial relationships, six stimulation stages were responsible for the earthquake sequence while nearly 100 stages at nearby wells at greater distances did not coincide with detected seismicity.

In Chapter 2, we apply our optimized template matching technique to a local network in Trumbull County, Ohio, to characterize microseismic events part of a $M \leq 2.1$ sequence near a pair of wastewater disposal wells. We also implement a subspace detector approach following Barrett & Beroza (2014) that further improved our microseismic catalog, producing a catalog of events as small as M_L -1.4. Our results support the Ohio Department of Natural Resource's decision to resume operations

In Chapter 3, we apply the optimized template matching routine to all cataloged earthquakes in Ohio between 2010-2014. Cataloged earthquakes that were within 5 km from fluid injection activities that lacked previously documented seismicity were found to have swarm-like behavior, while cataloged earthquakes in regions of previously documented seismicity or located away from fluid injection wells did not. We detected the induced sequences covered in the previous chapters and suggest that two additional cases (Belmont/Guernsey County and Washington Count) were also induced. We find that using template matching to identify swarm-like earthquake patterns are a promising method of improving the ability to detect induced seismicity over a regional scale.

In Chapter 4, we seek to address one of the principle problems of template matching: the detection/creation of a template event. We propose a new algorithm, called a Repeating Signal Detector (RSD), that uses agglomerative clustering to group signals of interest according to their temporal and frequency domain characteristics. Resulting signal families can be stacked, improving the signal-to-noise ratio of the recorded signals,

and then the signal stack can the used in template matching. We apply the technique to detect earthquake swarms in volcanic, subduction, and induced seismicity settings throughout North America. In each case, RSD duplicates or improves upon existing catalogs in rapid, computationally-efficient manner.

CHAPTER 1: Earthquakes induced by hydraulic fracturing in Poland Township, Ohio

1.1. Abstract

Felt seismicity induced by hydraulic fracturing is very rare with only a handful of reported cases worldwide. Using an optimized multi-station cross-correlation template matching routine, 77 earthquakes were identified in Poland Township, Mahoning County, Ohio that were closely related spatially and temporally to active hydraulic fracturing operations. We identified earthquakes as small as local magnitudes (M_L) ~1 up to M_L 3, potentially one of the largest earthquakes induced by hydraulic fracturing in the United States. These events all occurred from 4 to 12 March 2014 and the rate decayed once the Ohio Department of Natural Resources issued a shutdown of hydraulic fracturing at a nearby well on 10 March. Using a locally derived velocity model and double-difference relocation, the earthquakes occurred during six stimulation stages along two horizontal well legs that were located ~0.8 km away. Nearly 100 stimulation stages in nearby wells at greater distances from the earthquake source region did not coincide with detected seismicity. During the sequence, hypocenters migrated ~600 m along an azimuth of 083° defining a vertically-oriented plane of seismicity close to the top of the Precambrian basement. The focal mechanism determined for the M_L 3 event had a vertically-oriented left-lateral fault plane consistent with the earthquake distribution and the regional stress field. The focal mechanism, orientation, and depth of hypocenters were similar to that of the 2011 Youngstown earthquake sequence that occurred 18 km to the northwest and was correlated with wastewater injection instead of hydraulic fracturing. Considering the relatively large magnitude of the Poland Township events and the b-value of 0.89, it appears the hydraulic fracturing induced slip along a pre-existing fault/fracture zone optimally oriented in the regional stress field.

1.2. Introduction

As oil and gas well completions utilizing multi-stage hydraulic fracturing have become more commonplace, the potential for seismicity induced by the deep disposal of frac-related wastewater and the hydraulic fracturing process itself has become an increasingly important issue (e.g., NAS, 2012). While it is rare for a wastewater disposal well to induce felt seismicity, the recent increase in the number of wells and volumes injected are suspected to have contributed to a substantial increase of events $\geq M_L$ 3 in the continental U.S. over the past decade (e.g., Ellsworth, 2013). Felt earthquakes caused directly by hydraulic fracturing during well stimulations are even more rare, but due to the recent enhanced scrutiny regarding the practice and more sensitive seismic-monitoring tools, induced seismicity attributed to hydraulic fracturing has become more prevalent in the past few years. While microseismicity (local magnitude [M_L] < 1) is an inherent component of the hydraulic fracturing process (Warpinski et al., 2012), hydraulic fracturing has previously been well-correlated to only a handful of earthquakes sequences, including moment magnitude (M_w) 1.9 Oklahoma, 1979 (Nicholson and Wesson, 1990); M_L 2.9 Oklahoma, 2011 (Holland, 2013); M_L 3.8 British Columbia, 2011 (BCOGS, 2012); and M_L 2.3 England, 2011 (BGS, 2011); and M_w 2.2 Harrison County, Ohio, 2013 (Friberg et al., 2014). Between 5-14 March 2014, a series of 5 earthquakes ranging from M_L 2.1 to 3.0 were recorded in Poland Township, Mahoning County, Ohio

near the town of Lowellville. The epicentral locations for these event were less than 20 km southeast of the locations of the 2011-14 Youngstown Earthquake Sequence (YES), a series of M_L ~1.0-4.0 events that have been linked to a deep wastewater injection well (Kim, 2013; Holtkamp et al., 2015; Skoumal et al., 2014). Despite this proximity, there were no injection wells operating within 10 km of the Poland Township earthquakes. However, the earthquakes occurred within 1 km of a group of recently drilled oil and gas wells in the area, one of which (Hilcorp Energy CLL2 #1H; API 3409923199) was undergoing active hydraulic-fracture stimulation at the time of the M_L 3.0 seismic event. Because of this proximity, the Ohio Department of Natural Resources (ODNR) halted completion operations at the Hilcorp well on the afternoon of 10 March 2014.

Although the ODNR subsequently announced that there was a probable connection between hydraulic fracturing and the Poland Township events, to date, there has been no detailed scientific data released that demonstrates this relationship. This study seeks to investigate the Poland Township seismicity and its potential relationship to hydraulic fracturing by employing the seismographic template matching procedure utilized to characterize the nearby 2011-14 YES events (Holtkamp et al., 2015; Skoumal et al., 2014). If it can be demonstrated that the Poland Township earthquakes were induced by hydraulic fracturing, the M_L 3.0 event in the sequence would be one of the largest earthquakes directly linked to the process (Davies et al, 2013).

1.3. Data and Analysis

Our analysis followed the approach of Skoumal et al. (2014) that was optimized for the nearby 2011-14 YES. Data were obtained using IRIS WebServices, interpolated to 40 samples/sec, and then bandpass filtered between 5-15 Hz. Templates of 37 sec length were created from earthquakes identified by the ODNR, Lamont Doherty Earth Observatory (LDEO), and the USGS National Earthquake Information Center (NEIC). Templates began 10 s before the P-wave arrival on vertical components and 10 s before S-wave arrival on horizontal components. Cross-correlation coefficients (CCC) were calculated by correlating the template with years of data by shifting one datum at a time for each station and component. When executed in parallel with a peak usage of 72 simultaneous workers, we can achieve over 10^8 corr/s that allowed us to run templates through all available data in under an hour. We sum the CCC values across the network taking into account the lag values between different station-components established in the template event arrival times. So if O56A-BHE has an S-wave arrival 5 sec later than N54A-BHE, the CCC values from O56A-BHE starting at 5 sec are added to the CCC values from N54A-BHE starting at 0 sec. Network-normalized CCC (NNCCC) values were produced by dividing the sum of normalized CCC values for all stations and components by the number of contributing channels. We set an initial threshold of 15 times the median absolute deviation (MAD) of the daily NNCCC. Correlating a randomly generated template against a random year-long signal at 40 samples/sec would result in ~1 false positive based on the theoretical statistics of 15×MAD. We then sought to lower the 15×MAD threshold to increase the number of matched events without changing the temporal trend of matched events, while also maintaining coherent seismic arrivals.

Considering the presence of the EarthScope Transportable Array, various station combinations were investigated to determine the template that produced the highest number of positive detections and minimized false positives. While stations N53A and

YSLD were the closest to the source region (Figure 2.1), large and repetitive noise at these stations had detrimental effects on template-matching performance. The ideal network consisted of stations M54A, N54A, and O56A, which was the same combination found by Skoumal et al. (2014). The stations in the most successful template were installed in early November 2010, such that scans with this template were run from 6 November 2010 to 6 May 2014.

The earthquakes returned from the template-matching process were located through a combination of absolute and relative location techniques. The absolute location of the largest event (M_L 3.0, 3/10/2014 06:26:42) was determined using *elocate* (Herrmann, 2004). The inversion used the manually picked arrival times of the clearest P and S waveforms on 10 stations (labeled stations, Figure 2.1). We considered using the one-dimensional velocity models for the nearby Youngstown region presented by Kim (2013), as the two models developed for that study were based on sonic logs in the area and were appropriate for the local recordings used in that study (Table 2. 1). However, our study used regional stations such that seismic waves recorded in our study primarily sample deeper depths. Faced with a similar issue, similar studies have sought to identify a model that would be more appropriate for this case (Holtkamp et al., 2015; Skoumal et al., 2014). Beginning from the Northeastern Ohio velocity model, the parameters were adjusted through forward modeling to reduce the variance and the bootstrap error estimates (Table 2. 1). An additional lower crustal layer was added to help fit arrival times at more distal stations. Considering that the bedrock units in this portion of Ohio dip gently (~1°) to the southeast into the Appalachian Basin (Baranoski, 2013), the velocity models were adjusted to accommodate the thicker formations and deeper tops reported in a vertical well within 1 km from the Poland Township epicenters (CLL1 #1V; API 3409923185), and the deeper basement contact estimated for the well location (Table 2. 1). The absolute location errors were determined using bootstrapping, removing one station at a time from the location process and using the standard deviation as the error estimate (Efron, 1979) (Table 2. 2).

The relative locations of all matched events were determined by using a larger network of 26 stations (Figure 2.1) following the approach of Skoumal et al. (2014). Lag times and correlations were generated between the template and each matched event using a 10 sec long window that began 4 sec prior to the P-wave arrival on vertical components and 4 sec prior to the S-wave arrival on horizontal components. This process produced P- and S-wave arrival times and weights (proportional to the correlation coefficient) for all matched events, which were used with *elocate* and the velocity model to determine an initial set of catalog locations. A full set of lag and correlation matrices between all events for all channels were then used in a *HypoDD* double-difference algorithm to determine the relative locations of the events (Waldhauser and Ellsworth, 2000; Waldhauser, 2001). The median relative locations errors we found based on bootstrapping estimation were ±11 m horizontally and ±89 m vertically (Table 2. 2). When interpreting maps and cross-sections, we focus only on events with horizontal and vertical relative location uncertainties less than ±10 m and ±100 m, respectively. Relocated hypocenters were pinned to the absolute location determined for the largest event, preserving the relative locations.

We determined M_L through a Richter scale approach:

$$M_L = \log_{10} [A/A_0]$$

For each station and component in our template, we calculated the median scale factor (A_0) using the filtered S-waveform amplitudes (A) and catalog magnitudes for all 6 events reported by the ODNR/LDEO/NEIC. For each matched event, we calculated a magnitude from the scale factor and S-waveform amplitude at each station and component, and took the median value as our final magnitude.

To gain additional perspective on the stresses at work in this earthquake sequence, we calculated a fault plane solution for the largest event, which was just large enough to make reliable identifications of first motion polarities (nominally, $M_L \geq 3.0$). To determine the fault plane solution, we used *FocMec*, which performed a grid search of the focal sphere based on user-specified criteria (Snoke, 2003). Input files for *FocMec* were assembled using event-station information and careful examination of first motion polarities in all available waveforms. Takeoff angles were estimated using the pseudo-bending method within *tomoDD* (Zhang and Thurber, 2003). We used the default criteria within *FocMec* to calculate a set of fault plane solutions for the lowest number of allowable polarity errors, and then took the median of these solutions as the fault plane solution for a specific event.

1.4. Results

Using an initial threshold of 15×MAD, our template matching procedure identified 60 similar events that all occurred between 4-12 March 2014 (Figure 2.2; Table 2. 3). There were no matches before 16:23 4 March 2014, indicating no similar seismicity since recording began in November 2010 (Figure 2.2b). When the threshold was lowered to 12×MAD, 77 events were all identified during 4-12 March 2014. Thresholds below 12×MAD resulted in a few spurious matches in the years prior to the sequence based on visual inspection, thus the 77 events from the 12×MAD threshold were utilized for the remainder of our study. Based on the $M_L$we calculated for the 77 detected events, we estimated a magnitude of completeness at M_L 0.85 (Figure 2.2c), comparable to that obtained for the nearby Youngstown sequence with similar processing (Skoumal et al., 2014). We also calculated a Gutenberg-Richter b-value for the entire Poland Township sequence, which is 0.89 with the maximum likelihood estimate (Figure 2.2c). Seismicity directly resulting from hydraulic fracturing is expected to have a b-value of ~2 (Maxwell et al. 2009; Wessels et al. 2011), whereas seismicity associated with fluid injection is expected to have a b-value < 1 (Lei et al., 2008; Bachmann et al., 2014). For example, the overall Youngstown sequence b-value was 0.82 (Skoumal et al., 2014). Seismicity directly resulting from hydraulic fracturing is expected to be < M 1 (Warpinski et al., 2012). The relatively large magnitude of the events and the low b-value support the notion that the majority of earthquakes we detected were not signatures of actual hydraulic fracturing. Instead, the sequence could represent slip on a pre-existing fault during well stimulation.

We turned to the earthquake locations to investigate this hypothesis. The absolute location we obtained for the 06:26 10 March 2014 best recorded event was approximately 1 km east of the location reported by ODNR/LDEO/NEIC (Figure 2.3). While the original location for the event placed it near horizontal wells that had been completed by Hilcorp in 2012-2013 (CCL1), the location we determined placed it near horizontal wells that were proposed by Hilcorp for operation in 2014 (CCL2) (ODNR, 2014b). After completing our initial relocation location analysis, we contacted ODNR and were

informed that well CCL2-1H was being hydraulically fractured when the largest event occurred.

Once the full well stimulation reports were available ~4 months afterwards, we identified the earthquakes corresponded to hydraulic fracturing stages on legs #1H and #3H (Figure 2.2a). The 1H and 3H stages with coincident seismicity were the most northeastern stages that had been hydraulically fractured (Figure 2.3), but the two northwesternmost stages of 3H did not correlate with earthquakes. Note that 6H stages reach as far north as the 1H stages (Figure 2.3), but there are no earthquakes during these hydraulic fracturing stages on 23 February 2014. Following termination of completion operations on the afternoon of 10 March 2014, there was a marked decline in seismicity, with only six events in the following 12 hours and only a single event (13:58 12 March) in the next ~2 months.

Considering events with the lowest location uncertainties (horizontal < 10 m; vertical < 100 m), the western portion of our relocated epicenters primarily occurred during stimulation of well 3H and immediately following it (4-6 March). The eastern portion of our relocated epicenters primarily occurred during stimulation of well 1H (10 March). The events following termination of stimulations tended to occur in the western portion. In particular, the event on 12 March occurred at the western end of our epicenters and appears to be an aftershock of the 4-6 March sequence.

This suggested that slip migration away from the well ceased after hydraulic-fracturing operations were halted. The waveforms supported the location trends over time, as events during 3H stimulation and immediately following had distinctly similar waveforms (Figure 2.4), with the largest arrival at 17.5 sec, a small early arrival at 17.0 sec, and a prominent third arrival at 18.5 sec. Waveforms during 1H stimulation were similar overall, the early arrival at 17.0 sec was significantly larger, and the late arrival at 18.5 sec was smaller. Waveforms recorded after 1H stimulation was terminated returned to the pattern seen during 3H stimulation with larger second and third arrivals.

Given the calculated depths, geologic cross sections through the study region showed that the events most likely occurred near the basement contact based on comparisons between our relocated hypocenters, the well paths, and estimated basement depths (Figure 2.5). The borehole deviation survey reports for wells 1H and 3H indicate the horizontal trajectories through the target interval (the Ordovician Point Pleasant Formation). Using the depth error bars determined for the 10 March M_L 3.0 event as a guide, the range of calculated depths for the 77 earthquakes identified as part of this study indicate the events most likely occurred within 200 m of the Precambrian basement, approximately 500 m below the target interval. Note that while our absolute depth uncertainty was ±280 m, our best fitting absolute depth was at the basement contact, and our relative depth uncertainty was ±150 m. This relocated hypocentral distribution indicated that many, if not all, events in the sequence occurred along a roughly vertical, east-west oriented fault (or faults) with likely basement involvement.

In order to confirm the possible geometry of the potential fault system, we calculated the fault plane solution for the largest 10 March 2014 M_L 3.0 event. The fault plane solution was based on the best 20 P-wave arrivals (Figure 2.6) and revealed a near-vertical (82° dip) ENE-WSW oriented fault plane that had nearly the same strike (258°) as that outlined by the distribution of hypocenters (262°). The similarity to the previous 31 Dec 2011 Mw 4.0 of the Youngstown earthquake sequence (strike 265°, dip 72° N)

(Kim, 2013) indicated the potential for a consistent basement fault fabric across Mahoning County, Ohio. The focal mechanism and waveform similarity indicated that Poland Township earthquake sequence occurred as a series of left-lateral displacements on a near-vertical fault.

The comparison of timing and three-dimensional locations of the best-located earthquake hypocenters and well stimulations help demonstrate the apparent relationship. To further illustrate this, we examined each well stimulation stage and plotted the average distance from the portion of the well stimulated to the hypocenters during that stage or up to 1 hour after (Figure 2.7). If earthquakes did not occur during that stage, we plot the average distance from the stage to the five earthquakes closest in time. While this is still a simplistic comparison, it illustrates the 6 stimulations that correlated in time with seismicity were at distances of 750-850 m. None of the nearly 100 other stimulation stages in the CCL2 wells at distances larger than 850 m from the earthquake source region coincided with detected seismicity. The lack of seismicity coincident with the northernmost stages at 6H indicates that the seismogenic fault is limited in extent and does not reach that far west. Further support for this can be found in the limited number of correlations at well 3H, with the two northernmost stages apparently too far from the fault to generate seismicity.

1.5. Discussion

The temporal and spatial proximity of the Poland Township earthquakes to active hydraulic fracturing operations strongly suggested that the stimulation process triggered the seismic events. In addition, the relatively large magnitudes compared to hydraulic fracturing microseismicity and calculated b-value of the earthquakes indicated slip on a pre-existing fault as opposed to the creation of a new fault. Pore-fluid pressures may have been elevated due to hydraulic fracture fluids or pressurized formation waters that entered a pre-existing fault or fracture zone, either as a result of intersection with the well borehole (Hulsey et al., 2010) or along natural fractures induced during well stimulation (Wolhart et al., 2005; Davies et al., 2013). In this interpretation, the increase of fluid pressure reduced effective normal stress on the fault surface and permitted fault slip (Healy et al, 1968; Simpson, 1986; Nicholson and Wesson, 1990; Zoback and Harjes, 1997). The ~ENE-WSW orientation of the proposed fault was within the range of optimal orientations for reactivation given the NE-SW orientation of regional S_{Hmax} in eastern Ohio (Zoback, 1992).

We note that the well 3H stimulation report shows evidence for a "screen-out" in the stage immediately before the earthquakes began, which may have occurred as fluids injected to produce hydraulic fractures entered a permeable fault or fracture zone. The escaping fluids could have caused induced fractures closer to well bore to close, resulting in the elevated well bore pressures. Although this scenario is highly speculative, the report from ODNR shows likely screen-out related shut downs in stimulation activities between 02:00 and 10:20 (local time) on 04 March, approximately 6 hours prior to our first detected earthquake (16:23, 04 March).

Alternatively, fluid pressure may have also increased through poroelastic stress coupling between fractured lithologies and formation fluids (Lacazette and Geiser, 2013; Davies et al., 2013). As such, seismic events associated with hydraulic fracture-related fault reactivation can occur close to the borehole or up to several 100s of meters from a

well (Davies et al., 2013). Tomographic imaging of areas adjacent to wells undergoing hydraulic fracturing suggesting that pre-existing structures can be seismically activated as much as 1 km both horizontally and vertically from the borehole (Lacazette and Geiser, 2013). This observation could explain the spatial distribution of the Poland Township earthquakes that indicated hydraulic fracturing was likely influencing faults up to 850 m away from the well stimulations (Figure 2.7).

Our findings were similar to that from a study of 38 earthquakes (M_L 2.2-3.8) between April 2009 and December 2011 identified by Natural Resources Canada (NRC) in the Horn River Basin in NE British Columbia (BCOGS, 2012). Dense arrays of 20 and 151 stations were installed in the Etsho and Tattoo areas of the basin, respectively, and a combined 254 events of $M_L \geq 2.0$ were identified. Fault mapping in the area found abundant pre-existing faults. BC Oil and Gas Commission concluded these events were the result of fluids injected from nearby hydraulic fracturing operations that activated the pre-existing faults. In both the Etsho/Tattoo and Poland Township areas, there was no reported seismicity prior to the hydraulic fracturing operations. Although the Etsho/Tattoo operations had legs that were drilled ~1 km from each other, a leg that resulted in extensive seismicity could be adjacent to others that had little to no attributed seismicity. Almost all seismicity from the Etsho/Tattoo sequences were confined below the target interval and occurred horizontally adjacent to hydraulic fracturing operations. Further analysis of the largest events aligned along a cluster of seismicity oriented within 30 degrees of the principal horizontal stress direction below the reservoir (Baig et al., 2013). This alignment suggested that the stress redistribution from hydraulic injection is sufficient to cause larger-scale, optimally-oriented faults to slip in surrounding formations.

In April 2014, following the Poland Township earthquake sequence, the ODNR issued new regulations that will apply to new horizontal wells in Ohio located within 3 miles of a known fault or previously identified seismicity $M \geq 2.0$ (ODNR, 2014a). While we did not have access to any proprietary data from the operator, to the best of our knowledge, these new regulations would not have applied to the Hilcorp Energy wells in Poland Township as no known fault or historical seismicity had been identified in the area prior to hydraulic fracturing. This fact highlights the potential of rapid regional template-matching techniques that can analyze any seismicity that may be related to ongoing hydraulic fracturing operations to determine if they are part of a larger repeating sequence. Our characterization of the Poland Township sequence demonstrated the viability of the template matching approach, as we were able to complete the template matching process within 1 hour of being informed of the 10 March 2014 M_L 3.0 event. Had we been informed of the M_L 2.1 earthquake that occurred on March 5, we would likely have identified the majority of the $M_L < 2.0$ earthquakes that occurred during the first couple days of the sequence. If hydraulic fracturing of the CLL2 wells had been terminated at that point, the more broadly felt events that occurred later in the earthquake sequence might have been prevented. The seismic network utilized for our template matching will continue to be applicable for eastern Ohio and surrounding regions as the three EarthScope Transportable Array stations used in this study were adopted as permanent components of the Pennsylvania seismic network.

1.6. Conclusions

Using an optimized multi-station cross-correlation template matching routine, 77 events were identified in two temporal clusters during 4-12 March 2014 that temporally and spatially coincided with nearby hydraulic fracturing operations. We identified earthquakes as small as M_L ~1 up to M_L 3, some of the largest earthquakes induced by hydraulic fracturing in the United States. Using a locally-derived velocity model, a combination of absolute and double-difference relocations indicate the events less than ~850 m from two lateral wells that were actively hydraulic fracturing. The relocated events outline a fault with a strike of 262° near the top of the crystalline Precambrian basement. A focal mechanism calculated for the M_L 3 event has a left-lateral fault plane with nearly the same azimuth as the earthquake distribution that appears to be optimally oriented within the regional stress field. The relatively large magnitude of these events and the b-value of 0.89 suggested slip occurred along a pre-existing fault that was induced to rupture by nearby hydraulic fracturing.

Optimized template matching utilizes high-quality reliable stations within pre-existing seismic networks and is therefore a cost-efficient monitoring strategy for identifying and characterizing potentially induced seismic sequences. This is particularly important in places like Ohio where new state regulations on activities related to hydraulic fracturing are being implemented based on seismicity patterns.

1.7. Data and Resources

Seismic data and earthquake catalogs were obtained from the IRIS Data Management Center at www.iris.edu (last access March 2014). Plots were made using the Generic Mapping Tools version 4.2.1 (www.soest.hawaii.edu/gmt; Wessel and Smith, 1998).

1.8. Acknowledgements

Support for this work was provided by NSF grant EAR-0847688 (MB). We benefitted from discussions with Steve Holtkamp, Paul Friberg, Chris Grope, Tom Serenko, Mike Hansen, Mike Angle and many others at the Ohio Department of Natural Resources. Paul Friberg, Art McGarr, and Ivan Wong provided constructive reviews of the manuscript that significantly improved this publication.

1.9. References

Bachmann, C. E., W. Foxall, and T. Daley (2014). Comparing induced seismicity on different scales. Proceedings, *Thirty-Ninth Workshop on Geothermal Reservoir Engineering*. Stanford University, Stanford, CA.

Baig, A., T. Urbancic, and F. Viegas (2013). Characterizing Felt Seismicity During Hydraulic Fracture Stimulations. *Geological Society of America Abstracts with Programs*, 45-7.

Baranoski, M. T. (2013). Structure contour map on the Precambrian unconformity surface in Ohio and related basement features (ver. 2.0). Columbus, Ohio Department of Natural Resources, Division of Geological Survey Map PG-23, scale 1:500,000, 17.

BCOGS (British Columbia Oil and Gas Commission), 2012. Investigation of observed seismicity in the Horn River Basin. URL: http://www.bcogc.ca/investigation-observed-seismicity-horn-river-basin.

BGS (British Geological Survey), 2011. "Blackpool earthquake, Magnitude 2.3, 1 April 2011." Available at http://www.bgs.ac.uk/research/earthquakes/blackpoolApril2011.html.

Davies, R., G. Foulger, A. Bindley, and P. Styles (2013). Induced seismicity and hydraulic fracturing for the recovery of hydrocarbons. *Mar. Petrol. Geol.,* 45 171-185.

Efron, B. (1979). Bootstrap methods: another look at the jackknife. *The Annals of Statistics,* 1-26.

Ellsworth, W. L. (2013). Injection-induced earthquakes. *Science*, 341. doi: 10.1126/science.1225942.

Friberg, P.A., Besana-Ostman, G.M., Dricker, I. (2014). Characterization of an earthquake sequence triggered by hydraulic fracturing in Harrison County Ohio, *Seismological Research Letters*, 85. doi: 10.1785/0220140127.

Nicholson, C., and Wesson, R., (1990). Earthquake Hazard Associated With Deep Well Injection - A Report to the U.S. Environmental Protection Agency. *U.S. Geol. Surv. Bull.*

Healy, J.H., W.W. Rubey, D.T. Griggs, and C.B. Raliegh (1968). The Denver Earthquakes. *Science,* 161-3848 1301-1310.

Herrmann, R.-B., (2004). Computer Programs in Seismology, Version 3.30-GSAC.

Holland, A. (2013). Earthquakes triggered by hydraulic fracturing in south-central Oklahoma. *Bull. Seism. Soc. Am.* 103-3 1784-1792.

Holtkamp, S. G., M. R. Brudzinski, B. S. Currie (2015). Regional detection and monitoring of injection-induced seismicity: Application to the 2010-12 Youngstown, Ohio seismic sequence, AAPG Bull., 99(9), 1671-1688. doi: 10.1306/03311513194.

Hulsey, B.J., Cornette, B., and Pratt, D. (2010). Surface Microseismic Mapping Reveals Details of the Marcellus Shale. Society of Petroleum Engineers, Eastern Regional Meeting, 13-15 October, 2010, Morgantown, West Virginia. SPE-138806-MS, 7.

Kim, W.-Y. (2013). Induced seismicity associated with fluid injection into a deep well in Youngstown, Ohio. *J. Geophys. Res.* 118 3506–3518. doi: 10.1002/jgrb.50247.

Lacazette, A., and P. Geiser (2013). Comment on Davies et al. (2012) Hydraulic fractures: how far can they go? *Marine and Petroleum Geology,* 43.

Lei, X., G. Yu, S. Ma, X. Wen, and Q. Wang (2008). Earthquakes induced by water injection at ~3 km depth within the Rongchang gas field, Chongqing, China. *J. Geophys. Res.*, 113-B10. doi: 10.1029/2008JB005604.

Maxwell, S. C., M. Jones, R. Parker, S. Miong, S. Leaney, D. Dorval, D. D'Amico, J. Logel, E. Anderson, and K. Hammermaster (2009). Fault activation during hydraulic fracturing. *SEG Annual Meeting, Expanded Abstracts*.

National Academy of Sciences (NAS) (2012). Induced Seismicity Potential in Energy Technologies, *Natl. Acad. Press*, 225. Washington, D.C.

Nicholson, C., and R. L. Wesson (1990). Earthquake hazard associated with deep well injection: A report to the U.S. Environmental Protection Agency, *U.S. Geol. Surv. Bull. 1951*. URL: http://pubs.usgs.gov/bul/1951/report.pdf.

ODNR (2014a). "Ohio Announces Tougher Permit Conditions for Drilling Activities Near Faults and Areas of Seismic Activity", URL: http://oilandgas.ohiodnr.gov/oil-gas-home/post/ohio-announces-tougher-permit-conditions-for-drilling-activities-near-faults-and-areas-of-seismic-activity.

ODNR (2014b). "Ohio Oil & Gas Well Locator", URL: http://oilandgas.ohiodnr.gov/well-information/oil-gas-well-locator.

Skoumal, R. J., M. R. Brudzinski, B. S. Currie, and J. Levy (2014). Optimizing Multi-station earthquake template matching through re-examination of the Youngstown, Ohio sequence. *Earth Planet. Sci. Lett*. 405, 274-280.

Simpson, D. W. (1986). Triggered earthquakes. *Annual Review of Earth Planet. Sci.* 14 21-42.

Snoke, J. A., 2003. FOCMEC: FOCal MEChanism Determinations. Package URL: http://www.geol.vt.edu/outreach/vtso/focmec/.

Waldhauser, F., and W. L. Ellsworth (2000). A double-difference earthquake location algorithm: Method and application to the northern Hayward fault, California, *Bull. Seism. Soc. Am.* 90 1353–1368.

Waldhauser, F. (2001). Hypodd: A computer program to compute double-difference earthquake locations. *USGS Open File Rep*. 01-113;

Warpinski, N. R., J. Du, and U. Zimmer (2012). Measurements of hydraulic-fracture-induced seismicity in gas shales. *Soc. Pet. Eng*. 151597, SPE Hydraulic Fracture Technology Conference, The Woodlands, Texas. 6-8 February 2012.

Wessel, P., & Smith, W. H. (1998). New, improved version of Generic Mapping Tools released. Eos, Transactions American Geophysical Union, 79(47), 579-579.

Wessels, S., M. Kratz, and A. De La Pena (2011). Identifying fault activation during hydraulic stimulation in the Barnett shale: source mechanisms, b values, and energy release analyses of microseismicity. *SEG Annual Meeting, Expanded Abstracts*.

Wolhart, S., E. Davis, W. Roadarmel, and C. Wright (2005). Reservoir deformation monitoring to enhance reservoir characterization and management. *75th Annual International Meeting, SEG, Expanded Abstracts*, 2512-2515.

Zhang, H., and C. H. Thurber (2003). Double-difference tomography: The method and its application to the Hayward fault, California. *Bull. Seism. Soc. Am.*, 93-5 1875-1889.

Zoback, M. L. (1992). Stress field constraints on intraplate seismicity in eastern north America. *J. Geophys. Res.* 97-B8 11761–11782.

Zoback, M. D., and H.-P. Harjes (1997). Injection-induced earthquakes and crustal stress at 9 km depth at the KTB deep drilling site, Germany, J. Geophys. Res., 102-B8 18477-18491. doi: 10.1029/96JB02814.

Table 1.1. Layered velocity models considered in determining locations of the Poland Township earthquake sequence.

Model	Depth (km)	Vp (km/sec)	Vs (km/sec)
Preferred	0.0	4.50	2.60
	3.10	5.94	3.43
	4.00	6.12	3.54
	10.0	6.60	3.82
	40.0	8.10	4.68
Adjusted Kim (2013) A	0.0	3.86	2.19
	1.19	4.98	2.83
	2.46	6.13	3.48
	3.10	6.15	3.49
	10.0	6.62	3.76
	41.0	8.10	4.60
Adjusted Kim (2013) B	0.0	3.86	2.23
	1.19	4.98	2.88
	2.46	6.13	3.54
	10.0	6.62	3.83
	41.0	8.10	4.68
Adjusted Northeast Ohio	0.0	4.50	2.60
	3.10	6.12	3.54
	10.0	6.62	3.83
	41.0	8.10	4.68

Table 1.2. Performance of layered velocity models in determining locations of the Poland Township earthquake sequence

Model	Preferred	Adjusted Kim (2013) A	Adjusted Kim (2013) B	Adjusted N.E. Ohio
RMS Residual of Cross-Correlation Waveforms (s)	0.0084	0.080	0.0084	0.0077
Double Difference Hypocentral Location Variance (s)	44.3	45.6	45.7	45.2
Median Bootstrap Horizontal Error Estimate (deg)	0.00010	0.00033	0.00029	0.00013
Median Bootstrap Vertical Error Estimate (km)	0.089	0.11	0.19	0.083

Table 1.3. Largest earthquakes identified in the Poland Township earthquake sequence.

Date	Time (UTC)	Latitude	Longitude	Depth (km)	M_L
3/05/2014	03:05:16	41.01339±0.00005	-80.52670±0.00014	3.14±0.09	2.3
3/10/2014	06:26:42	41.01380±0.00006	-80.52370±0.00013	3.10±0.09	3.0
3/10/2014	06:42:41	41.01408±0.00005	-80.52449±0.00013	3.04±0.09	2.3
3/10/2014	15:03:44	41.01390±0.00006	-80.52288±0.00013	3.09±0.09	2.5
3/10/2014	15:44:03	41.01374±0.00006	-80.52404±0.00012	3.11±0.09	2.8
3/11/2014	07:01:10	41.01340±0.00006	-80.52769±0.00013	3.17±0.09	2.1

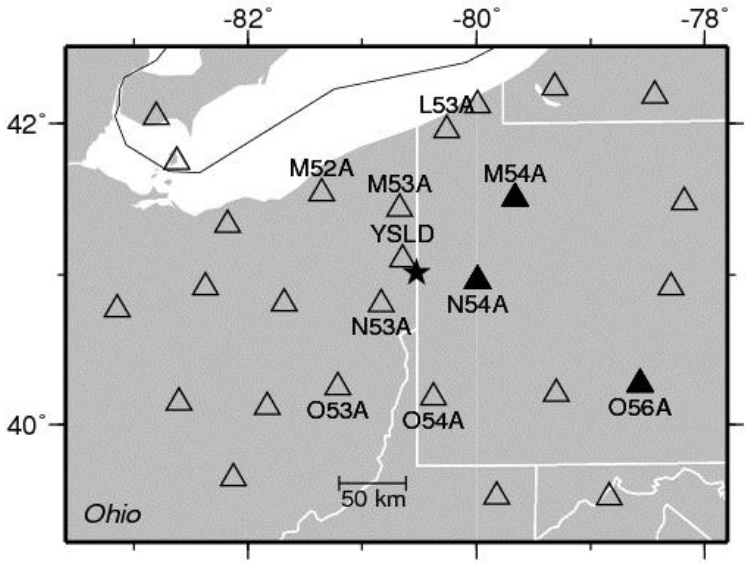

Figure 1.1. Regional map identifying seismic stations (triangles). Black stations were used for template matching, labeled stations were used to determine an absolute location of Poland Township sequence (star), and all stations shown were used in the relocation of matched events. The Youngstown sequence (Skoumal et al., 2014) occurred at the northwestern edge of the YSLD triangle.

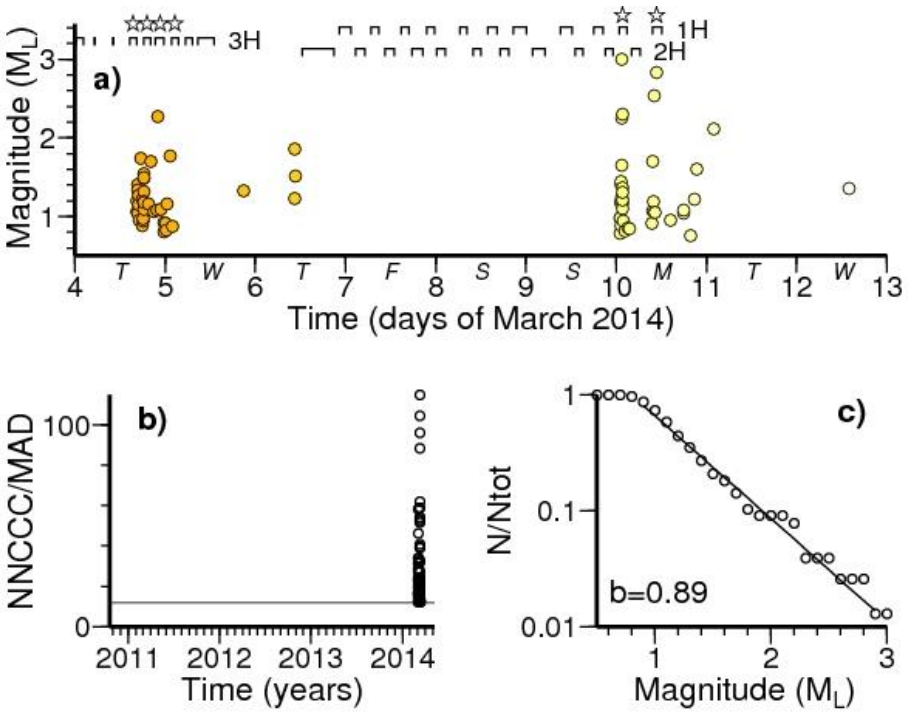

Figure 1.2. Summary of template matching results. (a) Magnitudes of matched events, shaded based on time. For well operations during this period (1H, 2H, 3H), timing of stimulations is marked across the top. Stars indicate stages that correlate with matched seismicity. X-axis is plotted in local time for comparison with daily operations. (b) Normalized network cross-correlation coefficient (NNCCC) over time, plotted with respect to the MAD value. The horizontal line marks 12×MAD, which is our threshold for detection. (c) Magnitude-recurrence relationship with calculated b-value.

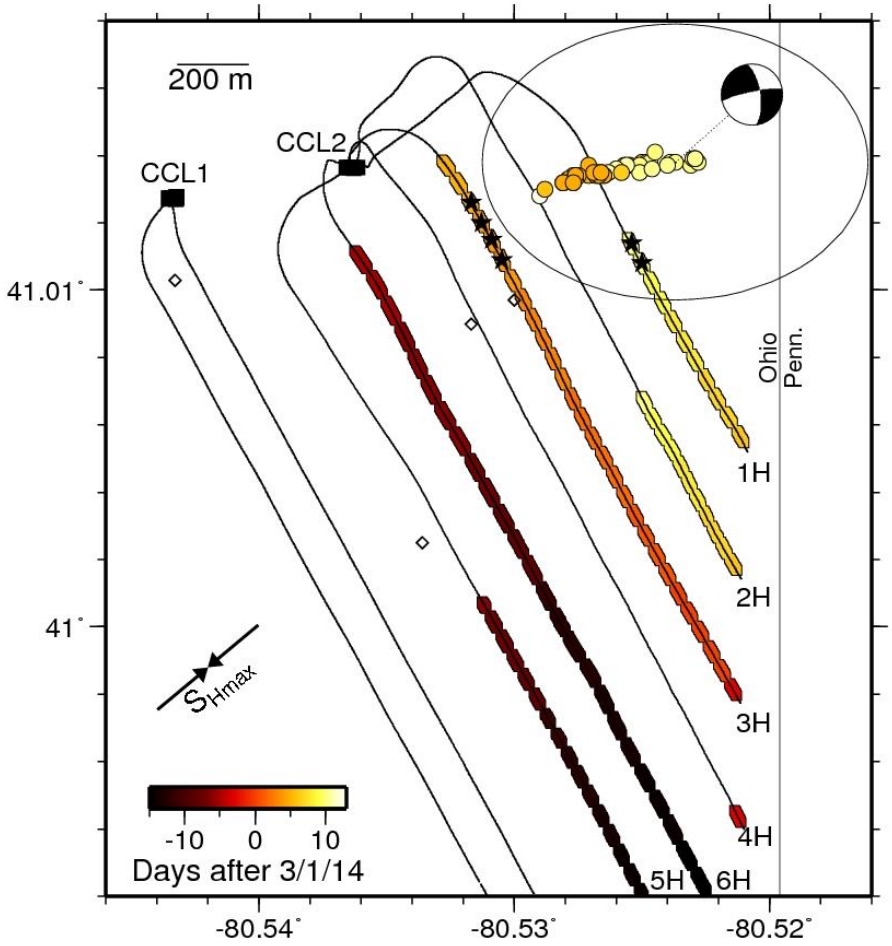

Figure 1.3. Map of the double-difference relocated earthquakes with the lowest relative location uncertainties shaded according to time. Curved lines indicate horizontal drilling well paths, with stimulation stages shaded using the same time scale. Stars indicate stages that correlate with times of seismicity. Well CCL1 was completed in 2013. Focal mechanism is from the 10 March 2014 06:26 M_L 3 event. Diamonds are reported ODNR/LDEO/NEIC locations of the largest earthquakes in this sequence.

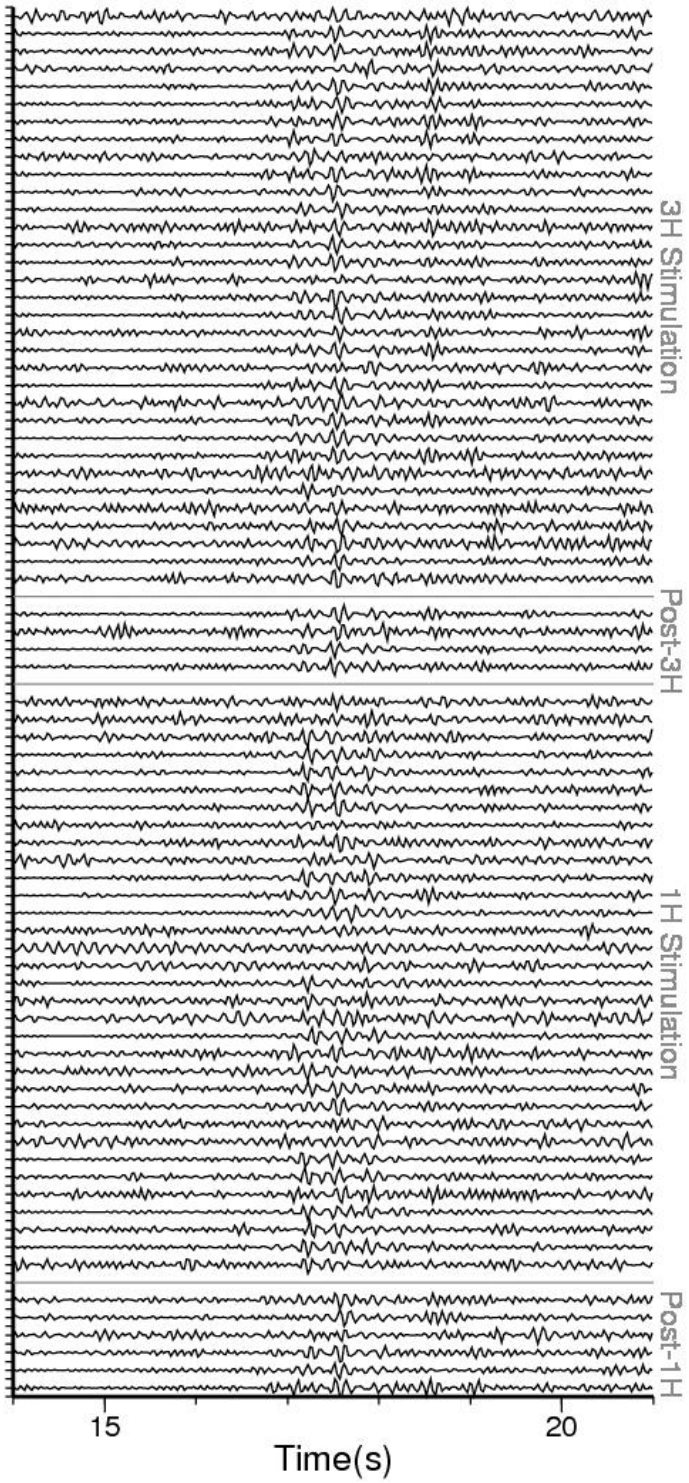

Figure 1.4. Horizontal component (BHN) waveforms at station N54A for the 77 identified events in chronological order from top to bottom. Grey lines divide key phases of well simulation. All traces are normalized to their maximum amplitude.

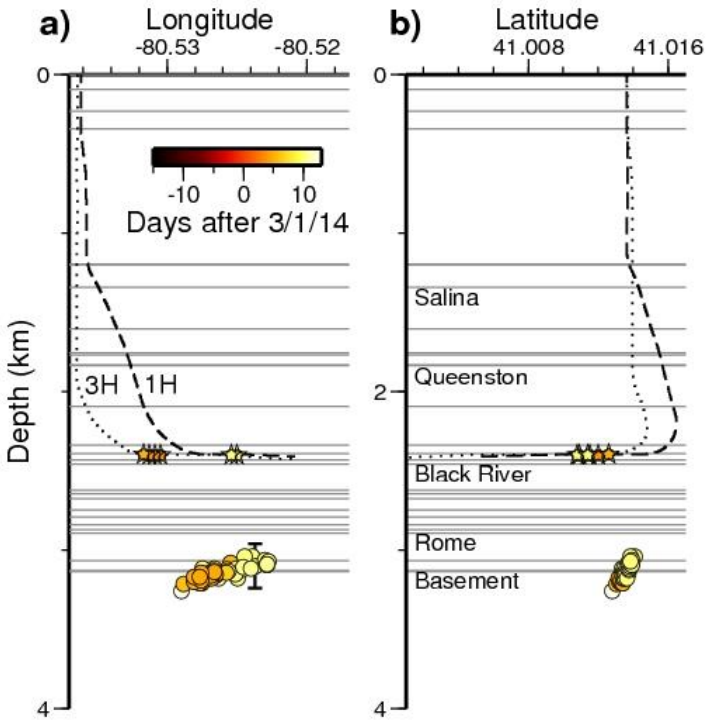

Figure 1.5. East-west (a) and north-south (b) cross-sections of the double-difference relocated seismicity shaded by time as in Figure 2.3. Absolute depths were based on the 10 March 2014 06:26 M_L 3 event, with the vertical error bar through this event based on bootstrap estimates of depth uncertainty indicating the events most likely occurred near the Precambrian basement contact. Horizontal grey lines mark key strata. The dashed and dotted black lines were the paths of Well 1H and 3H, respectively, targeting the Point Pleasant formation. No exaggeration.

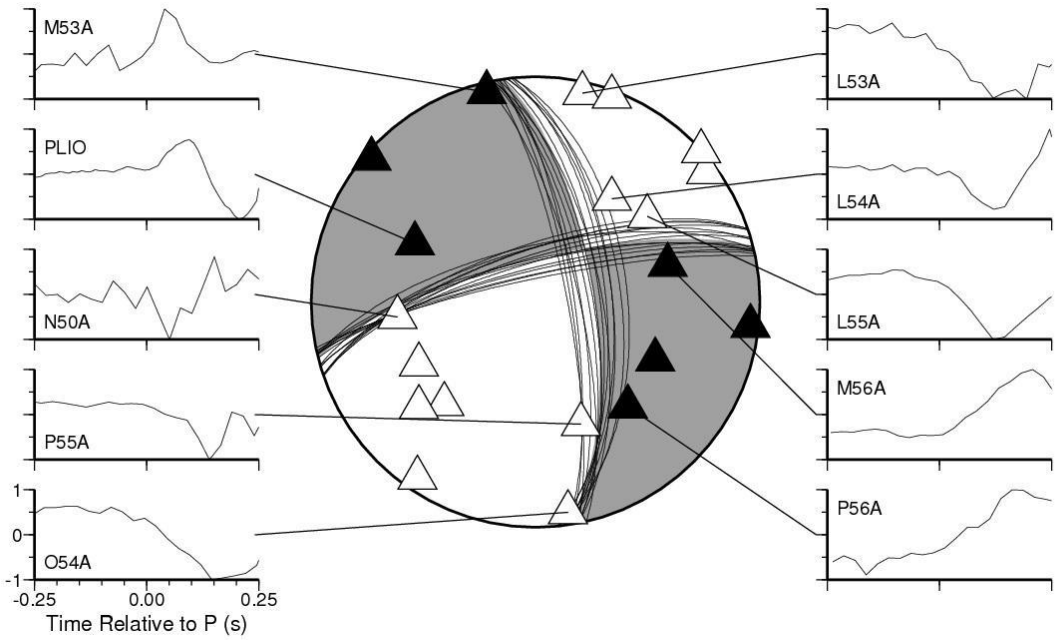

Figure 1.6. Fault plane solution and selected first arrival waveforms for the 06:26 10 March 2014 M_L 3 earthquake. Triangles on the focal sphere show station polarity data for compressional (black) and dilatational (white) first motions. Seismograms show 0.25 before and after the picked P wave arrival time at each station.

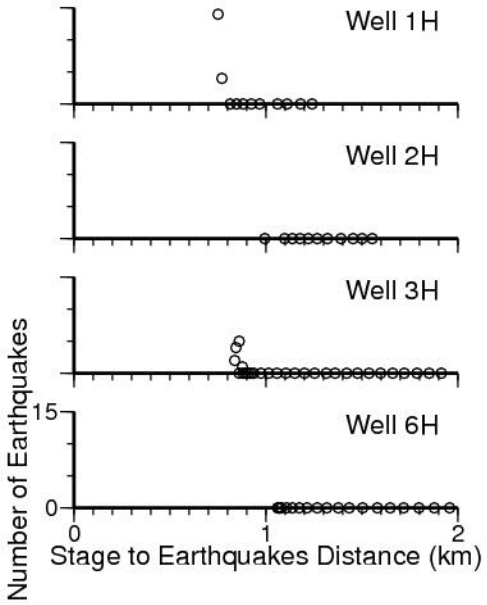

Figure 1.7. Estimate of three-dimensional distance from stimulation stage in horizontal wells to relocated earthquake hypocenters. Only the earthquakes with the lowest relative location uncertainties are considered (Figure 2.3).

CHAPTER 2: Microseismicity induced by deep wastewater injection in southern Trumbull County, Ohio

2.1. Introduction

As oil and gas well completions utilizing multi-stage hydraulic fracturing have become more commonplace, the potential for seismicity induced by the deep disposal of frac-related wastewater and the hydraulic fracturing process itself has become an increasingly important issue (e.g., NAS, 2012). While it is rare for a wastewater disposal well to induce felt seismicity, there have been several cases over the past half century that identify strong relationships between injected fluids and seismicity (e.g., Healy et al., 1968; Evans et al., 2012; McGarr et al., 2002; Nicholson and Wesson, 1990). Following the 2011 Youngstown earthquake sequence (YES) near a wastewater disposal well in northeastern Ohio (Figure 3.1), which included hundreds of earthquakes up to a M 4.0 (ODNR, 2012; Kim, 2013; Skoumal et al., 2014a), there has been a heightened concern over seismicity related to energy technologies in Ohio. The Ohio Department of Natural Resources (ODNR) is actively setting new regulations to deal with induced seismicity (ODNR, 2014), which could serve as a blueprint for other states. Seismic monitors are to be installed near certain injection wells before commercial injection began and will remain there for 12 months afterward. There are also a number of regional long-standing "backbone" seismic stations for over a decade and studies of the YES significantly benefited from early adoption of EarthScope Transportable Array (TA) stations in western Pennsylvania in late 2010.

The first earthquake detected by the ODNR and the USGS in the Trumbull County sequence was a M_L 2.1 earthquake on 31 August 2014 at 21:34 UTC (5:34 PM local), with only a single felt report. Epicentral locations placed it within 1 km of the American Water Management Services (AWMS) Weathersfield injection well site, near Warren, Ohio (Figure 3.1). There is a shallower well at this site (AWMS-1) that injects into the Silurian interval, and a deeper well (AWMS-2) that injects into Ordovician-Cambrian interval about 15 m above the Precambrian basement (Appendix A). AWMS-2 was approved on 4 March 2014 to inject at pressures up to 11.6 MPa (1680 psi). AWMS-1 was approved on 4 March 2014 at 7.1 MPa (1025 psi), which was later raised to 8.3 MPa (1200 psi) on 11 July 2014. As of 31 August 2014, > 9,160 and > 174,000 barrels of wastewater were injected into AWMS-1 and AWMS-2, respectively.

The ODNR issued a chief's order on 3 September 2014 suspending operations at both wells. The ODNR spokeswoman Bethany McCorkle said after analyzing data during the investigation, the agency found that the shallower of the two wells was not related to the seismic event. On 18 September 2014, the company was allowed to resume injection operations at the shallow well (AWMS-1), while the investigation continued on the deeper well (AWMS-2). In this study, we use multi-station waveform template matching as an earthquake fingerprint scanning technique to investigate the potential relationship between the earthquake and the injection operations.

2.2. Data and Analysis

Our analysis followed the approach of Skoumal et al. (2014a) that was optimized for the 2011-14 YES that occurred ~11.5 km away from the Trumbull sequence. Regional seismic data were obtained using IRIS WebServices (http://service.iris.edu) and

mainly consisted of high-quality broadband EarthScope Transportable Array stations recording at 40 samples/sec (Figure 3.1). The ODNR also sent a hard disk with seismic recordings from 1 July-30 September 2014 from a local 4 station network consisting of 3-component short period instruments recording at 200 samples/sec (Figure 3.1).

Templates using regional data were created for the M_L 2.1 and M_L 1.5 events using the same parameters (e.g. template length, sampling interval) as in previous work (e.g. Skoumal et al., 2014a). The preliminary analysis used data from M54A, N54A, O56A (begun in 6 November 2010) as well as closer stations M53A, N53A (begun 14 January 2013) and ran up to 14 January 2015. Local network data were interpolated to a common sampling interval of 100 samples/s and then bandpass filtered between 1-45 Hz. Templates of 6 sec length starting 1 second before the P-wave were created from the M_L 2.1 and M_L 1.5 earthquakes. Considering the higher resolution of the local data, empirical subspace detector was employed to expand the set of matches (Barrett and Beroza, 2014). With this approach, the stack of events and the time derivative of the stack are close approximations of the first two singular vectors. So, for each of the two template match results (M_L 2.1 and M_L 1.5), we created an additional template from the stack of those matches and a template from the time derivative of the stack. We also found that using the derivative of the original template waveforms detected some additional legitimate events. The matches from all 8 templates were then combined into our final set of events.

Multi-station template matching followed the approach of previous work (e.g. Skoumal et al., 2014a). Events were detected if the NNCCC exceeded an initial threshold of 12 times the median absolute deviation (MAD) of the daily NNCCC for regional data and 8×MAD for the local data. These thresholds were determined after inspecting the quality of the matched waveforms and the temporal patterns of the matches. Detections were considered legitimate earthquakes if they had a signal to noise ratio greater than 2 and visually resembled the template waveform at the quietest station.

Due to the proximity of this sequence to the YES, we used the velocity model B from Kim (2013) that was developed using sonic logs for location analysis with local data. A different velocity model for the Youngstown earthquake sequence was previously used since we were using regional data to locate those events (Skoumal et al., 2014a), but we found the Kim (2013) model B produced lower residuals in this case, likely due to the availability of local data.

Lag times and correlation coefficients were generated between the template and each matched event to determine wave arrival times and weights for all matched events, which were used with *elocate* (Herrmann, 2004) and the velocity model to determine an initial set of catalog locations. A full set of lag and correlation matrices between all events for all channels were then used in a *HypoDD* double-difference algorithm to determine the relative locations of the events (Waldhauser and Ellsworth, 2000; Waldhauser, 2001). The median relative locations errors we found based on bootstrapping estimation were 60 m horizontally and 100 m vertically. Relocated hypocenters were pinned to the absolute location determined for the M_L 2.1 event, preserving the relative locations.

Following the approach of Schaff and Richards (2014), the relative magnitudes of the earthquakes were estimated by comparing the unnormalized correlation coefficients of the events to the catalogued M_L 2.1 event. The estimation is given as:

$$\delta \text{ mag} = \log_{10} [\max(\mathbf{x} \star \mathbf{y})/(\mathbf{x} \cdot \mathbf{x})]$$

where **x** and **y** are the catalogued M_L 2.1 earthquake and a matched event, respectively. To validate these magnitude estimations, we also determined local magnitudes through a Richter scale approach similar to our previous work (e.g. Skoumal et al., 2014). While the two methods produced virtually identical magnitude estimations for the larger events, the Richter scale approach tended to overestimate the smaller magnitude events when poorer-quality stations were utilized. As demonstrated by Schaff and Richards (2014), correlation magnitude estimation techniques are ideally suited for estimating magnitudes of events with Gaussian white noise. Therefore, we utilized the correlation magnitude estimation in our analysis, which included the calculation of a Gutenberg-Richter *b*-value using the maximum likelihood estimate.

To gain additional perspective on the stresses associated with this earthquake sequence, we calculated a fault plane solution for the largest event, which was just large enough to make reliable identifications of first motion polarities at local and nearby regional stations. Takeoff angles were estimated using the pseudo-bending method within *tomoDD* (Zhang and Thurber, 2003). We used *FocMec* to performed a grid search of the focal sphere for a double couple solution (Snoke, 2003), and then took the median solution with 0 polarity errors. A grid search fit is justified by previous nearby studies that found clear double couple mechanisms along apparently pre-existing basement faults (Kim, 2013; Skoumal et al., 2015).

2.3. Results

Using the three long-standing regional stations (M54A, N54A, O56A), templates from the M_L 2.1 earthquake on 31 August identified the next two largest earthquakes, a M_L 1.5 on 29 July and a M_L 0.1 on 24 Aug 2014. Using the 3 closest TA stations (M53A, M54A, N53A), 3 additional earthquakes with M_L ~0 were found around the timing of the two largest events. The 6 epicenters determined using local data formed a band extending southwest of the well at distances 20-500 m from the wells in the basement at 3.1-3.3 km depth. Using the velocity model previously derived from nearby sonic logs (Kim, 2013), the absolute location errors for the M_L 2.1 were 60 m east-west and ~120 m north-south.

Utilizing local data, the multiple constructed templates identified 108 earthquakes with visually similar waveforms (Figure 3.2). 70% of the events were detected using waveforms associated with the M_L 2.1 templates, 30% from the M_L 1.5 templates. Using the stack and derivative templates provided a 25% increase beyond just the original two event templates. The 102 additional events discovered using local data had M_L -1.4 to 0, with a magnitude of completeness of approximately M_L -1.0 based on the frequency magnitude distribution.

The resulting set of all 108 matched events cover nearly the entire 3 month period for which local data was obtained, although there are only a handful of events during the first 3 weeks and after injection was halted (Figure 3.3a). The low seismicity rates appear to extend before the time period of local data we analyzed as single station scanning back to before injection began found no additional events (Paul Friberg, personal communication). The rate of very small ($M_L < 0$) seismicity tended to increase over time, but appears to have done so episodically. The seismicity rate increased quickly in the week preceding both the M_L 1.5 and 2.1 event, followed by a significant rate decrease. The reduced rate after the larger events implies a low aftershock rate that is unexpected for a stable continental region (Ben-Zion and Lyakhovsky, 2006). The jump of more than

an order of magnitude before the two larger events could be partly explained by the relatively narrow range of magnitudes in the remained of the events, such that the two larger events are anomalous.

The unusual pattern of earthquake magnitudes during this sequence is also evident in our attempts to estimate the Gutenberg-Richter *b*-value (Figure 3.4). While the *b*-value we calculate using the MLE method is close to 1 (0.91), the *b*-value we calculated using the LSQ method is (0.6). The discrepancy occurs because the frequency-magnitude distribution (FMD) does not follow a power law and suggests a different relationship is at work. A similar trend can be observed at the Youngstown injection well, although with larger magnitude events. However, the other nearby earthquake sequences induced by hydraulic fracturing in Harrison County and (Friberg et al., 2014) and Poland Township (Skoumal et al., 2015) do appear to follow a more typical power law FMD. In induced sequences with very high pore fluid pressure, the viscosity of the fault zone could be dictated by the fluid which would result in atypical FMDs. If fluid pressures are not as extreme, induce earthquakes may be followed by a sudden drop in pore pressure that could lead to more regular FMDs.

The earthquake activity appears to be correlated with injection at AWMS-2. The daily injection volumes provided to us by the American Water Management Services (AWMS) are the total for both wells, but based on the totalizers, AWMS-2 took 95% of the total volume before activities were suspended (AWMS, personal communication, 2015). Figure 3.3b shows weekly averages for volume (Vw) and pressure (Pw) for AWMS-2. The earthquake rates appear to increase once sustained injection pressures approach the maximum allowed surface pressure of ~11.6 MPa (1680 psi). This corresponds to pressures at the base of the injection interval of ~39.5 MPa (~5727 psi) given a ~1.1 g/cm^3 maximum density of injected fluids and slight friction-related reduction in pressure due to flow in through the injection tubing at reported maximum rates of 2 bbl/min (AWMS, personal communication, 2015).

It is also noteworthy that the volumes are reduced in late July once weekly pressures are near the maximum but the pressures only decrease slightly. When the volumes are raised again in late August, there is a corresponding increase in pressures and seismicity rate. After the injection was halted on 3 September, only 3 earthquakes were detected on 6 September. When the shallow injection was resumed on 18 September, we only found one earthquake on 30 September, about 2 days before the local data ends.

Figures 3.5 and 3.6 show map and cross-sectional views of the best located hypocenters with relative location bootstrap uncertainties less than 120 m horizontally and 150 m vertically. The average uncertainty of plotted events is ~60 m east-west, ~30 m north-south, and ~100 m vertically. The events form two clusters, one almost adjacent to the well and the other ~400 m southwest of the wells. The separation of these clusters was confirmed by performing absolute locations of the six largest events. The proximal cluster includes an event on 3 July, suggesting this cluster became active first, as one would expect for its proximity to the wells. The distal cluster became active on 13 July, but the M_L 1.5 event on 29 July occurred in the proximal cluster. Both clusters are active in August, but the M_L 2.1 event on 31 Aug occurred in the distal cluster. Intriguingly, the distal cluster has NNE-SSW trend (024°) different from previous nearby cases which followed a ENE-WSW trend (~080°). Although the trend in the proximal cluster is harder

to estimate due to fewer events, it appears to have a more ENE-WSW trend that aligns with seismicity along the northern edge of the distal cluster. We note that seismicity in the distal cluster initiates during a drop in weekly averaged pressure (Figure 3.3), which could indicate that fluid pressures migrating along a ENE-WSW fault drop upon reaching a NNE-SSW fault.

A sufficient number of *P*-wave first motions were available to calculate a focal mechanism for the M_L 2.1 event (Figure 3.7). The fault plane solution we determined was a strike slip mechanism, similar to previous nearby cases (Figure 3.5), but it shows a different azimuthal trend. In this case, the ESE-WNW left-lateral fault plane azimuth (110°) is rotated ~30° from the previous cases. This fault plane does not align well with either the overall trend of hypocenters or the trend of either event cluster. Instead, the NNE-SSW right-lateral fault plane azimuth (020°) matches better with the trend in the distal cluster where the M_L 2.1 event occurred. To quantify this comparison, we investigated the distances of epicenters in the distal cluster from a fault plane with either orientation. The standard deviation of epicenters from a 020° fault plane is ~3 times less than the average relative location uncertainty in the east-west direction, whereas the standard deviation of epicenters from a 110° fault plane is ~2 times more than the average relative location uncertainty in the north-south direction.

The hypocentral depths we determined also indicate the events in the proximal cluster occurred near the top of the Precambrian crystalline basement in close proximity to the bottom of the deep well. The distal cluster of events is about 500 m deeper but still in the upper Precambrian. These two depth ranges are similar to the nearby Poland Township and Youngstown induced sequences (Figure 3.6) (Skoumal et al., 2014a; Skoumal et al., 2015).

2.4. Discussion

The likelihood of inducing slip along a pre-existing fault is greater if the injection well or hydraulic fracturing stimulation is near a critically stressed fault that is optimally oriented to the regional stress field. The focal mechanism and azimuthal trend of the distal cluster of seismicity in the Trumbull sequence outlined a potentially different fault orientation (~020°) than nearby induced sequences of Youngstown (078°; Skoumal et al., 2014a), Poland Township (083°; Skoumal et al., 2015), and Harrison County (092°; Friberg et al., 2014) (Figure 3.1). However, the NE-SW orientations of the regional S_{Hmax} in eastern Ohio determined by Hurd and Zoback (2012) suggests that these two fault orientations (~020° and ~080°) are both ~30° from S_{Hmax} and hence optimal orientations for reactivation. Although the proximal cluster of Trumbull seismicity is only a handful of events, it may represent a ~080° basement fault or fracture trend extending from the well towards the distal cluster. If so, all four Ohio cases would represent ~500-800 m segments of strike-slip faults located within 1 km from the operations in map view. The slip appears to be located in the upper Precambrian basement in each case, such that there may be a network of faults or fractures in the shallow basement in eastern Ohio that are susceptible to being induced by human activities. A detailed study of the large number of injection wells and hydraulic fracturing stimulations that have not induced any detected seismicity could provide additional insight into the pervasiveness or scarcity of susceptible structures.

We recently proposed that induced earthquakes in Ohio could be identified using a checklist of possible indicators (Brudzinski et al., 2014): a close spatial correlation (< 10 km) between anthropogenic activities and observed seismicity, a close temporal correlation (< 1-2 years) between activities and observed seismicity, a repetitive swarm of seismicity, a low b-value or non-power law FMD, and the seismicity occurs in a region with no previously documented earthquakes. All of these criteria appear to be met in the Trumbull case, but we can further determine whether both the shallow and deep wells (AMWS-1 and -2) are responsible. Once the injection operations at both the shallow and deep Trumbull wells were halted, the seismicity rate quickly decreased. Following the resumed operations of the shallow well (AWMS-1), we find a lack of small earthquakes ($M_L < 0$) in the weeks after using the local data and an absence of any larger earthquakes ($M_L > 0$) in the months after using the regional data. Combining this finding with the relatively small amount of water injected into AWMS-1 and the large spatial distance between AWMS-1 and the Precambrian basement, we do not believe AWMS-1 has influenced slip along the fault. It appears that the sequence is solely a result of injection into the deep well (AWMS-2).

When the conditions are suitable for inducing earthquakes, a number of studies have suggested that the number and size of earthquakes are related to the volume of fluids injected (e.g., Holtkamp et al., in press; McGarr, 2014). This study supports those relationships in that the seismicity rate tends to increase with increasing cumulative injected volumes (Figure 3.3). In fact, the increasing rate of very small ($M_L < 0$) seismicity was a potentially diagnostic feature that the sequence was induced. However, the decrease in injected volumes beginning in late July while pressures remained relatively high indicates the absence of a simple relationship between injected volumes and number of earthquakes. Figure 3.8 illustrates how the weekly seismicity rate correlates better with the weekly average well pressures than the weekly average injected volumes. The trends are not linear so we calculated a Spearman's rank correlation and find the correlation coefficient is 62% between pressure and earthquakes and -22% between volume and earthquakes. The ~10% standard error indicates that correlation between pressure and earthquakes is much more statistically significant. The larger seismicity rates and majority of the earthquakes occur when the weekly average surface injection pressures are above 9.3 MPa (1350 psi). There appears to be a several day lag between changes in well pressure and corresponding changes in seismicity rate (Figure 3.3), which is similar to observations made in the Youngstown case (Holtkamp et al., in press) and implies a relatively fast communication between injection and seismic response.

Ellsworth (2013) identified two mechanisms for inducing earthquakes from wastewater injection: by 1) directly increasing the pore pressure along a fault or 2) changing the loading conditions above a fault. The pore fluid pressure mechanism would require a high-permeability pathway between the well and the fault. The fluids are expected to migrate via diffusion and could progressively lower effective normal stress that promotes fault slip. The diffusion of the water would be expected to create a pore pressure triggering front and back front when the high fluid pressure reaches and leaves the fault, respectively. Between the relatively slow moving triggering fronts, shorter time-scale variations in fluid pressures could also induce fluid pressure waves that more rapidly transmit dynamic changes in pore-fluid pressure along the fault. Inducing a fault

to slip through loading conditions could be possible in wells that have injected large volumes of water above a fault over long time frames, like the Prague case in Oklahoma (Keranen et al., 2013; Sumy et al., 2014). In this mechanism, the fluid pressure waves would not have to reach the fault. Rather, the volume and/or mass change of injected fluids above a fault would alter the shear and normal stresses, promoting slip. For the Trumbull and Youngstown sequences, the close temporal correlation between injection operations and seismicity are indications that fluid pressure changes are changing effective normal stresses directly on the fault. However the Trumbull sequence highlights 3 new observations from a wastewater injection case that also appear to be related: lack of aftershock productivity, narrow magnitude range, and non-power law FMD. Each of these observations is predicted by numerical simulations of a seismogenic zone governed by a viscoelastic damage rheology when the viscosity in the fault zone is reduced (Ben-Zion and Lyakhovsky, 2006). Such a reduction in viscosity is expected if deep wastewater injection increases fluid pressures in the fault zone to the point that the fault zone begins to dilate.

The formation of new fractures from hydraulic fracturing is expected to produce microseismicity with $M_L < 1$ and a *b*-value of ~2 (Warpinski et al., 2012; Maxwell et al., 2009; Wessels et al., 2011). Although rare, inducing a pre-existing fault to slip from hydraulic fracturing has been documented to produce seismicity with *b*-values < 1 and magnitudes up to M_L 4.2, as seen in the Septimus Basin in British Columbia (e.g. Skoumal et al., 2015 ; BCOGC, 2014). Two mechanisms are suggested for inducing earthquakes by hydraulic fracturing: 1) changes in viscoelastic stress transmitted primarily through rock and 2) changes in pore pressure transmitted through pore space. Tomographic imaging near wells undergoing hydraulic fracturing suggest pre-existing faults can be activated by viscoelastic stressing as much as 1 km horizontally and vertically from the borehole (Lacazette and Geiser, 2013). Those distances are harder to explain with fluid pressures considering the rapid onset and halt of seismicity with individual stages on the order of minutes in some cases. Moreover, the volumes injected and the duration of injection are both considerably smaller than for disposal wells. Using the Trumbull sequence as a guide, fluid pressure changes could result in lack of aftershock productivity, narrow magnitude range, and non-power law FMD, but these patterns are generally absent in the Poland Township and Harrison County cases, so we propose those cases are due to viscoelastic stressing.

Regardless of the specific mechanism for inducing seismicity, a number of cases of seismicity induced by fluid injection have been examined to investigate whether adjusting operations can reduce the degree to which seismicity is induced (NAS, 2012). The NAS report suggests that seismicity can be reduced by lowering injection volumes and pressures. Considering that the majority of seismicity occurred in our study region once weekly average pressures were above 9.3 MPa despite reductions in injected volumes, we suggest that keeping the sustained pressures below this level, perhaps via a lower maximum pressure, would be a key criterion for reducing seismicity if injection is resumed at the deep AMWS-2 well. We also hope this study demonstrates the utility of template matching for detection and evaluation of microseismicity ($M_L < 1$), which could then be used to adjust injection operations to help ensure seismicity remains below regulatory limits.

2.5. Conclusions

Multi-station cross-correlation template matching is a valuable tool to monitor for induced seismicity in addition to providing a more refined analysis of past seismic sequences. Utilizing both regional and local networks, 108 earthquakes were identified < 500 m from a pair of injection wells in southern Trumbull County, Ohio between 3 July and 30 September 2014. These events ranged in size from M_L -1.4 to 2.1, but there is a remarkable separation between the two largest events and the rest leading to an non-power law frequency-magnitude distribution. We also observed swarm behavior with low aftershock productivity for a continental interior. Each of these observations is consistent with recent numerical simulations when the viscosity in the fault zone is reduced by fluid injection. We suggest these could be diagnostic features that seismicity is being induced by injected fluid changing pore fluid pressures in the fault zone. The seismicity outlined a fault located in the uppermost Precambrian basement with an overall ENE trend similar to the orientation of other nearby induced sequences. However, the focal mechanism of the largest event and trend of the events cluster further from the well follow a NEN orientation. Both fault orientations are optimally oriented within the regional stress field. The operations at both wells were suspended by the ODNR on 3 September 2014. The lack of earthquakes after injection resumed at the shallower well (AWMS-1) and lack of earthquakes near this well during earlier injection indicates this well was not related to the seismicity and supports ODNR's decision to resume injection operations at this well. The deeper well (AWMS-2) is very likely related to the earthquakes based on strong spatial and temporal correlations between injection and seismicity. While seismicity rates generally grew with larger cumulative injected volumes, weekly seismicity rates were better correlated with weekly average well pressures. Seismicity primarily occurred when sustained pressures at AWMS-2 approached the maximum allowed, suggesting future deep injection at reduced pressures is a strategy that could preserve the current low seismicity rate. However, we advocate employing a multi-station cross-correlation template matching approach in real-time to monitor whether activity of microseismicity (M_L < 1) remains at low levels.

2.6. Supplementary Material

AWMS-1 and AWMS-2, are located in Weathersfield Township, Trumbull County, Ohio. The wells are located ~34 m (112 ft) apart on a north-south trend, at a surface elevation of 277 m (909 ft) above sea level. Based on well-completion records on file with ODNR, drilling of the AWMS-1 well (API 3415524076000) occurred between 13 September-2 November 2013. The well was drilled as a 44.5 cm-diameter (17.5 in) hole to a depth of 196 m (644 ft), where 34 cm-diameter (13.375 in) casing was set and cemented into the surface (Figure 3.S1). From 196 m to 1239 m (4061 ft) the well was drilled with a borehole diameter of 31.1 cm (12.25 in). The base of 22 cm-diameter (8.625 in) steel production casing was set at 1237 m (4056 ft) and cemented in up-hole to a depth of ~1145 m (~3756 ft). Injection tubing (11.4 cm-/4.5-in diameter) run from the surface was set with a packer the base of the production casing. AWMS-1 was drilled with a 7.85 in diameter from 1239 m to a total depth (TD) of 1342 m (4403 ft).

To facilitate wastewater injection, the lower 106 m (347 ft) of the well was completed "open-hole" between 1237 m (4056 ft) and TD. This interval corresponds to depths of between -959 m and -1065 m (-3147 to -3494 ft) below sea level. Drilling and

completion records indicate the injection interval is within the Silurian Newburg/Lockport Dolomite (Figure 3.S1). Prior to the initiation of waste-water injection, the open-hole interval was hydraulically fractured with ~55,865 liters (14,758 gallons) of produced water/friction reduces and treated with ~14385 L (2800 gal) of 28% HCl. Commercial injection was initiated in April, with an allowed maximum surface-injection pressure of ~7.1 MPa (1025 psi). Maximum injection pressures were increased to ~8.3 MPa (1200 psi) following approval on 11 July 2014 based on the actual specific gravity of the injection fluid at 1.05. During AWMS-1 well operations from April-August 2014, >9,1600 barrels of wastewater were injected (AWMS, personal communication).

Drilling of the AWMS-2 well (API 3415524075000) occurred between 14 September 2013 and 2 January 2014. The well was drilled as a 44.5 cm-diameter (17.5 in) hole to a depth of 279 m (914 ft), where 34 cm-diameter (13.375 in) casing was set and cemented into the surface (Figure 3.S1). From 279 m to 2225 m (7297 ft) the well was drilled with a borehole diameter of 31.1 cm (12.25 in). The base of 24.5 cm-diameter (9.625 in) steel production casing was set at 2195 m (7201 ft) and cemented in up-hole to a depth of ~2104 m (~6900 ft.). Injection tubing (11.4 cm-/4.5-in diameter) run from the surface was set with a packer the base of the production casing. AWMS-2 was drilled with a 21.6 cm-diameter (8.5 in) from 2225 m to a TD of 2592 m (8501 ft).

The lower ~396 m (1300 ft) of the AWMS-2 well was completed open-hole between 2195 m and TD. This interval corresponds to elevations of between -1918 m and -2315 m (-6292 to -7592 ft) below sea level. Drilling and completion records indicate the injection interval includes Ordovician Black River Group carbonates, Cambrian Knox Group dolostones and sandstones, and sandstone and carbonates of the Cambrian Conasauga Group (Figure 3.S1). The deepest penetration of the well was into the upper basal sandstones of the Conasauga Group (Marysville Formation, commonly referred to as the Mt. Simon Sandstone (ODNR, 2012)). Using geophysical logs, we correlated lithologic units in the Marysville Formation with similar horizons recorded in the Northstar well ~11.5 km to the southeast in Mahoning County that was drilled into Precambrian basement. This indicates the bottom of the AWMS-2 well was drilled to ~21 m (~68 ft) above the contact with crystalline rocks of the Precambrian basement, at an elevation of approximately -2330 m (~-7645 ft) below sea level. This projected elevation is support by regional structure contour maps of the Paleozoic-Precambrian contact constructed by Baranoski (2013).

Prior to the initiation of waste-water injection, hydraulic fracturing of the open-hole interval of the AWMS-2 well was attempted with ~924,600 liters (244,258 gallons) of produced water/friction reduces and treated with ~14385 L (2800 gal) of 28% HCl. However, fracture stimulation was unsuccessful due to insufficient downhole pressures (AWMS, personal communication). Commercial injection was initiated in April 2014 with an allowed maximum surface injection pressure of ~11.6 MPa (1680 psi). Throughout operation of the well through August 2014, >174,000 barrels of wastewater were injected into the Ordovician- Cambrian interval (AWMS, personal communication).

2.7. Acknowledgements

Seismic data and were obtained from the Incorporated Research Institutions for Seismology Data Management Center (IRIS) (www.iris.edu). Plots were made using the Generic Mapping Tools version 4.2.1 (www.soest.hawaii.edu/gmt). Geophysical log

interpretation software used in this study was supplied by the LMKR University Grant Program. Support for this work was provided by National Science Foundation Grant EAR-0847688 (MB) and the ODNR. The ODNR provided critical data and information for this study, and we specifically thank M. Angle, D. Blake, S. Dade, J. Fox, M. Hansen, and T. Serenko for their assistance. S. Kilper and AWMS provided injection volumes, pressures, and background information related to their wells. This research also benefited from discussions with P. Friberg, M. Hasting, B. Rish, and Y. Ben-Zion. This study benefitted greatly from the local network installed by M. Hasting and disposal reports provided by AWMS. Three anonymous reviewers and Zhigang Peng provided constructive reviews which significantly improved the manuscript. Our analysis relied heavily on Miami University's High Performance Computing, and we thank J. Mueller for his assistance.

2.8. References

Baranoski, M.T. (2013). Structure contour map on the Precambrian unconformity surface in Ohio and related basement features: Ohio Department of Natural Resources, Geological Survey Map PG-23, scale 1:500,000, 17.

Barrett, S. A. and G. C. Beroza (2014). An Empirical Approach to Subspace Detection: *Seismological Research Letters* **85** 3 594-600, doi: 10.1785/0220130152.

Ben-Zion, Y., V. Lyakhovsky (2006). Analysis of aftershocks in a lithospheric model with seismogenic zone governed by damage rheology, *Geophysical Journal International*, **165** 197-210.

British Columbia Oil & Gas Commission (BCOGC) (2014). Investigation of Observed Seismicity in the Montney Trend, http://www.bcogc.ca/investigation-observed-seismicity-montney-trend (last accessed Februrary 2015).

Brudzinski, M. R., R. J. Skoumal, B. C. Currie (2014). Optimizing Multi-Station Template Matching to Identify and Characterize Induced Seismicity in Ohio: Abstract S51A-4438 presented at 2014 Fall Meeting, AGU, San Francisco, California, 15-19 Dec.

Ellsworth, W. L. (2013). Injection-induced earthquakes, *Science*, **341**. doi: 10.1126/science.1225942.

Evans, K.F., A. Zappone, T. Kraft, N. Deichmann, and F. Moia (2012). A survey of the induced seismic responses to fluid injection in geothermal and CO_2 reservoirs in Europe, *Geothermics*, **41** 30–54, doi: http://dx.doi.org/10.1016/j.geothermics.2011.08.002.

Friberg, P. A., G. M. Besana-Ostman, I. Dricker (2014). Characterization of an earthquake sequence triggered by hydraulic fracturing in Harrison County Ohio, *Seismological Research Letters*, **85**. doi: 10.1785/0220140127.

Healy, J. H., W. W. Rubey, and D. T. Griggs (1968). The Denver earthquakes, *Science*, **161** 1301–1310, doi:10.1126/science.161.3848.1301.

Herrmann, R.-B. (2004). Computer Programs in Seismology, Version 3.30-GSAC: http://www.eas.slu.edu/eqc/eqc_cps/CPS/CPS330.html (last accessed February 2015).

Holtkamp, S. G., M. R. Brudzinski, B. S. Currie (2015). Regional detection and monitoring of injection-induced seismicity: Application to the 2010-12

Youngstown, Ohio seismic sequence, AAPG Bull., 99(9), 1671-1688. doi: 10.1306/03311513194.

Hurd, O., M. D. Zoback (2012). Intraplate earthquakes, regional stress and fault mechanics in the Central and Eastern US and Southeastern Canada, *Tectonophysics*, **581** 182-192.

Keranen, K.M., H.M. Savage, G.A. Abers, E.S. Cochran (2013). Potentially induced earthquakes in Oklahoma, USA: links between wastewater injection and the 2011 Mw 5.7 earthquake sequence: *Geology*, **41** 699–702. doi: http://dx.doi.org/10.1130/G34045.1.

Kim, W.-Y. (2013). Induced seismicity associated with fluid injection into a deep well in Youngstown, Ohio, *Journal of Geophysical Research*, **118** 3506–3518. doi: 10.1002/jgrb.50247.

Lacazette, A. and P. Geiser (2013). Comment on Davies et al., 2012 - Hydraulic fractures: How far can they go? *Marine and Petroleum Geology*, **43**. doi: 10.1016/j.marpetgeo.2012.12.008.

Maxwell, S. C., M. Jones, R. Parker, S. Miong, S. Leaney, D. Dorval, D. D'Amico, J. Logel, E. Anderson, and K. Hammermaster (2009). Fault activation during hydraulic fracturing, *SEG Technical Program Expanded Abstracts*, 1552–1556. doi: 10.1190/1.3255145.

McGarr, A., D. Simpson, L. Seeber (2002). Case histories of induced and triggered seismicity. In: Lee, W., Kanamori, H., Jennings, P., Kisslinger, C. (Eds.), *International Handbook of Earthquake and Engineering Seismology*, **40**, Academic Press, London, 647–664.

National Academy of Sciences (NAS) (2012). Induced seismicity potential in energy technologies, *National Academies Press*, Washington, D.C., **225**.

Nicholson, C. and R. L. Wesson (1990). Earthquake hazard associated with deep well injection: a report to the U.S. Environmental Protection Agency: U.S. Geological Survey Bulletin 1951, http://pubs.usgs.gov/bul/1951/report.pdf (last accessed Februrary 2015).

Ohio Department of Natural Resources (ODNR) (2012). Preliminary report on the Northstar 1 class II injection well and the seismic events in the Youngstown, Columbus, Ohio, 23.

Ohio Department of Natural Resources (ODNR) (2014). Ohio Announces Tougher Permit Conditions for drilling activities near faults and areas of seismic activity, http://ohiodnr.gov/news/post/ohio-announces-tougher-permit-conditions-for-drilling-activities-near-faults-and-areas-of-seismic-activity (last accessed December 2014).

Schaff, D. P. and P. G. Richards (2014). Improvements in magnitude precision, using the statistics of relative amplitudes measured by cross correlation, *Geophysical Journal International*, **197** 1 335-350. doi: 10.1093/gji/ggt433.

Skoumal, R. J., M. R. Brudzinski, B. C. Currie, and J. Levy (2014a). Optimizing multi-station earthquake template matching through re-examination of the Youngstown, Ohio, sequence: *Earth and Planetary Science Letters*, **405** 274-280. doi: 10.1016/j.epsl.2014.08.033.

Skoumal, R. J., M. R. Brudzinski, and B. C. Currie (2014b). Earthquakes induced by hydraulic fracturing in Poland Township, Ohio: American Geophysical Union Abstracts, S51A-4431, San Francisco, California, 15-19 December.

Skoumal, R. J., M. R. Brudzinski, and B. C. Currie (2015). Earthquakes induced by hydraulic fracturing in Poland Township, Ohio: *Bulletin of the Seismological Society of America*, **105** 1. doi: 10.1785/0120140168.

Snoke, J. A. (2003). FOCMEC: FOCal MEChanism Determinations. Package URL: http://www.geol.vt.edu/outreach/vtso/focmec/.

Sumy, D. F., E. S. Cochran, K. M. Keranen, M. Wei, and G. A. Abers (2014). Observations of static Coulomb stress triggering of the November 2011 M5. 7 Oklahoma earthquake sequence, *Journal of Geophysical Research: Solid Earth*, **119** 1904-1923.

Waldhauser, F. (2001). Hypodd: A computer program to compute double-difference earthquake locations, U.S. Geological Survey Open-File Report, 01-113.

Waldhauser, F., and W. L. Ellsworth (2000). A double-difference earthquake location algorithm: Method and application to the northern Hayward fault, California, *Bulletin of the Seismological Society of America*, **90** 1353–1368.

Wessels, S., M. Kratz, and A. De La Pena (2011). Identifying fault activation during hydraulic stimulation in the Barnett shale: Source mechanisms, b values, and energy release analyses of microseismicity, SEG Technical Program Expanded Abstracts, San Antonio, Texas, 18–23 September.

Zhang, H., and C. H. Thurber (2003). Double-difference tomography: The method and its application to the Hayward fault, California. *Bulletin of the Seismological Society of America*, **93** 5 1875-1889.

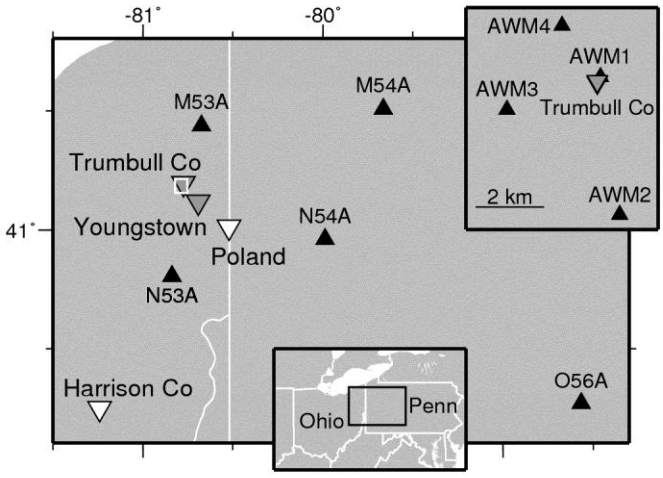

Figure 2.1. Map of study region (box in the lower inset), showing seismic stations (black triangles) and cases of seismicity potentially induced by injection wells (gray) or hydraulic fracturing (white). White box is the location of upper right inset that shows the local seismic network. Labels: T: Trumbull Co (this study), Y: Youngstown, P: Poland Township, H: Harrison Co.

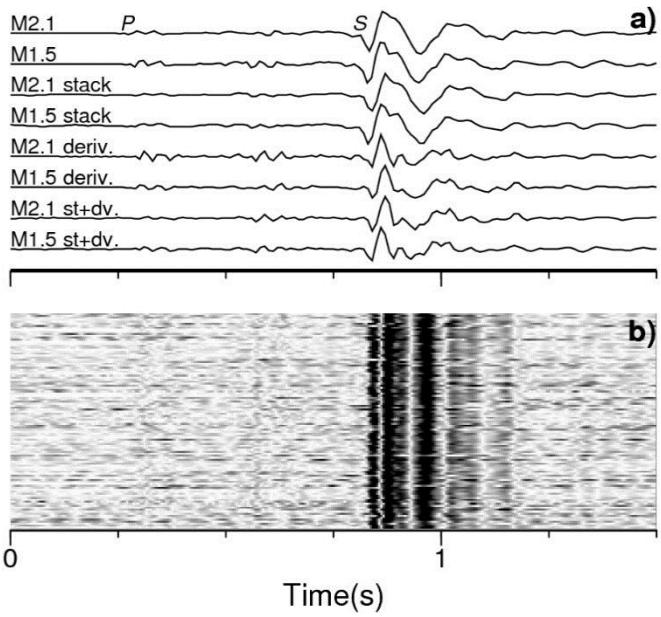

Figure 2.2. Normalized *P*- and *S*-waveforms recorded on the BHE component of AWM4. (a) Template waveforms from the M_L 2.1 31 August 2014 and M_L 1.5 28 July 2014 earthquakes, as well as stacks of events they matched with, derivatives of the template waveforms, and derivatives of the stacks. (b) Waveform amplitudes of the 108 matched events.

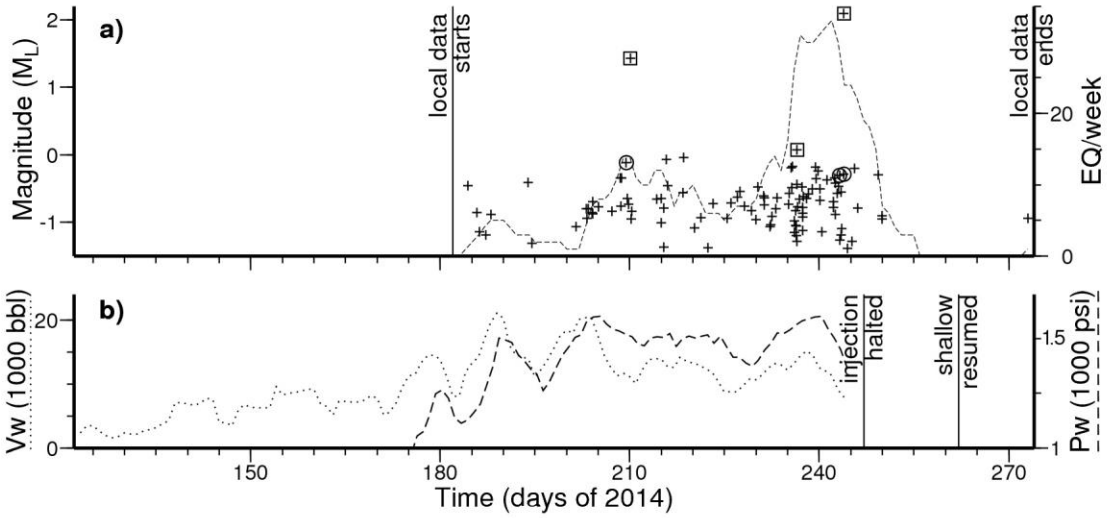

Figure 2.3. (a) Magnitudes of matched events using cross-correlation at the closest local station (crosses). Dashed line shows rate of detected earthquakes per week. Vertical bars mark time frame when local data has been analyzed. Shape outlines around crosses show events also detected by multiple combinations of regional stations (box) and events detected by the closest 3 regional stations (circle). No additional matches were found using regional data from November 2010 to January 2015. (b) Weekly averages of injection volume (Vw, dotted) and pressure (Pw, dashed). Vertical bars mark when the ODNR ordered injection halted, and when injection was allowed to continue at AWMS-1.

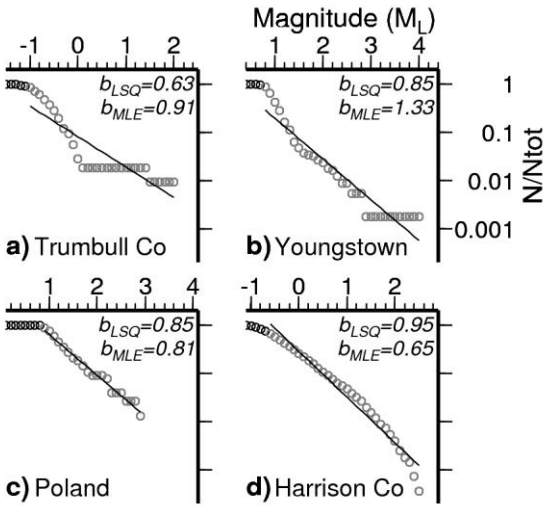

Figure 2.4. Magnitude-frequency estimates (circles) comparing (a) this study to (b) another case of seismicity during wastewater injection near Youngstown (Skoumal et al., 2014a), and two cases of seismicity during hydraulic fracturing in (c) Poland Township (Skoumal et al., 2015), and (d) Harrison County (Skoumal et al., 2014b). Black circles are below the estimated Mc. B-values are for least-squares power-law fit (LSQ, black line) and maximum likelihood estimate (MLE).

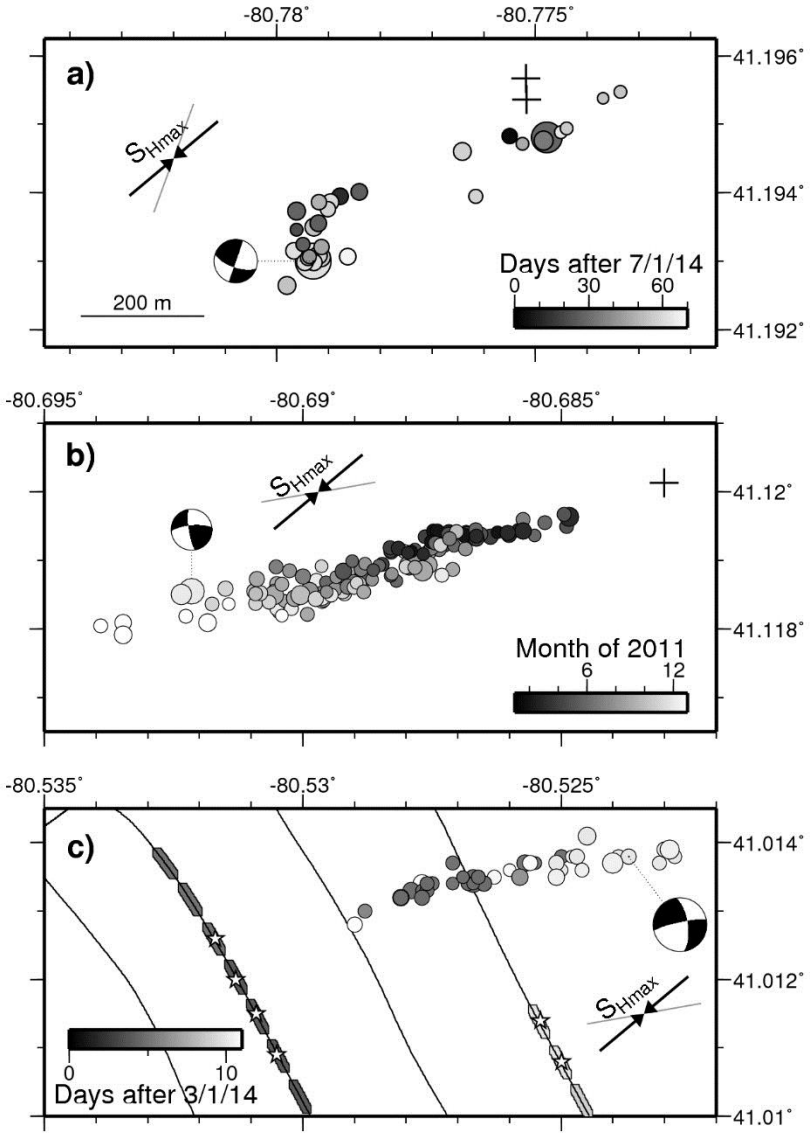

Figure 2.5. Map of the double-difference relocated earthquakes for the (a) Trumbull, (b) Youngstown (Skoumal et al., 2014), and (c) Poland Township, Ohio, (Skoumal et al., 2015) sequences. Only the best located events that exceeded a 12×MAD NNCCC threshold are shown. Circles are scaled according to magnitude. Focal mechanisms are shown for the largest events in each sequence (this study; Kim, 2013; Skoumal et al., 2015). Arrows show orientation of maximum horizontal stress, and gray lines are fault orientation suggested by focal mechanism and trend of hypocenters. In (a) and (b), the plus symbols represent the location of the injection wells. In (c), the black lines are the horizontal laterals of drilled wells, ovals are completed fracture stages, and stars denote stages temporally correlated with seismicity.

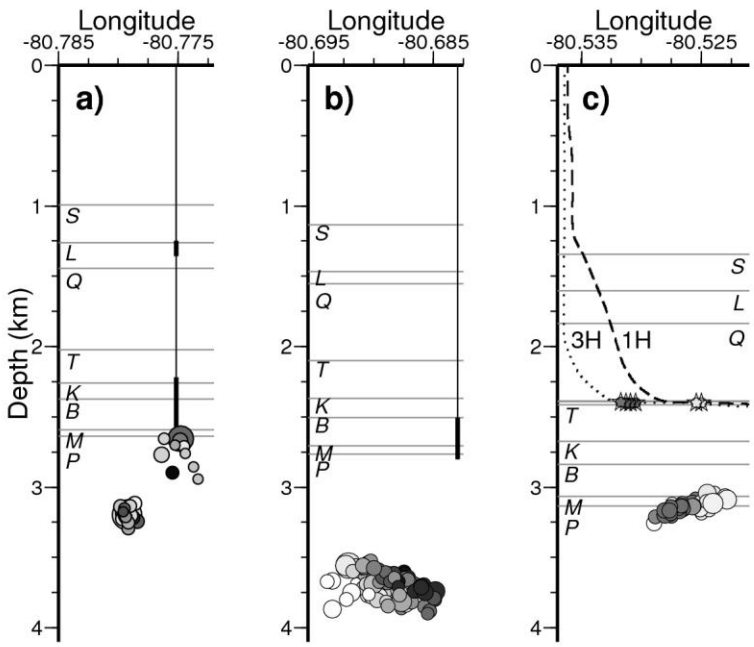

Figure 2.6. East-west cross sections of the double-difference relocated seismicity for the (a) Trumbull, (b) Youngstown (Skoumal et al., 2014a), and (c) Poland Township, Ohio (Skoumal et al., 2015). There is no vertical exaggeration. Horizontal gray lines mark key strata: S=Salina, L=Lockport, Q=Queenston, T=Trenton, K=Knox, B=B Zone, M=Mt Simon, P=Precambrian Basement. In (a) and (b), the black vertical line represents the location of the injection well with the screened interval in bold. In (c), the dashed and dotted black lines represent the paths of two wells into the Point Pleasant (not labeled). Stars indicate fracture stages that were temporally correlated with seismicity. Color scales same as in Figure 3.5.

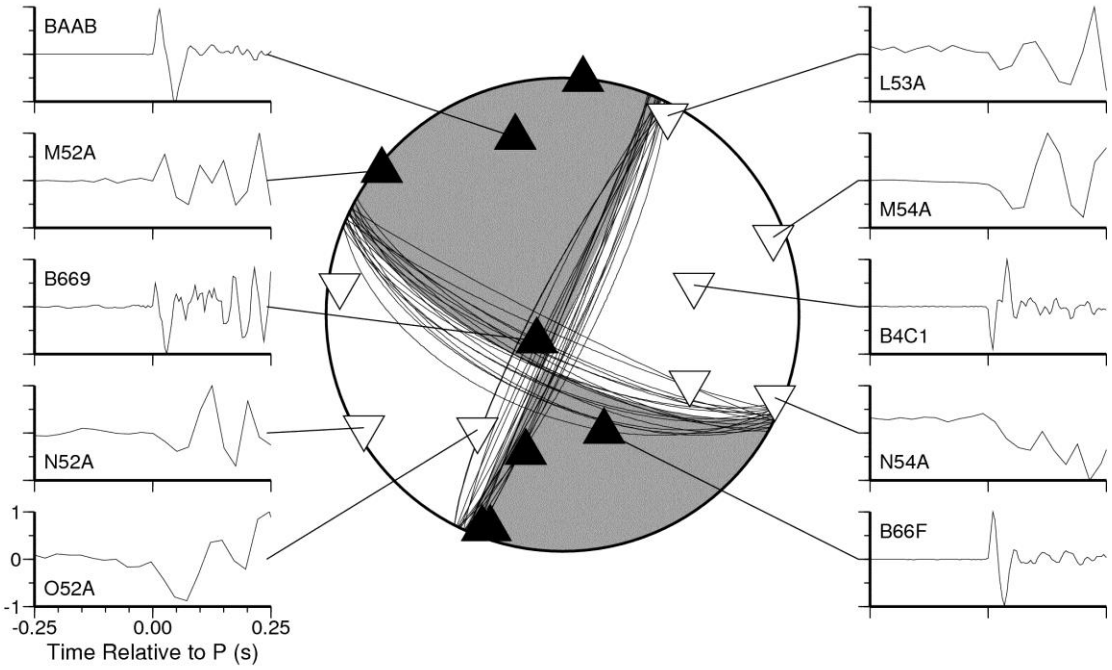

Figure 2.7. Fault plane solution and selected first arrival waveforms for the M_L 2.1 31 August 2014 earthquake. Triangles on the focal sphere show station polarity data for compressional (black) and dilatational (white) first motions. Seismograms are filtered but not interpolated, showing 0.25 before and after the picked *P* wave arrival time at each station.

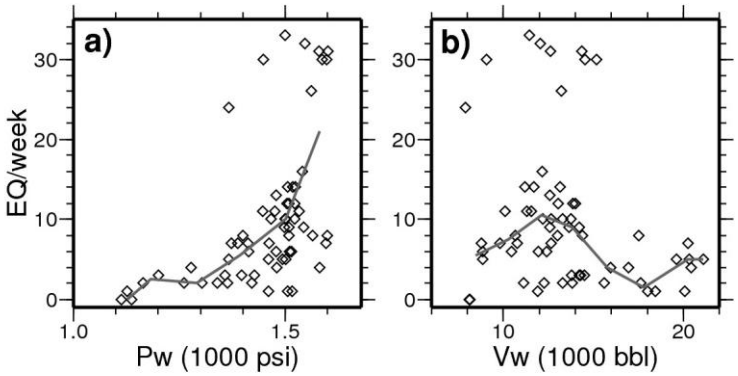

Figure 2.8. Comparison between seismicity rates and average weekly a) pressures and b) volumes injected for each week during the local data availability. Trend lines are median values in 8 evenly-spaced bins.

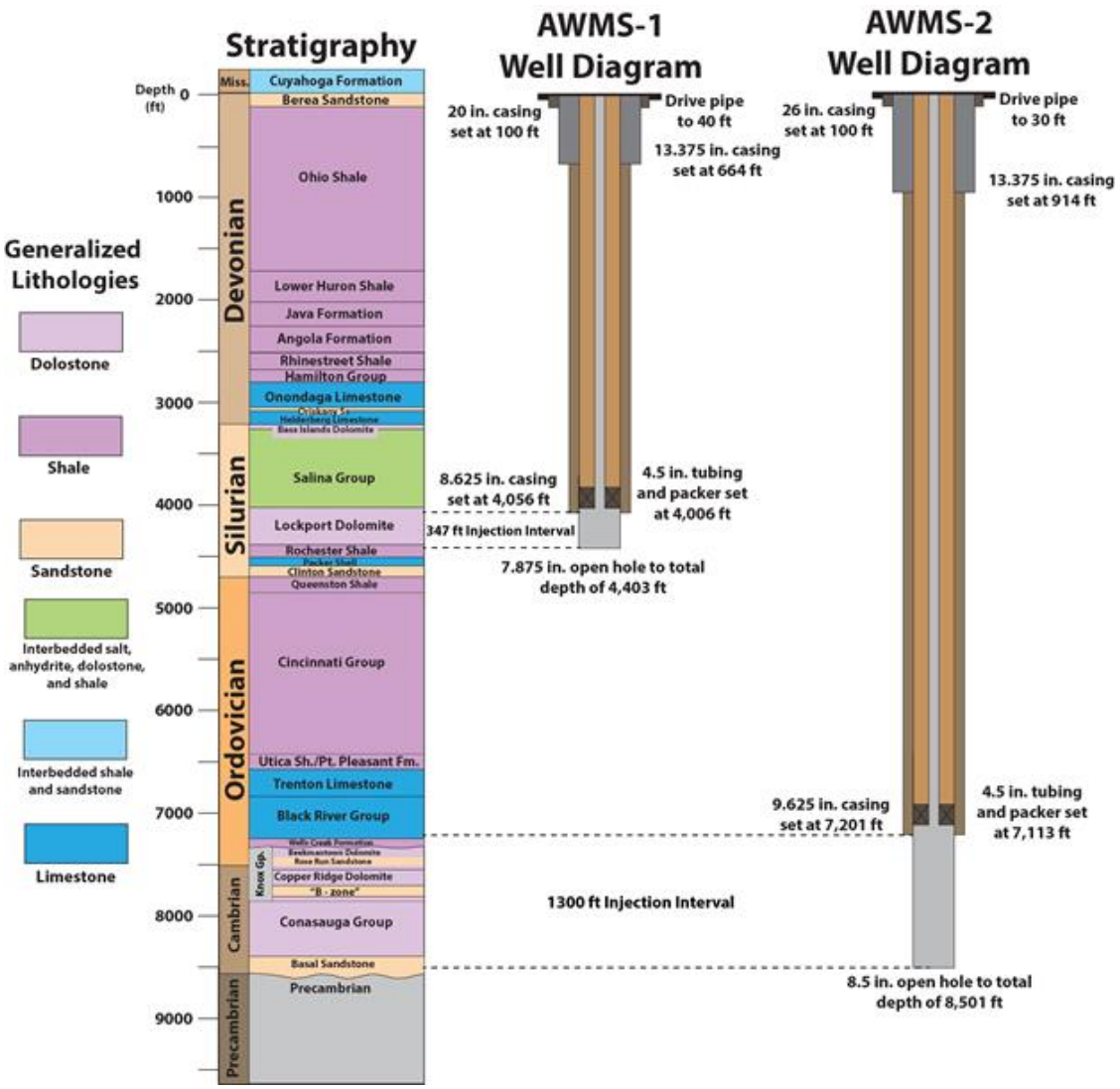

Figure 2.S1. Stratigraphy and well-construction diagram for the Trumbull County, Ohio AWMS wastewater disposal wells.

Table 2.S1. Seismic events detected in this study.

Date	Time	Latitude (°)	Lat. Error	Longitude (°)	Lon. Error	Depth (km)	Dep. Error	M_L
2014-07-03	09:24:12	41.19483	0.00030	-80.77550	0.00093	3.00	0.13	-0.46
2014-07-05	04:48:50	41.19627	0.00073	-80.77163	0.00146	3.30	0.31	-1.03
2014-07-06	05:12:03	41.19267	0.00264	-80.77402	0.01031	2.14	0.87	-1.05
2014-07-07	01:18:45	41.19000	0.00154	-80.77974	0.00293	1.33	0.90	-0.91
2014-07-12	20:21:55	41.19395	0.00032	-80.77878	0.00073	3.21	0.11	-0.38
2014-07-22	02:50:31	41.19347	0.00044	-80.77962	0.00140	3.17	0.09	-0.81
2014-07-23	03:08:26	41.19508	0.00142	-80.78420	0.00219	3.26	0.20	-0.66
2014-07-23	03:49:04	41.19130	0.00065	-80.78036	0.00132	2.28	0.36	-0.80
2014-07-24	02:14:11	41.19512	0.00067	-80.78019	0.00233	3.66	0.28	-0.75
2014-07-26	04:33:34	41.19311	0.00089	-80.77977	0.00092	3.01	0.40	-0.82
2014-07-27	11:34:59	41.19401	0.00052	-80.77841	0.00120	3.24	0.27	-0.34
2014-07-27	13:01:16	41.19325	0.00027	-80.77950	0.00076	3.15	0.08	-0.75
2014-07-27	17:00:35	41.19355	0.00027	-80.77921	0.00075	3.18	0.08	-0.33
2014-07-28	09:47:27	41.19373	0.00026	-80.77962	0.00072	3.19	0.07	-0.09
2014-07-29	02:31:52	41.19481	0.00026	-80.77478	0.00076	2.66	0.08	1.45
2014-07-29	08:30:04	41.19286	0.00035	-80.77978	0.00063	2.92	0.16	-0.73
2014-08-03	19:05:46	41.19476	0.00025	-80.77484	0.00077	2.67	0.08	-0.05
2014-08-06	10:56:21	41.19109	0.00258	-80.77756	0.01000	1.33	0.94	-0.56
2014-08-06	13:00:43	41.19355	0.00665	-80.78599	0.01868	2.86	0.72	-0.01
2014-08-09	05:09:58	41.19012	0.00570	-80.78668	0.01321	3.22	0.17	-0.93
2014-08-11	05:06:47	41.19306	0.00026	-80.77937	0.00075	3.21	0.08	-0.70
2014-08-14	00:51:23	41.19894	0.00924	-80.77740	0.02307	2.77	1.14	-0.77
2014-08-15	10:42:54	41.19320	0.00027	-80.77914	0.00073	3.29	0.09	-0.55
2014-08-16	03:05:53	41.19369	0.00255	-80.77363	0.00238	2.40	0.83	-0.75
2014-08-17	06:07:19	41.19472	0.00025	-80.77525	0.00073	2.70	0.08	-0.82
2014-08-18	07:29:49	41.19381	0.00185	-80.77480	0.00120	2.47	0.95	-0.47
2014-08-19	03:48:41	41.19386	0.00027	-80.77919	0.00076	3.25	0.09	-0.56
2014-08-21	08:45:05	41.19514	0.00125	-80.77725	0.00170	3.88	0.65	-0.64
2014-08-23	13:44:13	41.19350	0.00025	-80.77929	0.00073	3.17	0.07	-0.14
2014-08-23	15:00:22	41.19670	0.00321	-80.77492	0.00655	9.36	1.29	-0.47
2014-08-23	17:44:09	41.19265	0.00032	-80.77981	0.00086	3.14	0.10	-0.20
2014-08-24	02:24:13	41.19538	0.00000	-80.77369	0.00000	2.86	0.00	-0.97
2014-08-24	06:08:05	41.18741	0.01645	-80.80127	0.04416	5.43	0.75	-0.97
2014-08-24	06:10:29	41.19547	0.00031	-80.77336	0.00080	2.94	0.11	-0.81
2014-08-24	07:38:21	41.19068	0.01834	-80.74556	0.02829	3.85	0.67	-1.14
2014-08-24	11:18:06	41.19306	0.00026	-80.77915	0.00078	3.15	0.08	0.07
2014-08-24	12:05:57	41.19305	0.00026	-80.77940	0.00077	3.22	0.08	-0.43
2014-08-25	07:45:43	41.19592	0.00074	-80.76903	0.00690	3.81	0.50	-1.21
2014-08-25	07:48:26	41.19205	0.00301	-80.76821	0.01811	3.00	1.76	-0.95
2014-08-25	08:53:18	41.19494	0.00065	-80.77440	0.00138	2.76	0.24	-0.84
2014-08-25	10:25:59	41.18505	0.01365	-80.78667	0.00346	1.88	1.07	-0.63
2014-08-25	22:53:07	41.20335	0.01497	-80.75920	0.02754	2.10	2.22	-0.66
2014-08-26	21:24:05	41.18740	0.00241	-80.80731	0.01026	3.86	0.12	-0.47
2014-08-27	10:00:25	41.19308	0.00027	-80.77921	0.00074	3.19	0.08	-0.17
2014-08-27	11:34:18	41.19683	0.00033	-80.77150	0.00086	4.00	0.23	-0.34
2014-08-27	19:20:41	41.19460	0.00021	-80.77641	0.00069	2.77	0.08	-0.19

2014-08-28	02:53:00	41.19376	0.00025	-80.77902	0.00072	3.14	0.08	-0.47
2014-08-28	03:27:27	41.19395	0.00037	-80.77615	0.00062	2.66	0.21	-0.64
2014-08-28	09:24:51	41.19721	0.00592	-80.77979	0.00764	2.76	1.00	-1.00
2014-08-29	04:43:37	41.19002	0.00444	-80.79250	0.00895	3.43	0.97	-0.32
2014-08-30	05:27:19	41.19906	0.00371	-80.75988	0.01710	2.80	1.93	-0.69
2014-08-30	05:50:26	41.19171	0.00369	-80.78234	0.00614	2.30	1.02	-0.72
2014-08-30	09:59:35	41.19298	0.00027	-80.77946	0.00073	3.20	0.07	-0.35
2014-08-30	11:51:34	41.19386	0.00029	-80.77896	0.00078	3.20	0.10	-0.39
2014-08-30	13:00:52	41.18771	0.00293	-80.75951	0.00172	2.62	0.84	-0.88
2014-08-30	19:43:14	41.19631	0.00264	-80.77308	0.00591	4.24	0.33	-0.54
2014-08-31	01:01:58	41.19202	0.00229	-80.77225	0.00692	1.41	1.16	-0.48
2014-08-31	05:24:42	41.19299	0.00026	-80.77929	0.00075	3.19	0.08	-0.29
2014-08-31	09:49:41	41.19285	0.00228	-80.79997	0.01364	4.57	0.41	-1.14
2014-08-31	11:28:10	41.19031	0.00133	-80.77452	0.00209	2.62	0.34	-0.54
2014-08-31	13:31:42	41.18446	0.00706	-80.78306	0.00898	1.56	0.42	-1.08
2014-08-31	20:43:20	41.19315	0.00029	-80.77967	0.00081	3.23	0.08	-0.29
2014-08-31	21:34:18	41.19300	0.00026	-80.77930	0.00077	3.20	0.08	2.10
2014-09-01	10:43:08	41.18983	0.00744	-80.78109	0.00254	3.59	1.75	-1.33
2014-09-02	13:58:12	41.19522	0.00037	-80.77718	0.00085	4.04	0.17	-0.13
2014-09-03	01:27:11	41.19488	0.00027	-80.77451	0.00078	2.71	0.08	-0.77
2014-09-06	08:32:21	41.19307	0.00026	-80.77863	0.00076	3.12	0.08	-0.31
2014-09-06	22:07:31	41.19104	0.00860	-80.76762	0.01025	2.67	0.86	-0.94
2014-09-30	01:13:15	41.18267	0.00987	-80.76651	0.00475	1.63	0.61	-0.95

CHAPTER 3: Distinguishing induced seismicity from natural seismicity in Ohio: Demonstrating the utility of waveform template matching

3.1. Abstract

This study investigated the utility of multistation waveform cross correlation to help discern induced seismicity. Template matching was applied to all Ohio earthquakes cataloged since the arrival of nearby EarthScope TA stations in late 2010. Earthquakes that were within 5 km of fluid injection activities in regions that lacked previously documented seismicity were found to be swarmy. Moreover, the larger number of events produced by template matching for these swarmy sequences made it easier to establish more detailed temporal and spatial relationships between the seismicity and fluid injection activities, which is typically required for an earthquake to be considered induced. Study results detected three previously documented induced sequences (Youngstown, Poland Township, and Harrison County) and provided evidence that suggests two additional cases of induced seismicity (Belmont/Guernsey County and Washington County). Evidence for these cases suggested that unusual swarm-like behaviors in regions that lack previously documented seismicity can be used to help distinguish induced seismicity, complementing the traditional identification of an anthropogenic source spatially and temporally correlated with the seismicity. In support of this finding, we identified 17 additional cataloged earthquakes in regions of previously documented seismicity and away from disposal wells or hydraulic fracturing that returned very few template matches. The lack of swarminess helps to indicate these events are most likely naturally occurring.

3.2. Introduction

As oil and gas well completions utilizing multi-stage hydraulic fracturing have become more commonplace, the potential for seismicity induced by the deep disposal of frac-related wastewater and the hydraulic fracturing process itself has become an increasingly important issue (e.g., NAS, 2012). While it is rare for a wastewater disposal well to induce felt seismicity, the recent increase in the number of wells and volumes injected are suspected of contributing to a substantial increase of events ≥ M 3 in central and eastern United States in since 2010 (e.g., Ellsworth, 2013). More than 300 earthquakes with M ≥ 3 occurred in the 3 years from 2010 through 2012, compared with an average rate of 21 events/year observed from 1967 to 2000. Arkansas, Colorado, New Mexico, Ohio, Oklahoma, and Texas have recently experienced elevated levels of seismic activity near industrial activities, raising the likelihood that these events were induced by human activity (e.g., Frohlich, 2012; Horton, 2012; Kerenan et al., 2013; Kim, 2013; Rubinstein and Ellsworth, 2013). A more thorough investigation of recent earthquakes is needed to more clearly identify and characterize induced seismicity, and ultimately to determine whether human activity should be changed to reduce earthquake hazards and potential losses.

Beginning in March 2011, a series of 10 small (M ~2), shallow (~3 km depth) earthquakes were recorded and reported by the Ohio Department of Natural Resources (ODNR) near Youngstown in northeastern Ohio (Figure 4.1). The proximity of the Youngstown earthquake sequence (YES) to the recently activated D&L Energy Northstar 1 wastewater disposal well raised concerns of possible injection-induced seismicity.

ODNR and Lamont-Doherty Earth Observatory (LDEO) deployed a local seismic network in December 2011 that more closely constrained the proximity of events to the disposal well. Injection activities were ceased on 30 December 2011. On 31 December 2011, a M 4.0 earthquake occurred with an epicenter less than 1 km from the well. Several subsequent studies of this sequence have provided additional evidence that the earthquakes were induced by wastewater disposal (ODNR, 2012; Kim, 2013; Skoumal et al., 2014; Holtkamp et al., in press).

Although uncommon, the YES findings are consistent with earlier cases where the injection of fluids into underground formations has induced seismicity (e.g., Evans et al., 2012; McGarr et al., 2002; Nicholson and Wesson, 1990). Although the number of earthquakes near the Northstar 1 well reduced dramatically within a week of shut in, there is an ongoing moratorium on wastewater disposal within 7 km of the well and a small number of earthquakes, including a M ~2 event in November 2013, have continued to occur near the well (Skoumal et al., 2014).

Felt earthquakes induced by hydraulic fracturing during well stimulations are even rarer than those associated with wastewater disposal. However, due to the recent enhanced scrutiny regarding the practice and more sensitive seismic-monitoring tools, induced seismicity attributed to hydraulic fracturing has become more apparent in the past few years. While microseismicity (M < 1) is an inherent component of the hydraulic fracturing process (Warpinski et al., 2012), hydraulic fracturing has previously been well-correlated to a handful of earthquakes sequences, including M 1.9 Oklahoma, 1979 (Nicholson and Wesson, 1990); M_L 2.9 Oklahoma, 2011 (Holland, 2013); M_L 3.8 British Columbia, 2011 (BCOGS, 2012); M_L 2.3 England, 2011 (BGS, 2011); and M 2.2 Harrison County, Ohio, 2013 (Friberg et al., 2014).

Between 5-14 March 2014, a series of 5 earthquakes ranging from M_L 2.1 to 3.0 were recorded in Poland Township, Ohio. The epicentral locations for the Poland Township earthquake sequence (PTES) are less than 20 km southeast of the locations of the YES. Despite this proximity, there were no disposal wells operating within 10 km of the Poland Township earthquakes. However, the earthquakes occurred within 1 km of a group of recently drilled production wells in the area, one of which (Hilcorp Energy CLL2 1H) was undergoing active hydraulic-fracture stimulation at the time of the initial seismic events. Because of this proximity, the Ohio Department of Natural Resources (ODNR) halted completion operations at the Hilcorp well on the afternoon of 10 March 2014.

These two recent examples of induced seismicity have demonstrated that Ohio is a good target region for establishing how earthquakes hazards may be influenced by human activities. Foremost, Ohio has a relatively low background seismicity rate with ~4 recorded events/year between 1990 and 2004. By comparison, Ohio has seen that number jump to ~10 in the past 10 years as potential cases of induced seismicity have become more prevalent. The overall low background rate helps in distinguishing induced events from tectonic events as induced sequences tend to stand out relative to the background patterns. Another key factor is that Ohio is host to both active wastewater disposal wells and horizontal drilling/hydraulic fracturing associated with the Marcellus and Utica-Point Pleasant shale plays. The majority of the disposal wells and the area of active hydraulic fracturing are concentrated in eastern Ohio which limits the geographic extent of likely induced events. Additionally, the relatively limited number of disposal and horizontal

production wells compared to other states (for example Oklahoma) allows the effects of activities associated individual well acts to be evaluated.

Following the events of the YES, there has been a heightened concern over seismicity related to energy technologies in Ohio. The ODNR has established new regulations to identify induced seismicity before felt events occur (ODNR, 2014a), which could serve as a blueprint for other states. Additionally, Ohio requires detailed oil and gas and underground disposal control reports including horizontal well location surveys, completion and stimulation reports, and daily injection volume and pressure data that are publically available (ODNR, 2014b). From a seismological research perspective, Ohio benefits from being served by a number of regional long-standing "backbone" seismic stations for over a decade and the studies of YES and PTES significantly benefited from early adoption of EarthScope Transportable Array (TA) stations in western Pennsylvania in late 2010.

Utilizing the data sources outlined above, we attempted to broaden the template matching efforts to other recorded seismic events across Ohio to investigate whether additional cases of induced seismicity can be identified. Davis and Frohlich (1993) developed three primary criteria to determine if seismicity is induced by fluid injection activities: (1) coincident timing, (2) coincident location, and (3) adequate fluid pressures. In this study, we demonstrate that the identification of repetitive and/or swarm-like seismicity from template matching can also be a criteria for differentiating induced seismicity from natural seismicity in a stable cratonic interior where seismicity is generally rare.

3.3. Data and Analysis

Our template matching and event characterization approach has been optimized based on studies of the YES (Skoumal et al., 2014) and PTES (Skoumal et al., 2015). The ideal network consisted of stations early-adoption EarthScope TA sites M54A, N54A, and O56A in both the YES and PTES. This study investigates templates with these stations (referred to as MNO templates) from the time of installation (November 2010) until the end of this study (May 2014). TA stations formally arrived in Ohio during 2012, which provided opportunities to build templates using closer TA stations for some recent earthquakes (referred to as local templates). The closer proximity of these stations to the source events typically increased the signal to noise ratio and led to higher numbers of matches. In one earthquake sequence, there was an event of interest that occurred just before the installation of M54A, N54A, and O56A, such that we needed to construct a template from older regional stations.

Templates were created for all earthquakes in Ohio since 6 November 2010 from the catalogs provided by the ODNR, Lamont Doherty Earth Observatory (LDEO), USGS National Earthquake Information Center (NEIC), and EarthScope Array Network Facility (ANF). For the ANF catalog, we needed to identify surficial blasts related primarily to quarrying/surface mining activities based on the presence of clear R_g waves (e.g., Kafka, 1990). This step is important because the blast events register an average of over 100 matches if used as templates. This highlights the fact that the majority of seismic sources in Ohio are blasts, yet there is less concern about mining activities because they represent surficial processes and rarely involve pre-existing faults. While we examined waveforms to identify blasts manually, we developed a simple routine to aid this process. It involved

calculating the ratio of the high-frequency (>5 Hz) to low frequency (0.4-1 Hz) mean amplitude for a horizontal component seismogram during the event and dividing it by the ratio calculated in the minute before the event. We calculated this across the 10 closest stations, and found the average was typically less than 1 for blasts due to the prominent R_g waves, and greater than 5 for earthquakes.

After discarding 60 blast events, the culled catalog has 51 remaining earthquakes that were used for template matching (Table 1). As in our previous studies, waveforms were obtained using IRIS WebServices, interpolated to 40 samples/sec, and then bandpass filtered between 5-15 Hz. For each event, templates began 10 sec before the P-wave arrival on vertical components, and 10 sec before S-wave arrival on horizontal components, with a total length of 37 sec in both cases. Cross-correlation coefficients (CCC) were calculated by correlating the template with years of data by shifting one datum at a time for each station and component. We sum the CCC values across the network taking into account the lag values between different station-components established in the template event arrival times. Network-normalized CCC (NNCCC) values were produced by dividing the sum of normalized CCC values for all stations and components by the number of contributing channels. We set an initial threshold of 15 times the median absolute deviation (MAD) of the daily NNCCC. Correlating a randomly generated template against a random year-long signal at 40 samples/sec would result in ~1 false positive based on what 15×MAD represents, theoretically.

We determined local magnitudes through a Richter scale approach:

$$M_L = \log10\ [\mathbf{A}/\mathbf{A_0}]$$

For each station and component in our template, we calculated the median scale factor ($\mathbf{A_0}$) using the filtered S waveform amplitudes ($\mathbf{A}$) and catalog magnitudes for all events reported by the ODNR/LDEO/NEIC. For each matched event, we calculated a magnitude from the scale factor and S waveform amplitude at each station and component, and took the median value as our final magnitude.

Following template matching, earthquake locations are compared with the OhioSeis catalog to determine whether the events occurred in a region of previous seismicity. The epicenters of events we investigated are also compared with the location of unconventional Utica wells and class II disposal wells active during our study time frame based on information available from ODNR (Figure 4.1). We found there were ~850 Utica wells and ~160 wastewater disposal wells during this time frame.

3.4. Results

3.4.1. Previously Documented Cases

3.4.1.1 Mahoning County (Youngstown, Poland Township)

The results for these two cases are described in Skoumal et al. (2014) and Chapter 1.

3.4.1.2 Harrison County

In October 2013, a series of 7 earthquakes listed in the EarthScope catalog occurred in Harrison County, southeast Ohio (Figure 4.1) in an area with no previously documented seismicity. While there are nearby quarrying operations that produce frequent blasts, we have confirmed that these events lack the R_g wave characteristic of surficial blasts. There are no disposal wells within 10 km of the events, but hydraulic

fracturing operations were performed from 7 September to 6 October 2013 on 3 wells near the earthquake hypocenters. These well-completion operations have been previously correlated to the recorded seismicity (Friberg et al., 2014).

The MNO templates for the Harrison County events revealed 154 unique matching events when the results from each individual template scan were combined. However, local template scans of a station (O53A) from within 5 km of the events revealed 2,788 unique matching events with a magnitude of completeness of M_L -0.6 (Figure 4.2). The temporal distribution of these events is similar to that of Friberg et al. (2014) with bursts of activity during certain stimulation stages and a gradual decay of activity after operations ceased. We note, however, that our technique identified nearly an order of magnitude more events than the earlier study with a lower magnitude of completeness (478 events, M_c 0).

3.4.2. New Sequences

3.4.2.1 Belmont/Guernsey County

A series of five small (M_L ~2) earthquakes listed in the EarthScope catalog occurred on 18-19 May 2014 in western Belmont/eastern Guernsey counties in southeast Ohio (Figure 4.1). The catalog epicenters were within 5 km of 4 horizontal wells (Kirkwood A wells 1H-4H-33), with targets in the Ordovician Point Pleasant Formation at depth of ~2475 m. These wells underwent hydraulic-fracture stimulation in April-May, 2014. We relocated the 4 cataloged earthquakes by picking reliable arrival times and inverting for locations with *elocate* using the velocity model from neighboring Harrison County (Herrmann, 2004; Friberg et al., 2014). The absolute location errors were determined using bootstrapping, removing one station at a time from the location process and using the standard deviation as the error estimate (Efron, 1979). Based on drill survey reports from the ODNR, the 4 relocated earthquakes appear to have occurred west of the drilled laterals (Figure 4.3), although the location uncertainties are relatively large given the station coverage.

Scans using the MNO templates revealed 64 unique events down to M_L ~1 temporally restricted to May 2014 (Figure 4.4a). Template matching using the 3 closest TA stations (O53A, P53A, O52A) showed 180 unique events restricted to 28 April to 25 May 2014 (Figure 4.4b), with only a single event in each of the two subsequent months. State records indicate that drilling/completion occurred during April 28-May 21 along four horizontal wells, temporally coinciding with the seismicity we detected. We identified 8 seismic events during the concurrently operating Kirkwood A 1H-33 and 2H-33 stimulations, but the vast majority of seismicity occurs on 17-19 May during 3H-33 and 4H-33 stimulations. An 11 additional events were recorded on the following days when hydraulic-fracturing operations on these two wells were again active (Figure 4.4b). Based on the current location estimates, it appears that seismicity flourished during a set of 3H-33 and 4H-33 stages despite being further from the seismic source than 1H-33 and 2H-33.

The main cluster of seismicity started during stage 14 of well 3H-33 which does appear to be a routine stimulation based on the stimulation report available from ODNR, but the details for stage 4 of well 4H-33 which immediately preceded this are missing in the stimulation report. The other stage that may be important is stage 6 at well 4H-33 because a "sweep" was reported during the middle of that stage, and this term typically refers to temporary reduction in the proppant concentration to avoid clogging the well.

As a result, this stage lasted longer than normal, and the largest earthquake occurred at the end of that stage. This results in a day-long gap in stimulation that may have contributed to the reduced seismic activity afterwards. Unfortunately, the limited stimulation reports available at this time prevent more detailed analysis of the potential relationships between operations and seismicity.

Given that the Belmont/Guernsey County events display unusual swarm behavior that temporally and spatially correlates to the hydraulically fracturing operations, and that they occurred in an area with no prior documented earthquakes, there is a strong possibility that the April-May 2014 earthquake sequence was induced.

3.4.2.2 Washington County

There were a series of 5 recorded earthquakes in Washington County (Figures 4.1, 4.5) which we used to construct MNO templates that found 59 unique events (Figure 4.6). The seismicity rate based on our initial template matching decreased considerably after 2011. To further investigate this seismicity rate change, we generated a template for the 3 closest TA stations (P53A, P52A, Q52A) that recorded the last cataloged event (18 September 2012). Template matching with this event produced 80 matches from 27 August 2012 to 6 May 2014, most of which were $M_L < 1$ (Figure 4.6a). This suggests that the seismicity in this region may have been ongoing during 2011-2012, but below the magnitude detection threshold.

While the initial catalog locations of the 5 events used as templates covers a 25 km wide area (Table 1), the similarity of matched waveforms indicate the events occur within a much smaller source area. We proceeded to relocate these events by picking reliable arrival times and found all template epicenters are within 4 km of one another (Figure 4.5). The relocations were achieved using a 1-D velocity model derived from a sonic-velocity log of the 3489 m deep Amerada Petroleum, Ulman 1 well. This well was located in southern Noble County, ~25 km north of the earthquakes. The Ulman 1 well was spudded in Pennsylvanian sedimentary rocks and drilled through the entire Paleozoic stratigraphic section to the Proterozoic crystalline basement, the top of which was encountered at depth of 3478 m. The initial model contained 12 discrete velocity layers defined by changes in rock rheology associated with key stratigraphic intervals in the basin (Table S1, Supporting Information). This initial model was reduced to 4 layers to reflect primary thickness-associated weighted mean velocities exhibited by local stratigraphy, with the initial velocity increase at 2.572 km depth (Table S2, Supporting Information). The uncertainties associated with the latest cataloged events in 2012 are smallest due to the presence of TA stations in Ohio and a few portable instruments deployed by ODNR at that time. These best located events are less than 2 km west of a wastewater disposal well (Figure 4.5).

There are several wastewater disposal wells in the area of interest, but the closest to the seismicity is the Ohio Oil Gathering Corporation, Long Run Disposal Well 1. This well began injecting into the Clinton and Medina formations in September 2008 at depths of 2127-2146 m and 2170-2174 m. Since that time, the well has had one of the highest average monthly disposal volumes in Ohio. Monthly reported injected volumes have exceeded 40,000 BBL since 2009 and reached a maximum near 74,000 BBL in 2011 (Figure 4.6). Maximum reported injection pressures have been approximately constant at ~1900 psi since the beginning of 2011. However, ownership of the well changed in early

2012 and monthly disposal volumes have been reduced in cooperation with ODNR. As such, the reduction in rate of seismicity > M_L 1 after 2011 could be the result of reduced injected volume.

The depths of the relocated earthquakes prior to mid-2012 are not well constrained due to the lack of local data, with locations ranging in depth between 1.6-5.6 km. The most recent earthquake in the sequence (which is also the best located owing to more local data) has a depth of 3.6 ± 1.0 km. According to Baranoski (2013), the Precambrian basement depth in this location is ~3.6 km. The earthquakes could be located in the upper Precambrian basement, as seen in the better constrained induced Ohio sequences, or it could be located in the overlying Paleozoic strata. In both scenarios, the located events occurred below the Silurian injection interval. The presence of basement faults that extend upward through the Silurian in southern Washington county (Deyling, 1993; Baranoski 2013), suggest that either scenario is plausible.

About two weeks prior to the installation of the MNO template stations in November 2010, one M 2.8 earthquake was reported, but there are no other cataloged earthquakes in Washington County since 1950. We constructed a template from 3 regional stations that were recording earlier (ACSO, MCWV, BLA), but found no matches besides the template itself from 2008 to the end of our study time. To determine how effective these 3 different stations are as a template, we also constructed a template using these stations for the 4 September 2011 earthquake that had the largest number of matches using the MNO template stations (53). We identified about half as many matches (25), and none before November 2010. This suggests that the more regional template stations are sufficient to determine that the first event is essentially not repetitive, and that there is no evidence of seismicity from when injection began at the Long Run 1 well until the October 2010 event.

3.4.3. Lake and Ashtabula Counties

There were 4 earthquakes in Lake County and 1 earthquake in Ashtabula County during our 2010-2014 study time frame, which was interesting since these counties hosted seismic sequences that are thought to have been induced by deep wastewater disposal as far back as 1986 (Nicholson et al., 1988; Seeber and Armbruster, 1993; Seeber et al., 2004; Gerrish and Nieto, 2005) (Figure 4.7). We found that all 5 recent earthquake templates produced matching events, but the number of matches were small (2-4), and they appear to resemble more traditional foreshock/mainshock/aftershock patterns. To further investigate these cases, we created templates from closer TA stations (e.g., M53A, M52A, L53A) as all the recent events occurred in March 2013 or later, after the TA had arrived. Despite the significantly higher signal to noise ratios with these stations, only 2 sequences were expanded, one from 3 to 5 matches and another from 4 to 8 matches.

While these numbers are still small relative to the previously discussed cases, the fact they are not isolated events without any matches may simply be related to the increased prevalence of seismicity overall in this so-called Northeast Ohio Seismic Zone. There have been over 100 felt events since the early 1800s in this region, greater than any other area of Ohio (Hansen, 2012). The seismicity correlates with the prominent Akron magnetic lineament, likely reflecting different lithologies in the Precambrian basement, and a first order structural boundary interpreted from reflection data (Seeber and

Armbruster, 1993). It seems reasonable that this apparent deep fault zone could host several sets of similar small earthquakes that would explain the small number of matches we observed in this region. The recent earthquake epicenters are all greater than 10 km from active wastewater disposal wells and the older wells suspected to have induced seismicity in the 1980s, which suggests the recent events are likely to be of the same natural origin as those that date back to the 1800s.

3.4.4. Isolated New Cases

Template matching was performed on the remaining 12 cataloged earthquakes that were generally isolated and scattered around Ohio (Figure 4.1). Only 1 of the 12 templates (Medina County) found a match, which was a smaller apparent aftershock that occurred 45 days following the template event. As such, none of the 12 cataloged events appears to be part of a repeating sequence, but there has been previously recorded or historical seismicity in each of the counties where these events occurred. One of the events without any matches was a widely felt M_L 3.5 event recorded in Athens County in 2013 (Table 1). This earthquake has been analyzed in detail by ODNR and determined to have a depth of 8 km and was not considered to be induced (ODNR, personal communication).

Only 1 of the template epicenters occurred within 10 km of a disposal well. This exception is located in Meigs County, where a 2012 earthquake occurred ~7-10 km from a set of five low volume wells that had been injecting for decades into the shallow (640-975 m depth) Devonian Ohio and Marcellus Shale formations, with only 2 still active 10 km away by the time the earthquake occurred. The low porosity/permeability of these units suggests that the wells were injecting into fractured reservoirs likely related to fault zones interpreted to intersect the injection interval in the area (Baranoski and Riley, 2013). The recorded seismic event, however, is listed as having a hypocentral depth of 20 km and so there appears to be a large vertical offset between the earthquake hypocenter and the depth of the injection interval. Moreover, the Meigs County event did not produce any matches above the 15×MAD threshold.

3.4.5. Swarminess of Matched Earthquake Sequences

To gain perspective on the results of our template matching analysis, we sought to evaluate the degree to which the resulting sequences follow traditional mainshock-aftershock patterns common to natural earthquakes or whether they demonstrate the swarm-like patterns common to those in previous induced sequences such as Rocky Mountain Arsenal (Healy et al., 1968). One way to quantify swarminess of a sequence is to compare the magnitude of the largest event in a sequence to the overall number of events above a level of magnitude completeness (Vidale and Shearer, 2006; Holtkamp and Brudzinski, 2011). Plotting all of the sequences identified in this study in this way illustrates that 5 sequences (Youngstown, Poland Township, Harrison Co., Belmont/Guernsey Co., and Washington Co.) are significantly more swarm-like than the other investigated events (Figure 4.8). The 2011 Mw 5.8 Virginia earthquake sequence is also plotted as a reference for mainshock-aftershock sequences in the eastern US (McNamara et al., 2014). Additional characteristics of swarms are found in the 5 Ohio sequences that distinguish them from traditional mainshock-aftershock sequences including: 1) the largest earthquake occurring later in the sequence; and 2) the largest

event not being a full magnitude unit larger than other events (Vidale and Shearer, 2006; Holtkamp and Brudzinski, 2011). For example, a portion of the Washington Co. sequence in July 2011 shows the largest event occurs later in the sequence and the largest event is only 0.3 magnitude units greater than the next largest event (e.g., Figure 4.6).

3.5. Discussion

The general approach to classifying induced seismicity has been to identify: 1) an appropriate anthropogenic source that is potentially influencing the effective stress on a fault; 2) a correlation in timing of the human activity with the seismicity; and 3) a correlation in location between the potential source and the earthquake hypocenters (e.g., Davis and Frohlich, 1993). In this study we have sought to demonstrate that these criteria can be complemented by evidence for swarminess, which can be established through template matching. Table 2 summarizes the criteria, and a few others that may be complementary, for the Ohio earthquakes examined in this study.

Recent studies have shown that the Youngstown, Poland Township, and Harrison County cases have earthquakes less than 1 km from either wastewater disposal or hydraulic fracturing and display a close temporal correlation between the initiation of wastewater disposal or certain hydraulic fracturing completion stages (Skoumal et al., 2014, Skoumal et al., 2015, Friberg et al., 2014). These studies also identified an unusual swarm-like behavior lacking traditional foreshock/mainshock/aftershock sequences. While not typically used as such, we suggest that this swarminess characteristic could be applied as a criterion to help distinguish induced seismicity. In this study we demonstrated that all 3 sequences are swarm-like based on the large number of events relative to the largest magnitude (Figure 4.8). Additional evidence for swarminess can be found in the lack of a leading largest magnitude mainshock followed by significantly smaller aftershocks decaying over time (e.g., Figure 4.2). Finally, we draw attention to the fact that each of these sequences occurred in areas lacking previously documented seismicity. A region that has a significant number of naturally occurring events would not exclude the possibility of an induced earthquake sequence, but the determination of an induced sequence can be supported by a lack of previous seismicity in the region. Overall, we argue there appear to be four criteria that support the notion that these cases should be classified as likely induced seismicity (Table 2).

The Belmont/Guernsey County case identified in this study follows the pattern of the 3 previous cases such that we classify it as “likely induced seismicity.” This includes hydraulic fracturing that was spatially and temporally correlated with the seismicity, swarm-like behavior, and no previously documented earthquakes in this region. The results from the Washington County case are not quite as definitive. The seismicity is swarm-like and occurred in an area with no prior documented seismicity. However, the closest identified event may have occurred at a larger distance from the nearest wastewater disposal well (~2 km) than the previously discussed cases, and the first identified event was ~2 years after disposal operations began at the nearest well. Yet it may be that both of these two features could be explained by the seismogenic fault simply being further from the disposal well, especially considering this well is injecting into a reservoir over 1 km above the basement. Considering that this situation is not as clear as the previous cases, we classify this case as probably induced.

In contrast to these cases, we also found 12 earthquakes that show no evidence of swarminess and do not appear to be spatially or temporally related to wastewater disposal wells or hydraulic fracturing. These events occurred in counties where previous seismicity has been documented, although much of it is historical. We see no reason to believe that any of these 12 earthquakes are induced and have classified them as unlikely induced, consistent with the notion that the low number of matches from template matching is indicative of natural seismicity. The 5 earthquakes in Lake and Ashtabula Counties that we analyzed produced a few more matches (2-8), but are not as swarm-like as the likely induced cases that all produced over 50 matches (Figure 4.8). These 5 catalogued events in Lake and Ashtabula Counties were greater than 10 km from active wastewater disposal and hydraulic fracturing as well as some older waste disposal wells that were previously proposed to have induced seismicity. Considering that this has historically been one of the most seismically active regions in Ohio, these events were unlikely to have been induced.

We note that our study has identified two sequences induced by wastewater disposal wells and three sequences induced by hydraulic fracturing. When compared with the ~160 wastewater disposal wells and ~850 hydraulically fractured wells, we can estimate the fraction of operations that have induced seismicity. We find ~1.3% of disposal wells and ~0.35% of unconventional wells have induced seismicity large enough to be detected by the OhioSeis catalog (nominally M>2). While these are simple approximations, the order of magnitude larger incidence of induced seismicity from disposal wells suggests that they have a higher risk of producing seismicity than hydraulic fracturing. This is consistent with the findings of the National Academy of Sciences that the very low number of induced seismicity cases from hydraulic fracturing is likely due to the shorter duration of injection of fluids and the limited fluid volumes used in a small spatial area. (NAS, 2012).

3.6. Conclusions

This study sought to investigate the pervasiveness of induced seismicity in Ohio while also investigating the utility of multistation waveform cross-correlation to help discern induced seismicity. Application of template matching to all Ohio earthquakes cataloged since the arrival of nearby EarthScope TA stations detected 3 previously documented cases (Youngstown, Poland Township, and Harrison County) and provided evidence that suggested 2 additional cases of induced seismicity (Belmont/Guernsey County and Washington County). All earthquakes that were within 5 km of fluid injection activities in regions that lacked previously documented seismicity were independently found to be swarmy. This supports the notion that swarminess and lack of previously documented seismicity can be used to help distinguish induced seismicity, complementing the traditional identification of an anthropogenic source spatially and temporally correlated with the seismicity. Moreover, the larger number of events produced by template matching for these swarmy sequences helps to establish more detailed temporal and spatial relationships between the seismicity and fluid injection activities. In support of using swarminess as an indicator of induced seismicity, we identified 17 additional cataloged earthquakes in regions of previously documented seismicity and away from disposal wells or hydraulic fracturing that returned very few

template matches. The lack of swarminess helps to indicate these events are most likely naturally occurring.

3.7. Supplementary Material

The earthquake hypocentral relocations in Washington Country were achieved using a 1-D velocity model derived from a sonic-velocity log of the 3489 m deep Amerada Petroleum, Ulman 1 well. This well was located in southern Noble County, ~25 km north of the earthquakes. The Ulman 1 well was spudded in Pennsylvanian sedimentary rocks and drilled through the entire Paleozoic stratigraphic section to the Proterozoic crystalline basement, the top of which was encountered at depth of 3478 m. The initial model contained 12 discrete velocity layers defined by changes in rock rheology associated with key stratigraphic intervals in the basin (Table S1). This initial model was reduced to 4 layers to reflect primary thickness-associated weighted mean velocities exhibited by local stratigraphy, with the initial velocity increase at 2.572 km depth (Table S2).

3.8. Acknowledgements

Seismic data were obtained from the Incorporated Research Institutions for Seismology Data Management Center (IRIS) (www.iris.edu). Earthquake catalogues were obtained from IRIS, the ODNR (http://geosurvey.ohiodnr.gov), the LDEO (www.ldeo.columbia.edu/LCSN), NEIC (http://earthquake.usgs.gov/data/), and ANF (http://anf.ucsd.edu/). Plots were made using the Generic Mapping Tools version 4.2.1 (www.soest.hawaii.edu/gmt). Support for this work was provided by National Science Foundation Grant EAR-0847688 (MB). Geophysical log interpretation software used in this study was supplied by the LMKR University Grant Program. We would like to thank the ODNR for their assistance, specifically M. Angle, D. Blake, S. Dade, J. Fox, M. Hansen, D. Rush, and T. Serenko. This work benefited from discussions with P. Friberg and N. Smith. Our analysis relied heavily on Miami University's High Performance Computing, and we thank J. Mueller for his assistance. P. Friberg, A. McGarr, and R. Nowack provided helpful peer reviews that improved the manuscript.

3.9. References

Baranoski, M. T. (2013), Structure contour map on the Precambrian unconformity surface in Ohio and related basement features (version 2.0), Columbus, Ohio Department of Natural Resources, Division of Geological Survey Map PG-23, scale 1:500,000, 17.

Baranoski, M.T. and Riley, R.A. (2013), Analysis of Stratigraphic, Structural, and Production Relationships of Devonian Shale Gas Reservoirs in Meigs County, Ohio, Columbus, Ohio Department of Natural Resources, Division of Geological Survey Open-File-Report 88-3, 29 p.

BCOGS (British Columbia Oil and Gas Commission) (2012), Investigation of observed seismicity in the Horn River Basin. URL: http://www.bcogc.ca/investigation-observed-seismicity-horn-river-basin.

BGS (British Geological Survey) (2011), "Blackpool earthquake, Magnitude 2.3, 1 April 2011." Available at http://www.bgs.ac.uk/research/earthquakes/blackpoolApril2011.html.

Davis, S.D. and Frohlich, C., 1993. Did (or will) fluid injection cause earthquakes? – Criteria for a Rational Assessment, Seismol. Res. Lett. 64(3-4), 207-224

Deyling, T. H. (1993), Moss Run Prospect: Structure in Lawrence Township, Washington County, Ohio. *in* An Update on Ohio's Subsurface Geology. Ohio Geological Society, Columbus, Ohio.

Efron, B. (1979), Bootstrap Methods: Another Look at the Jackknife, *The Annals of Statistics*, 7(1), 1-26.

Ellsworth, W. L. (2013), Injection-induced earthquakes. Science, 341. doi: 10.1126/science.1225942.

Evans, K. F., A. Zappone, T. Kraft, N. Deichmann, and F. Moia (2012), A survey of the induced seismic responses to fluid injection in geothermal and CO2 reservoirs in Europe. Geothermics 41, 30–54. doi: 10.1016/j.geothermics.2011.08.002.

Fischer, J. A. (1990), Proceedings of Fourth U.S. National Conference on Earthquake Engineering, Palm Springs, California, pp. 649–658.

Friberg, P. A., G. M. Besana-Ostman, and I. Dricker (2014), Characterization of an Earthquake Sequence Triggered by Hydraulic Fracturing in Harrison County, Ohio. Seismological Research Letters. 85(6). doi: 10.1785/0220140127

Frohlich, C. (2012), Two-year survey comparing earthquake activity and injection-well locations in the Barnett Shale, Texas. Proc. Natl. Acad. Sci. U.S.A. 109, 13934–13938. doi: 10.1073/pnas.1207728109.

Gerrish, H. and A. Nieto (2005), Evaluation of reservoir information in relation to earthquakes in Ashtabula, Ohio. Developments in Water Science, 52, 377-401.

Hansen, M. C. (2012). Earthquakes and Seismic Risk in Ohio. State of Ohio, Department of Natural Resources, Division of Geological Survey.

Healy, J. H., W. W. Rubey, D. T. Griggs, and C. B. Raleigh (1968), The Denver earthquakes, Science 161, 1301–1310.

Herrmann, R.-B. (2004), Computer Programs in Seismology, Version 3.30-GSAC, http://www.eas.slu.edu/eqc/eqc_cps/CPS/CPS330.html (last accessed March 2008).

Holland, A. (2013), Earthquakes triggered by hydraulic fracturing in south-central Oklahoma. Bull. Seism. Soc. Am. 103-3 1784-1792.

Holtkamp, S. G., and Brudzinski, M. R. (2011), Earthquake swarms in circum-Pacific subduction zones. Earth Planet. Sci. Lett. 305(1-2), 215-225.
Holtkamp, S., M. R. Brudzinski, B. S. Currie (2015), Regional detection and monitoring of injection-induced seismicity: Application to the 2010-12 Youngstown, Ohio seismic sequence, AAPG Bul. doi: 10.1306/3311513194.
Horton, S. (2012), Disposal of hydrofracking waste fluid by injection into subsurface aquifers triggers earthquake swarm in central Arkansas with potential for damaging earthquake. Seismol. Res. Lett. 83, 250–260. doi: 10.1785/gssrl.83.2.250.
Kafka, A. L. (1990), Rg as a depth discriminant for earthquakes and explosions: a case study in New England, Bull. Seismol. Soc. Am., 80(2), 373-394.
Kerenan, K. M., H. M. Savage, G. A. Abers, and E. S. Cochran (2013), Potentially induced earthquakes in Oklahoma, USA: Links between wastewater injection and the 2011 Mw 5.7 earthquake sequence. Geology 41, 699–702. doi: 10.1130/G34045.1.
Kim, W.-Y. (2013), Induced seismicity associated with fluid injection into a deep well in Youngstown, Ohio. J. Geophys. Res. 118, 3506–3518. doi: 10.1002/jgrb.50247.
McGarr, A., D. Simpson, and L. Seeber (2002), Case histories of induced and triggered seismicity, in International Handbook of Earthquake and Engineering Seismology, chap. 40, pp. 647–664, Academic Press, London.
McNamara, D. E., H. M. Benz, R. B. Herrmann, E. A. Bergman, P. Earle, A. Meltzer, M. Withers, M. Chapman (2013), The Mw 5.8 mineral, Virginia, earthquake of August 2011 and aftershock sequence: Constraints on earthquake source parameters and fault geometry. Bull. Seismol. Soc. Am. 104(1), doi: 10.1785/0120130058.
National Academy of Sciences (NAS) (2012), Induced Seismicity Potential in Energy Technologies, Natl. Acad. Press, 225. Washington, D.C.
Nicholson, C., E. Roeloffs, R.L. Wesson (1988), The Northeastern Ohio earthquake of 31 January 1986: was it induced? Bull. Seismol. Soc. Am., 78(1), 188-217.
Nicholson, C., and R. L. Wesson (1990), Earthquake Hazard Associated with Deep Well Injection: A report to the U.S. Environmental Protection Agency, U.S. Geol. Surv. Bull. 1951, http://pubs.usgs.gov/bul/.
Ohio Department of Natural Resources (ODNR) (2012), Preliminary report on the Northstar 1 class II injection well and the seismic events in the Youngstown, Ohio, Area. Columbus, Ohio.
ODNR (2014a), "Ohio Announces Tougher Permit Conditions for Drilling Activities Near Faults and Areas of Seismic Activity", URL: http://oilandgas.ohiodnr.gov/oil-gas-home/post/ohio-announces-tougher-permit-conditions-for-drilling-activities-near-faults-and-areas-of-seismic-activity.
ODNR (2014b), "Ohio Oil & Gas Well Locator", URL: http://oilandgas.ohiodnr.gov/well-information/oil-gas-well-locator.
Rubinstein, J. L. and W. L. Ellsworth (2013), The 2001 - present triggered seismicity sequence in the Raton basin of southern Colorado/Northern New Mexico. Seismol. Res. Lett. 84, 374.

Seeber, L. and J. G. Armbruster (1993). Natural and induced seismicty in the Lake Erie-Lake Ontario region: reactivation of ancient faults with little neotectonic displacement. Géographie physique et Quaternaire, 47(3), 363-378.

Seeber, L., J. G. Armbruster, W. Kim (2004), A Fluid-Injection-Triggered Earthquake Sequence in Ashtabula, Ohio: Implications for Seismogenesis in Stable Continental Regions. Bull. Seismol. Soc. Am., 94(1), 76-87.

Skoumal, R. J., M. R. Brudzinski, B. S. Currie, and J. Levy (2014), Optimizing Multi-Station Earthquake Template Matching Through Re-Examination of the Youngstown, Ohio Sequence. Earth Planet. Sci. Lett. 405, 274-280. doi: 10.1016/j.epsl.2014.08.033.

Skoumal, R. J., M. R. Brudzinski, and B. S. Currie (2015), Induced Earthquakes During Hydraulic Fracturing in Poland Township, Ohio. Bull. Seismol. Soc. Am. 105(1). doi: 10.1785/0120140168

Vidale, J. E., P. M. Shearer (2006), A survey of 71 earthquake bursts across southern California: exploring the role of pore fluid pressure fluctuations and aseismic slip as drivers. J. Geophys. Res. 111.

Warpinski, N. R., J. Du, and U. Zimmer (2012), Measurements of hydraulic-fracture-induced seismicity in gas shales. Soc. Pet. Eng. 151597, SPE Hydraulic Fracture Technology Conference, The Woodlands, Texas. 6-8 February 2012.

Table 3.1. Earthquakes utilized as templates in this study, grouped by their region.

Date	Lat	Long	Dep (km)	Mag	Source	# Matches	County/Region
Youngstown							
2011-03-17T10:42:20	41.11	-80.70	5	2.1	OGSO	342	Mahoning
2011-03-17T10:53:09	41.11	-80.70	5	2.6	OGSO	276	Mahoning
2011-08-22T08:00:31	41.09	-80.71	5	2.7	ISC	310	Mahoning
2011-08-25T19:44:20	41.10	-80.73	5	2.4	OGSO	249	Mahoning
2011-09-02T21:03:26	41.12	-80.69	5	2.2	OGSO	246	Mahoning
2011-09-26T01:06:09	41.12	-80.70	5	2.4	ISC	325	Mahoning
2011-09-30T00:52:37	41.16	-80.69	3.7	2.5	ISC	235	Mahoning
2011-10-20T22:41:09	41.11	-80.68	5	2.3	OGSO	320	Mahoning
2011-11-25T06:47:26	41.10	-80.69	5	2.2	OGSO	125	Mahoning
2011-12-24T06:24:57	41.11	-80.69	3.5	2.7	OGSO	271	Mahoning
2011-12-31T20:04:58	41.16	-80.73	2.2	4.0	ISC	90	Mahoning
2012-01-13T22:29:33	41.11	-80.69	5	2.1	OGSO	163	Mahoning
2013-11-12T20:12:00	41.13	-80.71	7.7	2.1	ANF	49	Mahoning
Poland Township							
2014-03-10T06:26:45	41.01	-80.54	2.5	3.0	NEIC-PDE	45	Mahoning
2014-03-10T06:42:44	41.01	-80.56	5	2.4	NEIC-PDE	64	Mahoning
2014-03-10T15:03:47	41.01	-80.53	5	2.2	NEIC-PDE	56	Mahoning
2014-03-10T15:44:06	41.01	-80.53	5	2.6	NEIC-PDE	61	Mahoning
2014-03-11T07:01:13	41.00	-80.53	5.2	2.1	NEIC-PDE	73	Mahoning
Harrison County							
2013-10-02T00:01:26	40.23	-81.22	11.2	2.2	ANF	97	Harrison
2013-10-02T01:52:46	40.23	-81.24	8.5	2.0	ANF	95	Harrison
2013-10-02T03:19:10	40.24	-81.24	7.6	2.4	ANF	107	Harrison
2013-10-02T10:06:55	40.24	-81.24	10.8	2.4	ANF	93	Harrison
2013-10-05T00:16:14	40.25	-81.24	7.4	2.6	ANF	84	Harrison
2013-10-08T06:25:46	40.24	-81.25	9.6	2.1	ANF	89	Harrison
2013-10-19T06:48:38	40.24	-81.24	8.9	2.3	ANF	86	Harrison
Belmont/Guernsey County							
2014-05-18T23:05:27	40.06	-81.25	3	2.6	ANF/TS	54	Belmont
2014-05-18T23:22:45	40.06	-81.25	3	1.9	ANF/TS	45	Guernsey
2014-05-18T23:47:19	40.06	-81.25	3	1.9	ANF/TS	54	Guernsey
2014-05-19T00:18:50	40.06	-81.24	3	2.2	ANF/TS	49	Belmont
2014-05-19T05:11:57	40.06	-81.24	3	2.1	ANF/TS	51	Belmont
Washington County							

2010-10-24T08:12:45	39.39	-81.35	2	2.8	OGSO/TS	<1>	Washington
2011-08-31T09:35:12	39.37	-81.37	3	2.8	ISC/TS	36	Washington
2011-08-31T17:36:02	39.37	-81.37	2	3.1	ISC/TS	31	Washington
2011-09-04T13:21:59	39.38	-81.35	5	2.6	OGSO/TS	53	Washington
2012-05-29T11:52:54	39.38	-81.34	2	2.1	OGSO/TS	6	Washington
2012-09-18T21:05:19	39.39	-81.34	4	2.1	OGSO/TS	47 (77)	Washington
Lake and Ashtabula Counties							
2013-03-08T22:32:20	41.71	-81.47	5	2.1	NEIC-PDE	3 (5)	Lake
2013-07-01T07:48:43	41.79	-81.29	5	3.2	OGSO	3 (3)	Lake
2013-10-06T19:37:02	41.85	-81.01	5	2.4	NEIC-PDE	2 (2)*	Lake
2014-04-08T16:02:28	41.81	-81.00	5	2.2	NEIC-PDE	2 (2)*	Lake
2013-03-17T22:49:26	41.66	-80.89	5	2.2	OGSO	4 (8)	Ashtabula
Isolated Events							
2011-04-26T07:09:46	40.86	-83.54	5	2.4	OGSO	1	Hancock
2011-06-05T15:35:20	41.00	-82.04	0.7	3.0	ISC	2	Medina
2011-06-15T04:37:57	41.81	-81.79	5	2.0	OGSO	1	Lake Erie
2011-08-13T15:41:00	42.25	-81.02	5	2.1	OGSO	1	Lake Erie
2012-12-01T07:32:01	39.05	-82.17	20	2.6	ANF	1	Meigs
2013-02-17T04:12:55	42.02	-82.22	5	2.5	NEIC-PDE	1	Lake Erie
2013-03-27T09:10:48	38.67	-82.21	1.2	3.1	ANF	1	Gallia
2013-05-10T23:22:36	39.02	-82.32	17.9	2.0	ANF	1	Meigs
2013-10-11T02:25:40	38.51	-82.80	5.7	2.2	NEIC-PDE	1	Greenup
2013-11-20T17:59:39	39.45	-82.20	8	3.5	NEIC-PDE	1	Athens
2014-01-20T06:50:18	41.41	-81.91	13	2.1	NEIC-PDE	1	Cuyahoga
2014-01-27T05:52:58	38.95	-82.94	17.2	1.9	ANF	1	Scioto

* Events that only match with each other.
() Number of matches obtained with a local set of 3 TA stations.
<> Matches obtained with a regional set of 3 older stations.
TS: Locations are from this study.

Table 3.2. Summary of criteria to distinguish induced seismicity in Ohio.

Sequence	Suggested induced source	Distance to source[A]	Time delay[B]	Swarm-like nature[C]	Previous seismicity[D]	Induced?
[1]2011-2012 Youngstown	Waste Disposal	**< 1 km**	**2 weeks**	**Yes**	**No**	**Likely Induced**
[2]2014 Poland Township	Hydraulic Fracturing	**< 1 km**	**< 1 day**	**Yes**	**No**	**Likely Induced**
[3,4]2013 Harrison Co	Hydraulic Fracturing	**< 1 km**	**< 1 day**	**Yes**	**No**	**Likely Induced**
[4]2014 Belmont/Guernsey Co	Hydraulic Fracturing	**< ~5 km**	**< 1 day**	**Yes**	**No**	**Likely Induced**
[4]2010-2014 Washington Co	Waste Disposal	**< ~2 km**	2 years	**Yes**	**No**	**Probably Induced**
[4]2010-2014 Isolated (Section 3.4)	None	>10 km	N/A	No	Yes	Unlikely Induced
[4]2012-2013 Lake Co	None	>10 km	N/A	No	Yes	Unlikely Induced
[4]2013 Ashtabula Co	None	>10 km	N/A	No	Yes	Unlikely Induced

[1]Skoumal et al., 2014 ; [2]Skoumal et al., 2015 ; [3]Friberg et al., 2014 ; [4]This study.

[A]: Three-dimensional distance from industry operations to closest earthquake.

[B]: Time delay between start of wastewater disposal or hydraulic fracturing and the first recorded earthquake.

[C]: Swarm-like nature, lacking traditional mainshock/aftershock pattern (Figure 4.8).

[D]: Region of suspected induced events has prior reported seismicity.

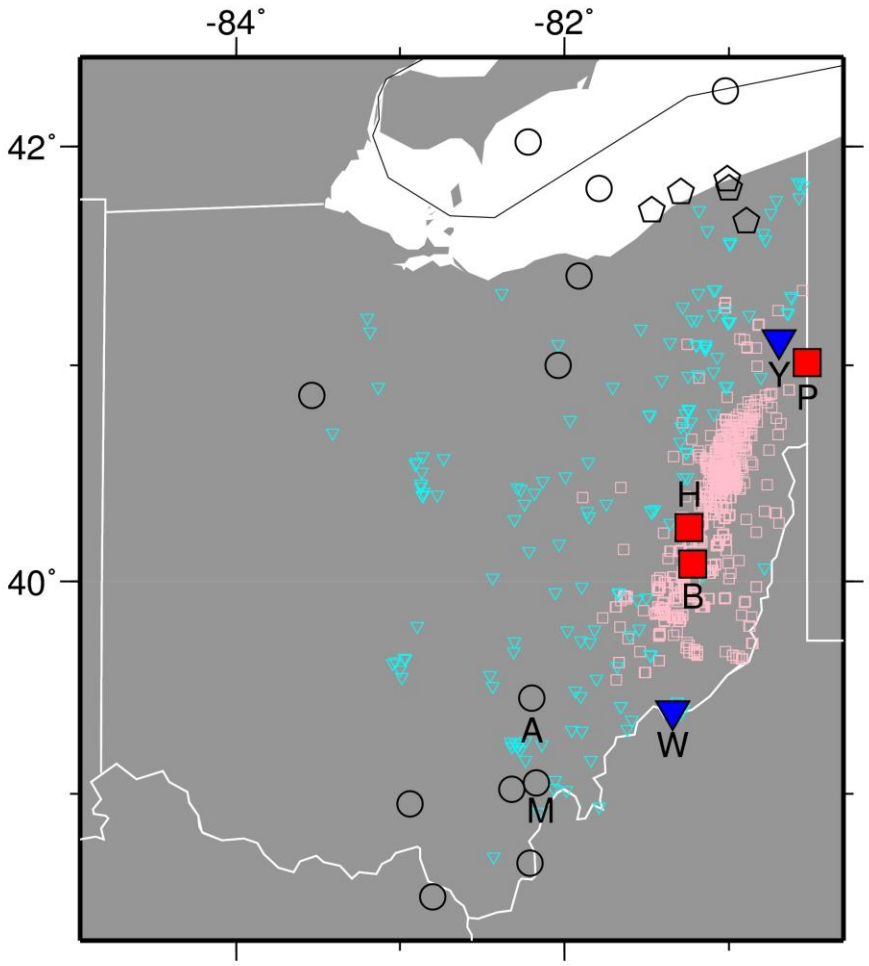

Figure 3.1. Map summarizing the template matching results. Some templates reveal repeating events with evidence they are induced by wastewater disposal (blue triangle) or hydraulic fracturing (red squares). Pentagons are recent earthquake templates that produced a handful of matches. Circles are recent isolated earthquake that produced 0-1 additional template matches and appear to be natural earthquakes. Pink squares and cyan triangles are all unconventional Utica wells and wastewater disposal wells active during the study time frame. Labels are: B – Belmont/Guernsey Co., H - Harrison Co., M - Meigs Co., P - Poland Township, A - Athens Co., W - Washington Co., Y - Youngstown.

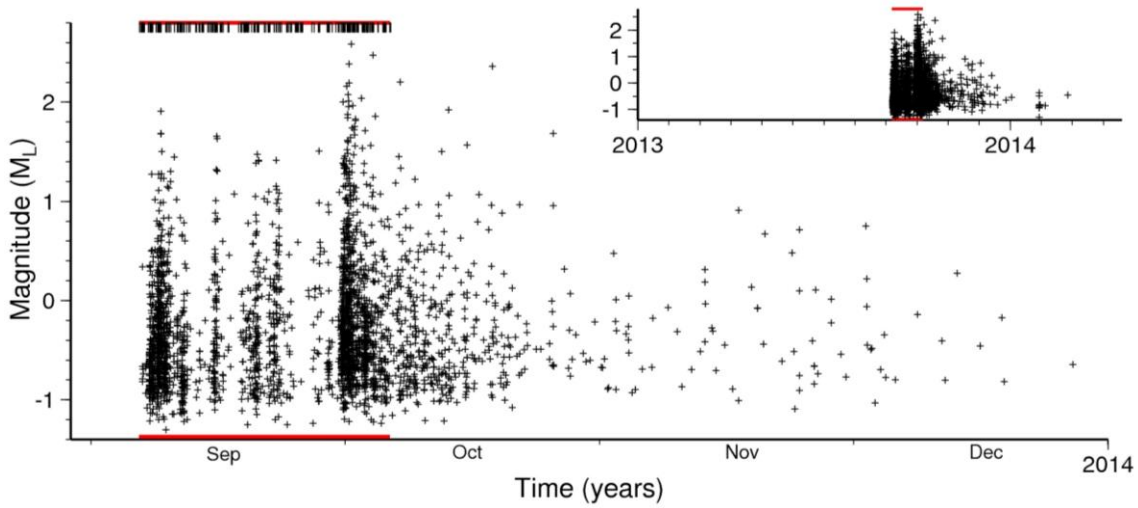

Figure 3.2. Magnitude of earthquakes in Harrison County (crosses) identified from template matching using nearby station O53A. Red bars indicate duration of nearby hydraulic fracturing, with black bars showing individual stages. Inset shows the entire time frame over which the template matching was performed based on nearby EarthScope station availability.

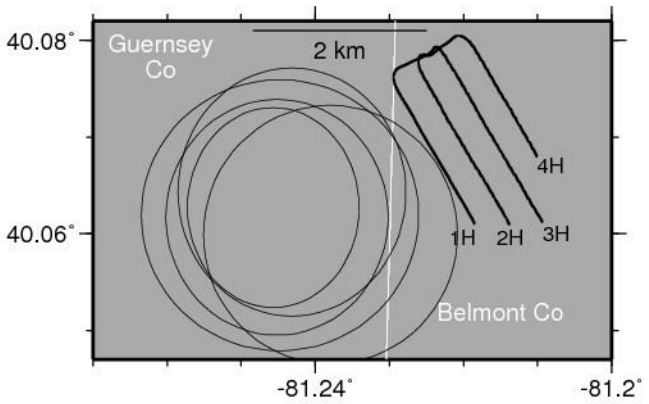

Figure 3.3. Map at the edge of Belmont and Guernsey Counties showing relocations and bootstrap uncertainties of 4 template earthquakes (ellipses) and the Kirkwood A horizontal wells 1H-33 through 4H-33 that underwent hydraulic fracturing around the time of the earthquakes.

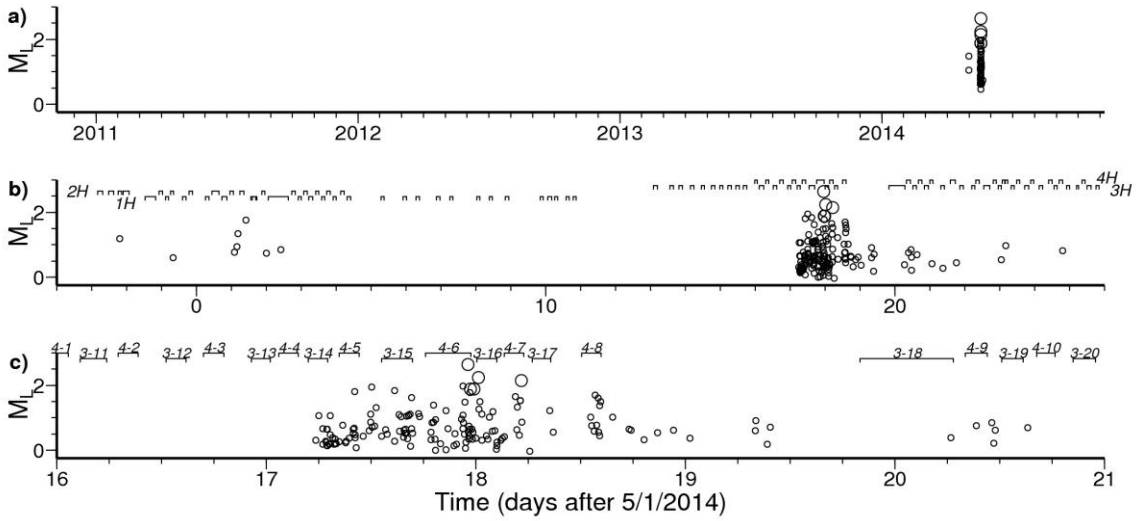

Figure 3.4. Magnitudes of earthquakes found through template matching in the Belmont/Guernsey County case using (a) typical 3 regional TA stations and (b and c) closest 3 TA stations. Large circles are templates, small circles are matches. Brackets indicate times of hydraulic fracturing stimulation at each well, and individual stages are labeled in the zoomed in view (c).

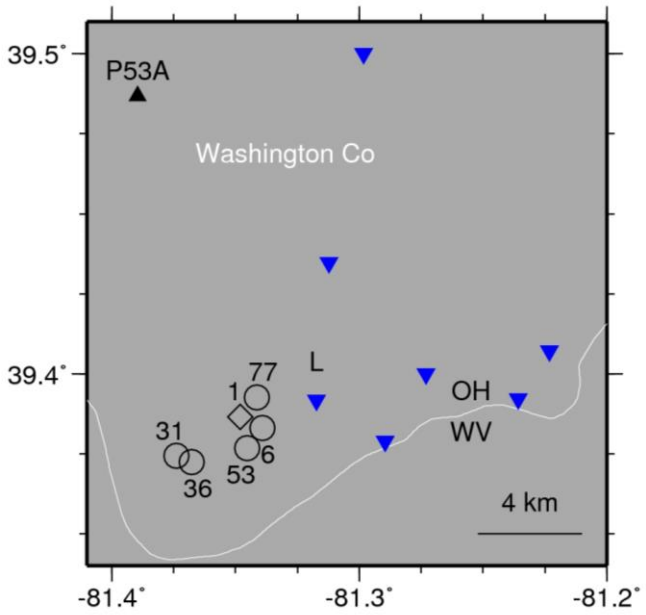

Figure 3.5. Map showing relocated epicenters of template events (circles), number of matches (numbers). Diamond shows the template event that used older regional data. Nearest TA station is a black triangle, and disposal wells are blue inverted triangles, where L = Long Run Disposal Well. White line shows state boundary (Ohio River).

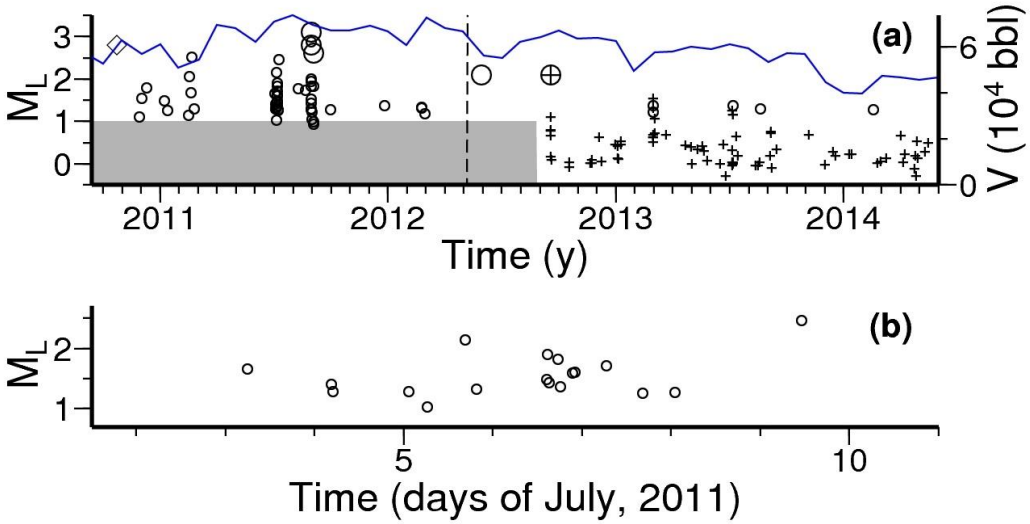

Figure 3.6. Magnitudes of earthquakes found through template matching in the Washington County region. Larger circles are templates, small circles are matches. (a) Events found with the traditional template stations (circles) and with the closest 3 TA stations using the last cataloged event in this region (crosses). Grey marks the time when the closer 3 TA stations were not available. Blue line is monthly injected volume at the nearest well. Dashed line is time when ownership changed at the nearest high volume disposal well. Diamond is earliest recorded event in this region, which occurred 2 weeks before the TA stations were installed. (b) Swarm of events illustrating the lack of mainshock-aftershock behavior.

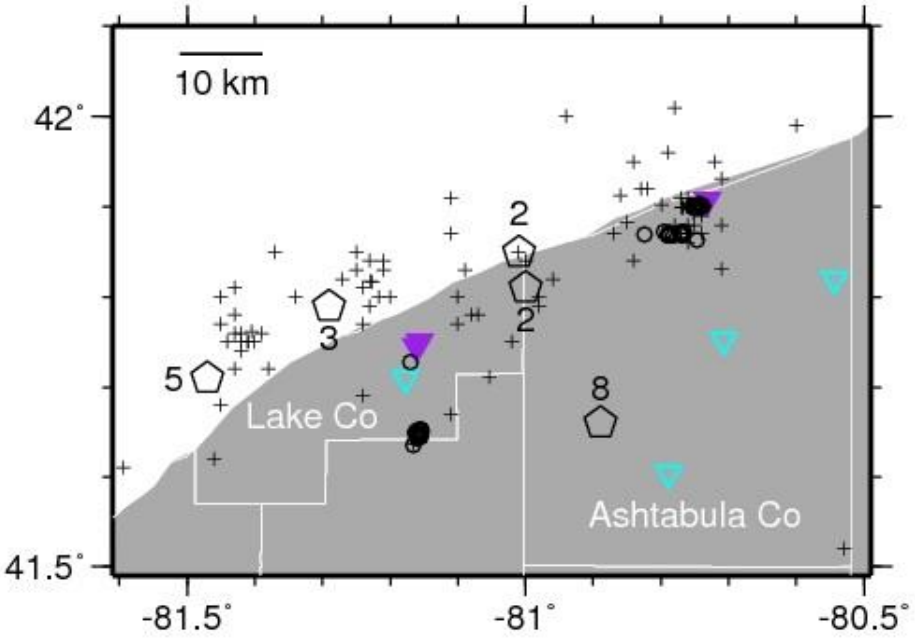

Figure 3.7. Map showing epicenters in the OhioSeis catalog (crosses), along with previously relocated events from the 1986 Lake Co sequence and 1987/2001 Ashtabula Co sequences (circles), and the 5 events analyzed by this study (pentagons). Numbers indicate how many matches found using a local set of TA stations. Inverted triangles show deep disposal wells suspected in the earlier sequences (purple) and those operating during the recent sequences (cyan).

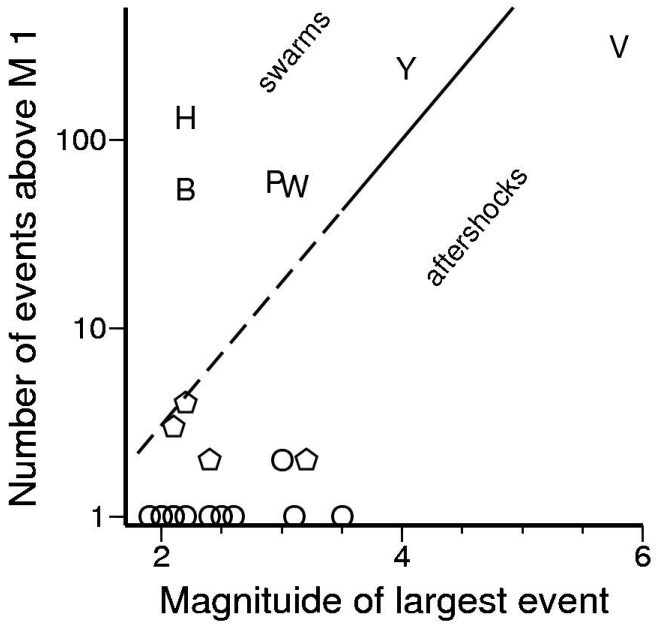

Figure 3.8. Swarminess of earthquake sequences analyzed in this study. Labels are those from Figure 4.1, with V added for the 2011 Virginia earthquake sequence. Solid line marks the proposed boundary between swarms and mainshock-aftershock sequences (Vidale and Shearer, 2006; Holtkamp and Brudzinski, 2011), and the dashed line is an extension following the same slope.

Table 3.S1. Statigraphic 1D velocity model based on the Amerada Petroleum Ulman 1 Well sonic logs.

Unit	Top depth (ft)	Thickness (ft)	Average velocity (uSec/ft)	Thickness (km)	Average interval velocity (km/s)
Pennsylvanian	0	1525	86.1	0.46	3.5
Mississippian	1525	382	73.6	0.12	4.1
Upper Devonian	1907	2822	73.5	0.86	4.1
Middle Devonian	4729	76	135.2	0.02	2.3
Lower Devonian-Silurian	4806	2084	55.6	0.64	5.5
Upper Ordovician	6889	1415	104.3	0.43	2.9
Point Pleasant	8304	133	124.2	0.04	2.5
Upper Cambrian-Middle Odovician	8437	1537	60.7	0.47	5.0
Rose Run Sandstone	9974	176	61.5	0.05	5.0
Copper Ridge-Conasauga Group	10150	1045	51.8	0.32	5.9
Basal Cambrian	11195	215	70.7	0.07	4.3
Precambrian Basement	11409	30	69.9	0.01	4.4

Table 3.S2. Seismic velocity model used for earthquake relocation in Washington County.

Depth (km)	Vp (km/s)	Vs (km/s)
0	4.117	2.377
2.572	5.261	3.037
10	6.62	3.83
41	8.1	4.68

CHAPTER 4: An efficient signal detector to investigate earthquake swarms

4.1. Abstract

Repetitive earthquake swarms have been recognized as key signatures in fluid injection induced seismicity, precursors to volcanic eruptions, and slow slip events preceding megathrust earthquakes. We investigate earthquake swarms by developing a Repeating Signal Detector (RSD), a computationally efficient algorithm utilizing agglomerative clustering to identify similar waveforms buried in years of seismic recordings. Instead of relying on existing earthquake catalogs of larger earthquakes, RSD identifies characteristic repetitive waveforms by rapidly identifying signals of interest above a low signal-to-noise ratio and then grouping based on spectral and time-domain characteristics, resulting in dramatically shorter processing time than more exhaustive autocorrelation approaches. RSD produces remarkably similar results to a prior study of volcanic seismicity at Mammoth Mountain that relied on 30 stations and templates constructed from a catalog of >1500 events. RSD identifies 10 times more events in a subduction-related seismic swarm in Oaxaca, Mexico than the traditionally constructed catalog. We then focus on induced seismicity swarms, which has proliferated recently such that rapid, efficient detection can aid in mitigation. In Central Alberta, Canada, RSD detects seismicity correlated with hydraulic fracturing over distances up to ~50 km from the station, performing as well as template matching using cataloged events. In Harrison County, Ohio, RSD identifies 18 seismic sequences that correlate temporally and spatially to separate hydraulic fracturing operations, 15 of which were previously unreported. Due to the smaller computation overhead and success at regional distances, RSD is well-suited for real-time detection of earthquake swarms over larger geographical regions.

4.2. Introduction

4.2.1. Repetitive seismic events

Relationships between earthquakes are observed by the clustering of seismic events in space and time. This clustering commonly occurs as mainshock-aftershock sequences, which are generally interpreted to contain the initial rupture of a fault (the mainshock) and a decaying cascade of smaller ruptures on or very near to the initial rupture plane (aftershocks) (Lay & Wallace, 1995). Clustering of earthquakes in space and time can also occur as earthquake swarms, which are empirically defined as an increase in seismicity rate above the background rate without a clear triggering mainshock earthquake (Mogi, 1963). Earthquake swarms are often associated with volcanic regions and are studied because of their relationship to eruptions (McNutt, 1996). Earthquake swarms have also been correlated with subduction zone slow slip events (Hirose et al., 2014), including a case that led into the 2011 Tohoku earthquake (Kato et al., 2012). Earthquake swarms are also well associated with many induced ("human influenced") earthquake sequences (e.g., Horton, 2012). Understanding the mechanisms that lead to earthquake swarms and the rapid detection of these events are key factor in reducing the hazard posed by these events.

Recent advances in seismic waveform template matching techniques have improved the detection of similar earthquakes, such as those that occur in swarms (e.g., Kato et al., 2012, Shelly et al., 2015). Two earthquakes from a given swarm are likely to

have a similar source mechanism and be located in close proximity, such that the radiated energy from both events is expected to have the same polarity, similar seismic wave arrival times, and interact with the same rock layers while follow a common pathway to a seismic station. The resulting ground motions for both events would be similar, enabling detection through correlation-based processing.

4.2.2. Induced seismicity overview

As enhanced oil and gas operations have proliferated over the past decade in North America, the potential to generate induced seismicity has also grown (NRC, 2013; Ellsworth, 2013). New industrial technologies have broadened the geographic area over which hydrocarbons can be economically recovered, meaning the areas at risk for associated induced seismicity is broadening as well. In response, regulations have been implemented in some states and countries in an attempt to limit the occurrence of induced earthquakes (GWPC & IOGCC, 2015). In Ohio, for example, if a hydraulic fracturing operation (HF) is associated with a magnitude (M) > 1 earthquake, operations at the well may be terminated (ODNR, 2014). This magnitude threshold is below the detection capabilities of traditional earthquake detection methods that utilize regional seismic data. To distinguish whether a well is associated with low magnitude seismicity, local seismic deployments and/or new earthquake detection algorithms would be required.

A monitoring strategy for induced seismicity is needed that can rapidly analyze this growing geographic region that may experience induced seismic events. Since 2010, induced seismicity associated with enhanced recovery has been observed in Arkansas (Horton, 2012), Colorado (Rubinstein et al., 2014), Kansas (Buchanan, 2015), New Mexico (Rubinstein et al., 2014), Ohio (Skoumal et al., 2015c), Oklahoma (Walsh & Zoback, 2015), Texas (Frohlich et al., 2011), as well as British Columbia (BCOGC, 2012) and Alberta (Schultz et al., 2015). Most of this seismicity is attributed to deep disposal of large volumes of leftover water following oil and gas well stimulation or recovery (McGarr et al., 2015; Walsh & Zoback, 2015; Weingarten et al., 2015). Although less common, there are also a number of cases where HF itself has been well correlated to earthquakes (Nicholson & Wesson, 1990; BCOGS, 2012, Holland et al., 2013; Clarke et al., 2014; Schultz et al., 2015, Skoumal et al., 2015a). In both cases, the induced seismicity tends to occur as seismic swarms that can be effectively detected with advanced correlation algorithms (Frohlich et al., 2011; Benz et al., 2015; Schultz et al., 2015; Holtkamp et al., 2015; Huang & Beroza, 2015; Skoumal et al., 2015c). Multi-channel cross-correlation using waveforms from a previously cataloged seismic event (template matching) is well-suited for the identification of similar, small magnitude events (e.g., Gibbons & Ringdal, 2006; Shelly et al., 2007). Due to the swarm-like nature that is commonly associated with induced sequences, template matching is ideally suited for lowering the magnitude detection threshold, increasing the confidence in classifying a sequence as natural or induced (e.g., Skoumal et al., 2015c). The question remains whether other induced sequences exist below the catalog detection threshold.

The swarm-like nature of induced seismicity creates an opportunity to develop a new algorithm to identify these repeating signals at lower magnitude than traditional earthquake detection methods. We first develop our algorithm by applying it to previously studied natural earthquake swarms at Mammoth Mountain, California, and Oaxaca, Mexico. We then applied our algorithm by investigating seismicity associated

with HF, as the shorter time of fluid injection (typically weeks) relative to wastewater disposal (typically years) helps to discern whether seismicity is related to HF. Our study focuses on Ohio where 3 sequences of induced seismicity have been attributed to wastewater disposal (Kim, 2013; Skoumal et al., 2015b; Skoumal et al., 2015c) and 3 associated with HF (Friberg et al., 2014; Skoumal et al., 2015a; Skoumal et al., 2015c). One advantage of this study region is that each case was spatially or temporally separated from other industrial operations, which allows us to simplify the investigation by examining a single area with HF seismicity. Since the previously identified sequences associated with HF were characterized via catalog-based template matching, each had to have at least one earthquake with M > 2, but none were larger than M 3. These seismic sequences were all shown to occur at or the below the basement contact with hypocentral distributions and focal mechanism orientations consistent with reactivation of pre-existing faults (Kim, 2013; Friberg et al., 2014; Skoumal et al., 2015b; Skoumal et al., 2015c). Operationally induced microseismicity typically produces M < 0 in the stimulated formation (Warpinski, 2013), suggesting that sequences with seismicity in the M 0-2 range should be the target for improving detection of induced seismicity on preexisting faults.

Another region with prevalent HF and correlated seismicity that was investigated in this study is the Duvernay Play in Central Alberta (Eaton & Mahani, 2015; Schultz et al., 2015). HF had previously been thought to pose little risk of inducing felt seismicity (NRC, 2013), but the Kaybob area near Fox Creek has had several earthquakes with M > 4 in 2015 near HF operations. Induced subsequences found in this region had remarkable inter-event similarity with average normalized correlation coefficients > 0.8 that aided detection via template matching (Schultz et al., 2015). The nearest publicly available seismometer is ~30-50 km away, providing an opportunity to test whether a new algorithm can successfully detect small, repeating seismic events at regional distances.

4.2.3. Previous repeating seismic event detection algorithms

Template matching has been demonstrated as a valuable tool to characterize low-magnitude induced seismic events, but it is inherently reliant on another algorithm to identify the template signals. A short-term / long-term average amplitude (STA/LTA) earthquake detection algorithm is commonly used to detect seismic wave arrivals, and then a data acquisition and processing system (e.g., Earthworm, Antelope) will determine if enough stations recorded arrivals at appropriate times to be from a single location in the Earth. Traditionally, the application of these algorithms to regional networks results in a magnitude detection threshold of M ~2.5. Consequently, catalog-based template matching relies on the detection of a M > 2 event before smaller magnitude events could be identified. If an induced sequence has not yet produced a M > 2 earthquake (or if it is not cataloged), the sequence would go undetected unless a local network is present. Induced seismicity often contains swarms of smaller magnitude events that precede larger events (e.g., Friberg et al., 2014; Huang & Beroza, 2015; Skoumal et al., 2015c), increasing the importance of rapidly detecting M < 2 seismicity. Ideally, a real-time detection algorithm would not rely on the identification of a M > 2 event that may occur later in the sequence.

Autocorrelation has the potential to identify repeating signals below the magnitude detection thresholds from multi-station STA/LTA detection, and it is also not

reliant on the prior identification of a seismic event. However, autocorrelation is computationally intensive when large time windows are considered, with $N\,(\,N-1\,)\,/\,2$ correlations required. A previously proposed solution to this computational challenge is to implement a time step between windows used in autocorrelation (Brown et al., 2008). While this will reduce the number of correlations to $N\,(N-1)\,/\,(\,2\times \text{step})$, it fails to address the quadratically increasing nature of the computations. Additionally, a significant step size would fail to detect repeating signals that have windows that are not aligned and is therefore not be an ideal detection tool. Due to the computationally intensive nature of autocorrelation, it is currently not practical to implement the algorithm on a regional scale for many months or years, which are common durations for induced seismicity.

Another proposed solution for the detection of repeating seismic events is the Fingerprint and Similarity Thresholding (FAST) algorithm (Yoon et al., 2015a). FAST utilizes locality-sensitive hashing, which groups similar waveforms together in hash buckets based on the discriminative features of the signals. Correlations are only performed on similar events, reducing the number of required calculations. In a week-long trial in Central California, the algorithm successfully identified 21 of the 24 cataloged earthquakes in addition to detecting 68 uncataloged earthquakes, while also identifying 12 false positives (Yoon et al., 2015a). With computations that scale near-linearly instead of quadratically, FAST has been demonstrated as having significant runtime advantages over autocorrelation, with 3 months of single-channel data processed in 16 days (Yoon et al., 2015b). While FAST is significantly more efficient than autocorrelation, its utilization for real-time earthquake detection on a regional scale may still be limited by its computational overhead.

Another technique that addresses the challenge of identifying a template event targeted for low-frequency earthquakes was proposed by Frank & Shapiro (2014). Using a three-dimensional grid of potential sources and a velocity model to estimate phase moveouts, recorded seismic energy peaks are summed to create templates in a near-automated manner similar to the source scanning algorithm (Kao and Shan, 2004). For a 2.5 year dataset using 10 stations spaced ~10 km apart, 8 days of computation time were required when used in parallel with 8 GPUs (Frank et al., 2014). The required number of seismometers, creation of accurate velocity models, and computation time may potentially impede this algorithm from being rapidly utilized for real-time monitoring over large regions with significant seismometer spacings where induced seismicity has been observed, like the Midcontinental United States, Alberta, and British Columbia.

4.3. Methods

4.3.1. Data sets

We utilized continuous seismic data from four regions in North America: 1) Mammoth Mountain, California, 2) Oaxaca, Mexico, 3) Central Alberta, Canada, and 4) Harrison County, Ohio. For the Mammoth Mountain study area, data was obtained from station NN OMMB (40 Hz) during 2-18 February 2014, and we compared our results to an earthquake catalog generated by Shelly et al. (2015) created during the same time window. In Oaxaca, Mexico, we used data from station MU OXTT (40 Hz) during 10-30 July 2006 and compared our results to the earthquakes identified by Fasola et al. (in press). For Central Alberta, we applied RSD to station BRLDA of the Raven network

from 15 August 2014 to 27 November 2015 after downsampling the data from 100 Hz to 40 Hz. Catalog earthquakes in Alberta were obtained from Natural Resources Canada (NRCAN). In Harrison County, we utilized station O53A (40 Hz) in Harrison County, Ohio, originally part of the EarthScope Transportable Array, from 14 December 2012 to 27 November 2015. To aid in characterization of the detected signals, we utilized a Freedom of Information Act request to Ohio Department of Natural Resources (ODNR) to obtain data from two three-component short-period stations, and we also deployed a broadband seismometer on 13 September 2015. Catalog earthquakes in Ohio were obtained from ODNR and Advanced National Seismic System (ANSS). Times and locations of HF for the Harrison County and Central Alberta regions were obtained from ODNR, FracFocus, and FracFocus.ca.

4.3.2. The Repeating Signal Detector (RSD) algorithm

In an effort to make the initial identification of small magnitude, repetitive events more efficient and effective, we propose a new algorithm, referred to as a Repeating Signal Detector (RSD). The initial step of RSD is identifying signals of interest (SoI) using continuous seismic data for a single station in a manner similar to the traditional STA/LTA detection algorithms. We employ a relatively low signal-to-noise threshold where the average amplitude in the previous 1 sec is at least 5 times larger than the average amplitude in the previous 30 sec. When the threshold is exceeded using 5-15 Hz bandpassed data, we reserve a 30 sec unfiltered window of the SoI centered on the peak amplitude. At this stage, many of these SoI are expected to consist of non-earthquake signals. To distinguish the repeating earthquakes, these SoI are grouped into families. For each SoI, the Fast Fourier Transforms of each component ($[E_{freq}]$, $[N_{freq}]$, and $[Z_{freq}]$) considering frequencies above 5 Hz are concatenated ($[E_{freq}\ N_{freq}\ Z_{freq}]$) to represent each SoI as a single point in *n*-dimensional space where *n* is 285, the number of points in the concatenated array. Agglomerative clusters are then created using a complete-linkage clustering approach by calculating the average, unweighted Euclidean distances between these points while considering the shortest distances between clusters. The maximum number of possible families is set as the total number of SoI divided by five, an experimentally derived coefficient that provided the optimal balance between grouping visually similar waveforms and a manageable numbers of output families.

While this initial family clustering step is effective at sorting like-signals into families, variations in waveforms may still be present (Figure 5.1). The small temporal offsets between different family members would create destructive interference if stacked at this stage. To account for these temporal arrival variations, the signals are bandpass filtered between 5-15 Hz and the largest amplitude signal in each family is identified and then cross-correlated against the other members in the family to adjust for any temporal offsets. For each individual family, the agglomerative clustering is then performed similar to before. However, this time the clustering is performed in the time domain by taking the medial 10 sec of the adjusted bandpassed waveforms from each of the three components ($[E_{time}]$, $[N_{time}]$, and $[Z_{time}]$) and concatenating them ($[E_{time}\ N_{time}\ Z_{time}]$) so that each SoI can once again be represented as a single point in *n*-dimensional space, where this time *n* is 1,200, the number of points in the concatenated array. This time domain clustering step identifies subfamilies that can then be stacked, improving the signal-to-noise ratio and providing characteristic repetitive signals that can then be used

as templates in a cross-correlation routine. In an effort to remove families identified by RSD that consisted of harmonic noise, we removed stacks with low frequency (< 3 Hz) normalized amplitudes above 0.3, an experimentally determined threshold that sufficiently removed the undesired signals in our study areas. To remove non-repetitive signals, we excluded identified subfamilies from further analysis if they had fewer than 5 members in cases where the station was further (>30 km) from the source (Oaxaca and Central Alberta) or 20 members in cases where the station was near (<10 km) the source (Mammoth Mountain and Harrison County). These differences highlight how the thresholds are likely both station and region specific, and should be expected to vary depending on the target. The objective of this manuscript is to describe the promise of RSD and encourage the community to modify the algorithm to suit their individual needs.

Computational overhead for the identification of SoI depends on the type of data compression and sample rate. Using an Intel Xeon Processor E5520 (2.26 Ghz), SoI from a day of 40 Hz MiniSEED data can be identified in ~1-2 seconds, which largely consists of reading data from the disk. Computation time for the family clustering process is dependent on the number of SoI identified, but it is capable of producing stacked subfamilies from 10,000+ SoI in ~1-2 minutes. Subsequent template matching using the stacked waveform requires ~15 minutes per template through each year of data. These relatively unintensive computational requirements allow for a year of continuous seismic data to be processed well within one hour in serial, but the calculations are also readily parallelizable. As a result, the computational overhead of RSD is a fraction of the amount required by autocorrelation or FAST, RSD does not rely on a velocity model or a relatively dense regional network required by an automated beamforming algorithm, and RSD has the potential to be employed in real-time processing of seismic data on a regional scale. Next, we demonstrate how successfully RSD can identify repetitive, small magnitude earthquakes below the detection threshold of traditional STA/LTA.

4.3.3. Investigating signals identified by the Repeating Signal Detector

For the remaining subfamily stacks, we use the medial 10 sec of each SoI as a template in a three component normalized cross-correlation routine using a detection threshold of 15 times the daily median absolute deviation (MAD) of the stacked correlation coefficients, a previously demonstrated conservative detection threshold (e.g., Skoumal et al., 2014). We perform template matching over the same time window that RSD was run (ranging between a few weeks and ~3 years, depending on the study region) in order to identify the temporal patterns of the repetitive signals. To ensure duplicate event detections by multiple templates were excluded, detected events that were analyzed were a minimum of 30 sec apart, consistent with previous studies (e.g., Skoumal et al., 2014).

To further investigate the results of template matching using RSD-derived templates, we performed manual inspection of the matched waveforms recorded by the station used for RSD in addition to other seismometers in the region to look for appropriate seismic wave characteristics. In particular, we looked for evidence of different P- and S-wave signatures on the vertical and horizontal components that would indicate a non-cultural source that can located. The remaining signals were bursts of energy recorded by the station used for RSD, but with no coherent signals on other nearby stations. Moreover, there was typically no time separation between noise signals

on the vertical and horizontal channels at the RSD station and hence no indication of separate P- and S-wave arrivals. We interpret these signals to be cultural noise near the seismometer, but the lack of seismic wave information prevents further investigation. Due to the vast number of matches to investigate in the larger sequences we identified, we utilized a grid-plot of the events to help discriminate seismicity from noise (see Supporting Information).

We approximated local magnitudes through a simplified Richter scale approach:

$$M_L = \log_{10}[A / A_0]$$

The median scale factor (A_0) was calculated using the peak-to-peak filtered S waveform amplitude and utilized existing catalog magnitudes of events in the corresponding catalog whenever present. For each matched event, we calculated a magnitude from the scale factor and S waveform amplitude at each station and component, and took the median value as our final magnitude. The largest magnitude events in each of the temporal clusters were then located using *elocate* (Herrmann, 2013) on manually picked P and S times using seismic data that were available at the time of the events. In Harrison County, we used a locally derived 1D velocity model (Friberg et al., 2014) adjusted to a basement depth of 3.4 km. In the Kaybob region, we derived a velocity model from sonic logs in the area (see Supporting Information).

4.4. Results

We first describe our comparisons to three documented swarms based on earthquake catalogs in volcanic, subduction, and induced seismicity cases. We then apply RSD to an induced seismicity case of interest where there is limited documentation of prior swarms but indications that it could be more pervasive.

4.4.1. Mammoth Mountain, California

Located in the Long Valley Caldera, Mammoth Mountain has been host to numerous earthquake swarms and outgassing events within the past few decades (Hill et al., 1990; Sorey et al., 1998; Lin, 2013; Lewicki et al., 2014). A previous large-scale template matching effort at Mammoth Mountain that utilized 1,545 cataloged earthquakes identified 6,179 events during 2-18 February 2014 from a swarm associated with fluid migration (Figure 5.2) (Shelly et al., 2015). The detection of this earthquake swarm was aided by the presence of a dense seismic network, including 6 seismometers within a few km horizontally from the swarm (Shelly et al., 2015). Using three-component waveforms from a single broadband station (NN OMMB) between 2-18 February 2014, RSD identified 6,026 SoI that were grouped into 1,206 families following the frequency domain grouping step. When these families were used in the time domain grouping, 18 sub-families were found that contained more than 20 members. Using stacks of these 18 sub-families as templates in a template matching routing, the temporal earthquakes pattern identified by Shelly et al. (2015) were duplicated. Nearly identical numbers of events were detected (6,197 vs. the 6,121 from RSD) between the methods (Figure 5.3). Approximately 87% (5,397) of the events from Shelly et al. (2015) were detected by RSD. Considering the reliance on an existing earthquake catalog and the large number of computations required by the large-scale template matching study, the relative ease by which RSD produced similar results with a single station and two orders

of magnitude less templates to process shows the promise for rapid earthquake identification.

4.4.2. Oaxaca, Mexico

Earthquake swarms, episodic slow slip, and tectonic tremor have previously been observed in Oaxaca, Mexico, associated with the subduction of the Cocos plate (e.g., Brudzinski et al., 2007; Brudzinski et al., 2010; Fasola et al., in press). In mid-July 2006, a swarm with $M_W \leq$ ~3.5 occurred ~20 km east of the city of Pinotepa Nacional (Fasola et al., in press). While this swarm has not been studied in detail, previous work on subduction zone swarms indicates they are potentially driven by slow slip and/or fluid flux (Holtkamp and Brudzinski, 2011), both of which are possible in this region (Brudzinski et al., 2007; Brudzinski et al., 2010; Song et al., 2009).

Using a single station (MU OXTT) of data between 10-23 July 2006 that was located ~30 km southeast from the July 2006 swarm (Figure 5.4), RSD identified 1,586 SoI that were grouped into 318 families following the frequency domain grouping step. Using these 318 families in the time domain grouping step, 33 sub-families were found that contained more than 5 members. Using stacks of these 33 sub-families in a template matching routine, 9 stacks each matched with > 15 real earthquakes (average of ~89 detections per stack) during expected seismically active periods, 9 stacks matched fairly continuously with noise, and 15 stacks matched with < 15 events and were discarded (Figure 5.5). A similar temporal seismicity pattern was observed to the catalog created by Fasola et al. (in press), with two primary bursts of activity on July 12 and 15-16. Moreover, RSD identified a ten-fold increase in the amount of detected events. Of the 43 earthquakes included in the catalog of Fasola et al. (in press) catalog that constituted the swarm, RSD detected 35 events (~81%).

4.4.3. Central Alberta, Canada

RSD was also applied to Alberta, Canada, where relatively large earthquakes have been related to hydraulic fracturing in the Kaybob area of Duvernay Formation, including a M_W 3.8 in August 2014 and a M_L 4.4 in January 2015 (Eaton & Mahani, 2015; Schultz et al., 2015). Station RV BRLDA is located in Central Alberta, ~250 km northwest of Edmonton and ~40 km south of the 2015 M_L 4.4 event (Figure 5.6) (Schultz et al., 2015). While there has been no record of a major, destructive earthquake in Alberta, moderate (< M 6) historical seismicity is common, occurring principally along the Rocky Mountain foreland basin (e.g., Stern et al., 2013). Between 1985-2012, there were 3 earthquakes with $M_L > 3$ in the NRCAN catalog in our study region (118-116.5°W, 53.5-55°N), compared with the 25 cataloged earthquakes with $M_L > 3$ in 2013-2015.

Using continuous seismic data recorded by station RV BRLDA between 15 August 2014 and 27 November 2015, a total of 9,984 SoI were grouped into 1,997 families following the frequency domain grouping, with 120 families containing more than 5 members. Following the time domain grouping, 88 subfamilies were identified that contained more than 5 members. Single-station normalized cross-correlation revealed 49 productive subfamilies that each matched with more than 100 events (Figure 5.7). Of these productive subfamilies, 42 were found to have matched consistently with real seismic events, while 7 matched with cultural noise fairly continuously throughout the sampling period. Template matching using the 42 productive subfamilies identified 4,411

unique events. Following manual inspection, ~93% of these events were confirmed as real seismic events, although distinguishing earthquakes from cultural noise was more difficult without a local network.

The Canadian National Earthquake Database (CNED) catalog identified 58 earthquakes during this time frame in this region (118-116.5°W, 53.5-55°N), with magnitudes between M_L 2.0 and M_W 4.6. Most earthquakes were clustered ~30 km away from station BRLDA (Figure 5.6). During the time frame considered, hydraulic fracturing occurred as close as ~5 km from station BRLDA, but most operations were > 30 km away (Figure 5.7a). These CNED catalog earthquakes were used in a template matching routine in a manner similar to the stacked subfamilies identified by RSD (Figure 5.7b). The cumulative number of event detections found using RSD were similar to the results obtained from using the catalog, and 91% of the template matched events using the catalog were also found using our RSD method. These results demonstrate the potential ability of RSD to duplicate results obtained using traditional earthquake detection over moderate (~50 km) source-receiver distances (Figure 5.7b-c).

4.4.4. Harrison County, Ohio

In September 2013, an earthquake sequence with magnitudes up to M_W 2.2 was induced by hydraulic fracturing in Harrison County, Ohio (Friberg et al., 2014). Two earthquakes in this sequence were included in the ODNR catalog following the published study. Despite ongoing industry activity near the vicinity of the sequence, the only other documented earthquake in the region was a M_L 2.1 on 30 September 2015, initially reported in the ANSS catalog.

Transportable Array (TA) station O53A is located only a few kilometers from this seismicity in an area of Harrison County where unconventional wells are actively being drilled and stimulated to target the Utica/Point Pleasant formation (Figure 5.8). Between 14 December 2012 and 27 November 2015, a total of 30,157 SoI were detected and grouped into 6,032 families following the frequency domain grouping, with 138 families containing more than 20 members. Following the time domain grouping step using the 138 families, 85 subfamilies were identified that contained more than 20 members. Using the 85 subfamilies, single-station normalized template matching revealed 38 productive subfamilies that each matched with more than 600 matched events, which we grouped into 4 categories based on inspection of waveforms.

The first group of 17 productive subfamilies were found to have matched with real seismic events nearly exclusively. A second group of 2 subfamilies matched with cultural noise at a small rate (averaging ~2 detections/day), but also had detection rate increases during times of real seismic events, although those detections essentially reproduced the events found with the first group of 19 subfamilies. A third group of 2 subfamilies matched with cultural noise fairly continuously throughout the sampling period (averaging ~5 detections/day). The fourth group of 17 subfamilies matched with cultural noise, but had a large increase in March-April 2013 that occurred while the Boy Scout 4-33H well was being drilled less than 1 km away from station O53A. Intriguingly, we detected very few events during the hydraulic fracturing of this well (23-28 May 2013). We focused our analysis on the first group of 17 productive subfamilies with the most limited cultural noise detections (Figure 5.9), and matching using the stacked subfamily templates identified 14,270 unique events. Using manual inspection of

individual waveforms for smaller sequences and correlated waveform grid-plots for larger sequences (see Supporting Information), we estimate that >95% of these events were confirmed as real seismic events.

Our culled seismicity catalog reveals 4 primary time periods of seismic activity, each with at least 500 events and an average of 3,300 events (Figure 5.9). To investigate whether these 4 sequences were induced, we compared the seismicity with the time and location of hydraulic fracture stimulations based on reports available from ODNR and FracFocus. In each of the 4 cases, the locations correlate with unconventional wells (Figure 5.8), and the timing of detections occur during the hydraulic fracturing of those wells or immediately after (Figure 5.10). We further examined these 4 sequences in Figure 5.11. The September-December 2013 sequence was previously reported as induced (Friberg et al., 2014) (Figure 5.11a). While the temporal patterns are similar to previous studies, the number of detections have dramatically increased when compared to previous work; Friberg et al. (2014) and Skoumal et al. (2015c) reported 698 and 2,788 events, respectively, while this analysis brings the number of events in the sequence to 7,231. The other three primary sequences (September 2014, December 2014-January 2015, and August-November 2015) had previously gone unreported (Figure 5.11b-d). Note that the lack of M_L 0-1.5 events in the September 2014 sequence is not erroneous (Figure 5.11b). Rather, location analysis of this sequence suggests the majority of the $M_L \leq 0$ events clustered along a separate feature ~1 km north of where the $M_L > 1.5$ events occurred (Brudzinski et al., 2015; Friberg et al., 2015). Another intriguing observation is the identification of a M_L 2.7 event in the August-November 2015 sequence that was not reported in any of the available catalogs, but was well-recorded on regional seismometers and was also felt by the local population (J. Butler, personal comm., 2015). This underscores the importance of utilizing a technique like RSD that does not rely on a catalog to search for seismicity.

14 additional smaller sequences that contained between 2 and 210 identified earthquakes (~30 events on average) were also found to correlate temporally with separate hydraulic fracturing operations (Figure 5.10). Events from eight of these additional sequences were able to be located using P and S arrivals from at least 3 stations, and each was found to be in close proximity (< 1 km) to the wells being stimulated during the seismicity (Figure 5.9). Accurate locations could not be determined for six sequences that occurred either prior to the deployment of additional stations or after the data obtained via FOIA request. Although data was only available for O53A for these six sequences, S-P times are consistent with distances between the station and well locations that were being actively hydraulically fractured when the seismicity was detected. Two sequences were detected > 10 km from O53A, both of which occurred in Belmont County, south of Harrison County (Figure 5.8b). This includes the Horseshoe well (~15 km from O53A) in addition to the previously reported May 2014 sequence associated with the Kirkwood well, near the border of Belmont/Guernsey Counties (~19 km from O53A) (Skoumal et al., 2015c). These two wells are the closest wells to the south of the Harrison County sequences in an area that has not been as heavily targeted. If wells are stimulated in this area in the future, the risk of generating induced seismicity may be higher than previously recognized.

Considering that only three of the 18 detected sequences were previously reported (Skoumal et al., 2015c), this case study demonstrates the potential of RSD to identify

characteristic, repeating seismic signals below the detection threshold of traditional earthquake detection methods. It is remarkable that > 99% of seismicity in the culled catalog correlates in space and time with hydraulic fracturing operations, but a more detailed study of each sequence is needed to characterize the nature of how seismicity is related to industry operations.

4.5. Discussion

4.5.1. Limitations and future work

This study principally seeks to show the results that can be obtained by applying RSD to a single seismometer with limited potential human interaction to demonstrate its capability for monitoring smaller seismicity in a near real-time environment. To determine the effectiveness of the algorithm, detected events were manually investigated to classify them as earthquakes or noise. More detailed investigation of the frequency and time domain characteristics of the noise signals could provide a means to automate the discrimination of these cases in the future. Such a discriminant would be particularly effective at the stage where stacked subfamilies are formed, as subfamily stacks formed primarily from cultural noise tend to find more noise than earthquakes.

Further analysis is also needed to clarify the connection between the identified seismicity detected in the Harrison Co region and the HF operations to determine if these sequences were induced. For example, one could utilize an empirical subspace detector on the events from each smaller sequence to increase the number of detections (Barrett & Beroza, 2014; Skoumal et al., 2015b). Considering many of the smaller sequences also have small magnitudes, a detailed location study utilizing improved velocity models, correlated arrival times, and/or double difference relocation could potentially improve the precision of hypocentral depths to differentiate whether these are operationally induced microseismicity in the target formation or earthquakes in the Precambrian basement. The other recent documented induced seismicity sequences in Ohio with M > 2 have all occurred near or below the basement contact (Kim, 2013; Friberg et al., 2014; Skoumal et al., 2014; Skoumal et al., 2015a; Skoumal et al., 2015b; Skoumal et al., 2015c). The lack of locations for newly detected events also limited the accuracy of magnitudes calculated in this study. Event magnitudes in the Ohio region further from O53A than the prominent seismic sequence in 2013 are likely to be underestimated with the single-station calculation we used. The most extreme example are the events associated with the Kirkwood wells that were estimated ~ 1 magnitude unit below their reported values (Skoumal et al., 2015c).

While we focused on two regions known to have induced seismicity from HF, previous work has indicated induced seismicity in the Midcontinental United States is largely attributed to disposal of large volumes of wastewater or produced water (McGarr et al., 2015; Walsh & Zoback, 2015; Weingarten et al., 2015). Considering the lifespan of wastewater disposal wells often last years or decades relative to HF operations that may last less than a couple of months, seismicity patterns between the two source of induced seismicity are expected to differ. In this study, we did not initially determine whether RSD stacked subfamily templates were real seismic signals or as noise. Rather, after template matching, we found that signals that found matches “continuously” throughout the time of the study were noise and discarded them. While this may be appropriate to identify seismicity induced by HF, this approach would not be viable for long-lived

wastewater disposal wells that may have associated seismicity for many years. For these cases, confirming a stacked subfamily represents an earthquake through additional frequency analysis, identifying the characteristics of P- and S-waves, and/or utilizing recordings on multiple seismometers may be required to ensure high detection fidelity and low false positive rate.

4.5.2. Induced seismicity regulations

In April 2014, new permit conditions set forth by the ODNR stated that new HF wells within 3 miles of a known fault or earthquake with M > 2 will be required to install seismic monitors (ODNR, 2014). If the seismometers detect a M > 1 event associated with the HF, the operations would be suspended. Had the four primary sequences in Harrison County been permitted following this regulation was enacted, operations may have been ceased. In March 2015, a new regulatory system was established by the Alberta Energy Regulator (AER) in the Kaybob area near Fox Creek that would require operators to adjust operations if a M > 2 event was associated with HF and suspend operations if it was responsible for a M > 4 event. HF operators in and around Harrison County and the Kaybob area should be aware of the increased likelihood of inducing seismicity based on the prevalent prior activity, and we propose implementing an algorithm such as RSD to maximize the detection capabilities of existing seismic networks.

4.5.3. Application to other repetitive seismic signals

While the application of RSD was focused on improving the detection of induced seismicity, we have sought to demonstrate that RSD also has the potential to improve characterization of natural earthquake swarms in areas with limited station coverage. Template matching approaches have been successfully applied to natural earthquake swarms in a variety of tectonic settings, including imaging of fault fluid interactions in volcanic settings (Shelly et al., 2015) and detecting slow slip in advance of megathrust earthquakes (Kato et al., 2012). While the use of earthquake swarms for forecasting subduction zone behavior is still only a hypothesis (Holtkamp & Brudzinski, 2014), earthquake swarms are considered to be a key component of eruption forecasting (McNutt, 1996). Much like in the induced seismicity examples, RSD would improve upon the previous studies that utilized catalog-based template matching by detecting natural earthquake swarms below the catalog detection level. This should improve the forecasting capabilities, particularly in areas without dense seismic networks.

4.6. Conclusion

While the commonly used multi-station STA/LTA earthquake detection algorithms are ideally suited for identifying M > 2 seismicity using existing regional networks in the United States, this approach struggles to effectively identify smaller magnitude earthquakes. When traditional detection techniques are employed using these regional networks, swarms of M < 2 events would go undetected until a larger magnitude event is observed. The RSD algorithm was created to efficiently identify these small magnitude, repeating earthquakes, such as in the increasingly more prevalent cases of induced seismicity. This algorithm identifies signals of interest on a single regional

station using a low-threshold STA/LTA amplitude detector and then sorts these signals into families according to their frequency and time domain characteristics.

When RSD was applied to a seismometer near Mammoth Mountain during the time of a volcanic swarm, it produced a remarkably similar pattern of seismicity to that from catalog-based template matching (Shelly et al., 2015). In the Oaxaca portion of the Mexico subduction zone, RSD identified ~10 times more events than a traditionally constructed catalog (Fasola et al., in press). In Central Alberta, Canada, template matching using RSD applied over moderate distances (~50 km) from the station was able to independently duplicate template matching results using cataloged events. When this algorithm was applied in Harrison County, Ohio, 18 potentially induced earthquake swarms were identified between 2013-2015, 15 of which were previously unreported. Although M > 1 seismicity induced by HF is likely rare and typically restricted to small magnitudes, our study indicates it may be more common than previously thought. While autocorrelation and FAST have both been proven effective at identifying repeating seismic events, the computationally intensive nature of these algorithms may impede the wide-scale application of these algorithms. Considering the minimal computational requirements of RSD, this algorithm may be better suited for the real-time detection and characterization of small magnitude earthquake swarms. As more observations typically lead to improved interpretations, techniques like RSD are important tools for the future understanding of earthquake swarms in a variety of settings.

4.7. Supplemental Material

Using the Repeating Signal Detector (RSD) algorithm, a portion of the repetitive earthquake waveforms identified by the most productive family from the 1) Oaxaca, Mexico, 2) Harrison County, Ohio, and 3) Central Alberta, Canada, studies are shown. Waveforms shown have been bandpass filtered 5-15 Hz, the same passband used in the RSD processing.

The earthquake hypocentral relocations in the Kaybob region of Alberta were achieved using a 1-D velocity model derived from a sonic-velocity log of the 3500 m deep Mobil KAYBOBS 6-12-61-20 well. This well was located in the eastern portion of our study region (54.260462° N, 116.868905° W). The initial model contained 6 discrete velocity layers defined by changes in rock rheology associated with key stratigraphic intervals in the study region (Table S1).

4.8. Acknowledgements

Support for this work was provided by ODNR, NSF grant EAR-0847688 (M.B.), and USGS NEHRP grant 2015-0176 (M.B. and B.C.). Seismic data were obtained through the Incorporated Research Institutions for Seismology Data Management Center (IRIS) (www.iris.edu; last accessed November 2015), through the Northern California Earthquake Data Center (NCEDC) (www.ncedc.org; last accessed February 2016), and by submitting Freedom of Information Act request for local seismic data collected by the Ohio Department of Natural Resources (ODNR). Waveforms from OXTT are available by contacting M. Brudzinski and will be available at the IRIS DMC under the network code MU in June 2016. Earthquake catalogs were obtained from the Ohio Department of Natural Resources (ODNR) (http://geosurvey.ohiodnr.gov; last accessed December 2015), U.S. Geological Survey National Earthquake Information Center (NEIC)

(http://earthquake.usgs.gov/data; last accessed December 2015), and the Canadian National Earthquake Database (http://earthquakescanada.nrcan.gc.ca; last accessed December 2015). Well data was retrieved from the Ohio Department of Natural Resources (https://gis.ohiodnr.gov/website/dog/oilgaswells; last accessed December 2015), FracFocus (https://fracfocus.org; last accessed December 2015), and FracFocus.ca (https://fracfocus.ca; last accessed December 2015). Plots were made using the Generic Mapping Tools version 4.2.1 (www.soest.hawaii.edu/gmt; last accessed December 2015). We would like to thank ODNR for the assistance, specifically D. Blake, S. Dade, J. Fox, M. Hansen, and D. Rush. The work in Harrison Co was greatly aided by P. Friberg. We also benefitted from discussions with G. Beroza, D. Eaton, O. Kaven, C. Yoon. Comments from two reviewers and an associate editor helped improve this manuscript. Our analysis relied heavily on Miami University's High Performance Computing, and we thank J. Mueller for his assistance.

4.9. References

Barrett, S. A., G. C. Beroza (2014).An empirical approach to subspace detection, Seismol. Res. Lett. 85, no. 3, 594–600.

Benz, H. M., N. D. McMahon, R. C. Aster, D. E. McNamara, D. B. Harris (2015). Hundreds of Earthquakes per Day: The 2014 Guthrie, Oklahoma, Earthquake Sequence, 86(5). doi: 10.1785/0220150019.

British Columbia Oil and Gas Commission (BCOGC) (2012). Investigation of observed seismicity in the Horn River basin, Technical Rept., http://www.bcogc.ca/investigation-observed-seismicity-horn-river-basin (last accessed December 2015).

Brown, J. R., G. C. Beroza, D. R. Shelly (2008). An autocorrelation method to detect low frequency earthquakes within tremor, Geophys. Res. Lett., 35. doi: 10.1029/2008GL034560.

Brudzinski, M.R., Cabral-Cano, E., Correa-Mora, F., DeMets, C., Márquez-Azúa, B. (2007). Slow slip transients along the Oaxaca subduction segment from 1993 to 2007. Geophys. J. Int. 171 (2), 523-538.

Brudzinski, M.R., Hinojosa-Prieto, H.R., Schlanser, K.M., Cabral-Cano, E., Arciniega-Ceballos, A., Diaz-Molina, O., DeMets, C. (2010). Nonvolcanic tremor along the Oaxaca segment of the Middle America subduction zone. J. Geophys. Res. Solid Earth 115 (B8).

Brudzinski, M. R., R. J. Skoumal, B. S. Currie (2015). Multistation template matching to characterize frequency-magnitude distributions of induced seismicity in the Central and Eastern US. Presented at *2015 Fall Meeting, AGU*, San Francisco, California, 14-18 December 2015, Abstract T43D-3047.

Buchanan, R. C. (2015). Increased seismicity in Kansas, The Leading Edge, 34(6), 614-617. doi: 10.1190/tle34060614.1.

Clarke, H., L. Eisner, P. Styles, P. Turner (2014). Felt seismicity associated with shale gas hydraulic fracturing: The first documented example in Europe, Geophys. Res. Lett., 41. doi: 10.1002/2014GL062047.

Eaton, D. W., A. B. Mahani (2015). Focal mechanisms of some inferred induced earthquakes in Alberta, Canada. Seismol. Res. Lett., 86(4).

Ellsworth, W. L. (2013). Injection-Induced Earthquakes. *Science*, 341.

Fasola, S., M. R. Brudzinski, N. Ghouse, K. Solada, S. Sit, E. Cabral-Cano, A. Arciniega-Ceballos, N. Kelly, C. DeMets, K. Jensen (in press). New perspective on the transition from flat to steeper subduction in Oaxaca, Mexico based on seismicity, nonvolcanic tremor, and slow slip, J. Geophys. Res.

FracFocus.ca, BC Oil & Gas Commission. http://www.fracfocus.ca/find_well/AB. (last accessed September 2015).

Frank, W. B., N. M. Shaprio (2014). Automatic detection of low-frequency earthquakes (LFEs) based on a beamformed network response. Geophys. J. Intl. Seis. doi: 10.1093/gji/ggu058.

Frank, W. B., N. M. Shapiro, A. L. Husker, V. Kostoglodov, A. Romanenko, M. Campillo (2014). Using systematically characterized low-frequency earthquakes as a fault probe in Guerrero, Mexico, J. Geophys. Res. Solid Earth, 119. doi:10.1002/2014JB011457.

Friberg, P. A., G. M. Besana-Ostman, I. Dricker (2014). Characterization of an earthquake sequence triggered by hydraulic fracturing in Harrison County, Ohio. Seismol. Res. Lett., 85(6), 1295-1307.

Friberg, P. A., M. R. Brudzinski, B. S. Currie, R. J. Skoumal (2015). Observations of a hydrofracture induced earthquake sequence in Harrison County Ohio in 2014. Presented at *2015 Fall Meeting, AGU*, San Francisco, California, 14-18 December 2015, Abstract S11C-03.

Frohlich, C., C. Hayward, B. Stump, and E. Potter (2011). The Dallas-Fort Worth earthquake sequence: October 2008 through May 2009, Bulletin of the Seismological Society of America, 101, 327-340.

Gibbons, S. J., F. Ringdal (2006). The detection of low magnitude seismic events using array-based waveform correlation. Geophys. J. Intl., 165 (1), 149-166.

GWPC (Ground Water Protection Council) and IOGCC (Interstate Oil and Gas Compact Commission) (2015). Potential Injection-Induced Seismicity Associated with Oil & Gas Development: A Primer on Technical and Regulatory Considerations Informing Risk Management and Mitigation.

Herrmann, R. B. (2013) Computer programs in seismology: An evolving tool for instruction and research, Seism. Res. Lettr. 84, 1081-1088, doi:10.1785/0220110096.

Hill, D. P., W. L. Ellsworth, M. J. S. Johnston, J. O. Langbein, D. H. Oppenheimer, A. M. Pitt, P. A. Reasenberg, M. L. Sorey, and S. R. McNutt (1990). The 1989 earthquake swarm beneath Mammoth Mountain, California: An initial look at the 4 May through 30 September activity, Bull. Seismol. Soc. Am., 80, 325–339.

Hirose, H., T. Matsuzawa, T. Kimura, H. Kimura (2014). The Boso slow slip events in 2007 and 2011 as a driving process for the accompanying earthquake swarm. Geophys. Res. Lett., 41(8), 2778-2785.

Holland, A. (2013). Earthquakes triggered by hydraulic fracturing in south-central Oklahoma, Bull. Seismol. Soc. Am. 103, no. 3, 1784–1792.

Holtkamp, S. G., Brudzinski, M. R. (2011). Earthquake swarms in circum-Pacific subduction zones. Earth Planet. Sci. Lett., 305, 215–225.

Holtkamp, S. G., M. R. Brudzinski, (2014). Megathrust earthquake swarms indicate frictional changes which delimit large earthquake ruptures, Earth and Planetary Science Letters, 390, 234-243.

Holtkamp, S. G., M. R. Brudzinski, B. S. Currie (2015). Regional detection and monitoring of injection-induced seismicity: Application to the 2010-12 Youngstown, Ohio seismic sequence, AAPG Bull., 99(9), 1671-1688. doi: 10.1306/03311513194.

Horton, S. (2012). Disposal of hydrofracking waste fluid by injection into subsurface aquifers triggers earthquake swarm in central Arkansas with potential for damaging earthquake, Seismol. Res. Lett., 83, 250–260. doi: 10.1785/gssrl.83.2.250.

Huang, Y., G. C. Beroza (2015). Temporal variation in the magnitude-frequency distribution during the Guy-Greenbrier earthquake sequence, Geophys. Res. Lett., 42, 6639–6646.Kao, H., S.-J. Shan (2004). The Source-Scanning Algorithm: mapping the distribution of seismic sources in time and space, Geophys. J. Int.,157 (2), 589-594.

Kao, H., S-J. Shan (2004). The Source-Scanning Algorithm: mapping the distribution of seismic sources in time and space. Geophys. J. Intl., 157(2), 589-594. doi: 10.1111/j.1365-246X.2004.02276.x.

Kato, A., K. Obara, T. Igarashi, H. Tsuruoka, S. Nakagawa, and N. Hirata (2012). Propagation of slow slip leading up to the 2011 Mw 9.0 Tohoku-Oki earthquake, Science, 335, 705–708. doi:10.1126/science.1215141.

Kim, W.-Y. (2013). Induced seismicity associated with fluid injection into a deep well in Youngstown, Ohio. J. Geophys. Res.118, 3506–3518.

Lay, T., T. C. Wallace (1995). Modern global seismology, Academic Press, San Diego, 521pp.

Lewicki, J. L., G. E. Hilley, D. R. Shelly, J. C. King, J. P. McGeehin, M. Mangan, and W. C. Evans (2014), Crustal migration of CO2-rich magmatic fluids recorded by tree-ring radiocarbon and seismicity at Mammoth Mountain CA, USA, Earth Planet. Sci. Lett., doi:10.1016/j.epsl.2013.00.832.

Lin, G. (2013). Seismic investigation of magmatic unrest beneath Mammoth Mountain California, USA. Geology, 41, 847–850.

McGarr, A., B. Bekins, N. Burkardt, J. Dewey, P. Earle, W. Ellsworth, S., Ge, S. Hickman, A. Holland, E. Majer, J. Rubinstein, A. Sheehan (2015). Coping with earthquakes induced by fluid injection. Science, 347(6224), 830-831.

McNutt, S.R. (1996). Seismic monitoring and eruption forecasting of volcanoes: A review of the state-of-the-art and case histories. Monitoring and Mitigation of Volcano Hazards, 99-146.

Mogi, K. (1963). Some discussions on aftershocks, foreshocks and earthquake swarms — the fracture of a semi-infinite body caused by an inner stress origin and its relation to the earthquake phenomena. Bull. Earthq. Res. Inst. Univ. Tokyo 41, 615–658.

National Research Council (NRC) (2013). Induced Seismicity Potential in Energy Technologies, 225 pp., Natl. Acad. Press. Washington, D.C.

Nicholson, C., R. L. Wesson (1990). Earthquake Hazard Associated with Deep Well Injection: A report to the U.S. Environmental Protection Agency, U.S. Geol. Surv. Bull. 1951.

Ohio Department of Natural Resources (ODNR) (2014). Ohio Announces Tougher Permit Conditions for Drilling Activities Near Faults and Areas of Seismic Activity, http://ohiodnr.gov/news/post/ohio-announcesougher-permit-conditions-for-drilling-activities-near-faults-and-areas-ofseismic-activity (last accessed December 2015).

Rubinstein, J. L., W. L. Ellsworth, A. McGarr, H. M. Benz (2014). The 2001–Present Induced Earthquake Sequence in the Raton Basin of Northern New Mexico and Southern Colorado, Bull. Seismol. Soc. Am., 104(5), 2162-2181. doi: 10.1785/0120140009.

Schultz, R., V. Stern, M. Novakovic, G. Atkinson, Y. J. Gu (2015). Hydraulic fracturing and the Crooked Lake sequence: Insights gleaned from regional seismic networks. Geophys. Res. Lett., 42, 2750-2758.

Shelly, D. R., G. C. Beroza, S. Ide (2007). Non-volcanic tremor and low-frequency earthquake swarms. Nature, 446. doi: 10.1038/nature05666.

Shelly, D. R., T.'a. Taira, S. G. Prejean, D. P. Hill, and D. S. Dreger (2015). Fluid-faulting interactions: Fracture-mesh and fault-valve behavior in the February 2014 Mammoth Mountain, California, earthquake swarm, Geophys. Res. Lett., 42, 5803–5812. doi:10.1002/2015GL064325.

Stern, V. H., R. J. Schultz, L. Shen, Y. J. Gu, D. W. Eaton (2013). Alberta earthquake catalogue, version 1.0: September 2006 through December 2010, Alberta Geological Survey Open File Report 2013-15.

Skoumal, R. J., M. R. Brudzinski, B. S. Currie, J. Levy (2014). Optimizing multi-station earthquake template matching through re-examination of the Youngstown, Ohio sequence. Earth Planet. Sci. Lett., 405, 274–280.

Skoumal, R. J., M. R. Brudzinski, B. S. Currie (2015a). Induced earthquakes during hydraulic fracturing in Poland Township. Ohio, Bull. Seismol. Soc. Am., 105(1), 189–197. doi:10.1785/0120140168.

Skoumal, R. J., M. R. Brudzinski, B. S. Currie (2015b). Microseismicity induced by deep wastewater injection in Southern Trumbull County, Ohio. Seismol. Res. Lett., 86(5). doi: 10.1785/0220150055.

Skoumal, R. J., M. R. Brudzinski, B. S. Currie (2015c). Distinguishing induced seismicity from natural seismicity in Ohio: Demonstrating the utility of waveform template matching. J. Geophys. Res., 120. doi: 10.1002/2015JB012265.

Song, T.-R. A., D. Helmberger, M. R. Brudzinski, R. W. Clayton, P. Davis, X. Pérez-Campos, and S. K. Singh (2009). Subducting slab ultra-slow velocity layer coincident with silent earthquakes in southern Mexico, Science, 324, 502–506.

Sorey, M. L., W. C. Evans, B. M. Kennedy, C. D. Farrar, L. J. Hainsworth, and B. Hausback (1998). Carbon dioxide and helium emissions from a reservoir of magmatic gas beneath Mammoth Mountain, California, J. Geophys. Res., 103, 15,303–15,323, doi:10.1029/98JB01389.

Switzer, S. B., W. G. Holland, D. S. Christie, G. C. Graf, A. S. Hedinger, R. J. McAuley, R. A. Wierzbicki, J. J. Packard (2008). Duvernay Interval Isopach and Lithofacies (GIS data, line features). Alberta Geological Survey. DIG 2008-0123.

Walsh, F. R., M. D. Zoback (2015). Oklahoma's recent earthquakes and saltwater disposal. Science Advances, 1(5).

Warpinski, N. R. (2013). Understanding Hydraulic Fracture Growth, Effectiveness, and Safety through Microseismic Monitoring. Effective and Sustainable Hydraulic Fracturing. Tech Croatia, Chapter 6.

Weingarten, M., S. Ge, J. W. Godt, B. A. Bekins, J. L. Rubinstein, J. L. (2015). High-rate injection is associated with the increase in US mid-continent seismicity. Science, 348(6241), 1336-1340.

Yoon, C., O. O'Reilly, K. Bergen, G. Beroza (2015a). Earthquake detection through computationally efficient similarity search, *Sci. Adv.*, 1.

Yoon, C., O. O'Reilly, K. Bergen, Y. Huang, W. Ellsworth, G. Beroza (2015b). Searching for Unknown Earthquakes in the Guy-Greenbrier, Arkansas, Earthquake Sequence Using Efficient Waveform Similarity Search, Presented at *2015 Fall Meeting, AGU*, San Francisco, California, 14-18 December 2015, Abstract S13B-2850.

FIGURES

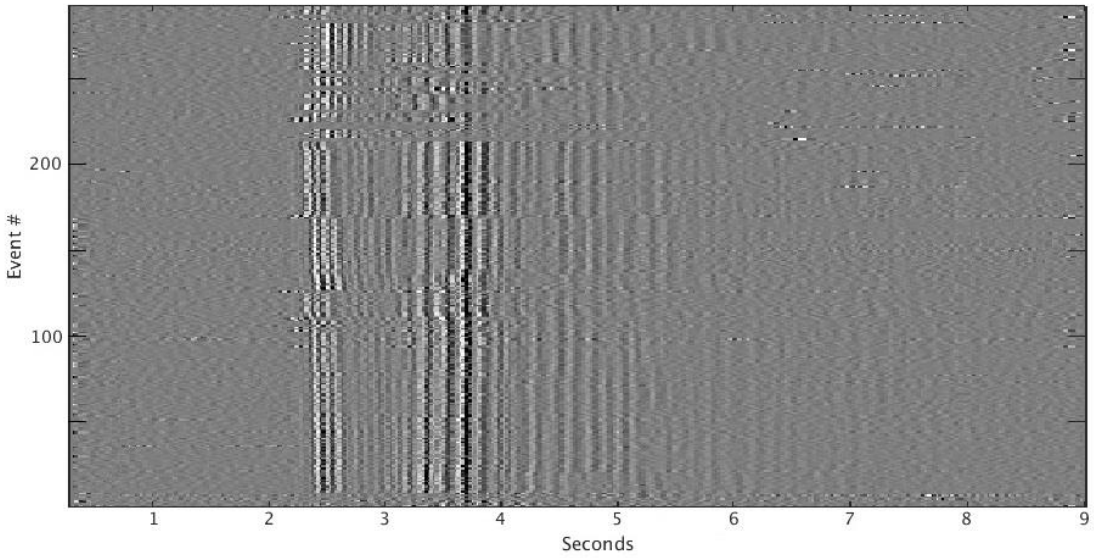

Figure 4.1. Example waveforms for a family. P and S waveforms from TA O53A BHZ in Harrison County showing the 292 members of one family identified by the initial frequency domain sorting step of RSD. Note that while the frequency content for these signals were similar, differential phase arrival times (and the absence of phases for some members) occurred, highlighting the importance of the secondary sorting step in the time domain.

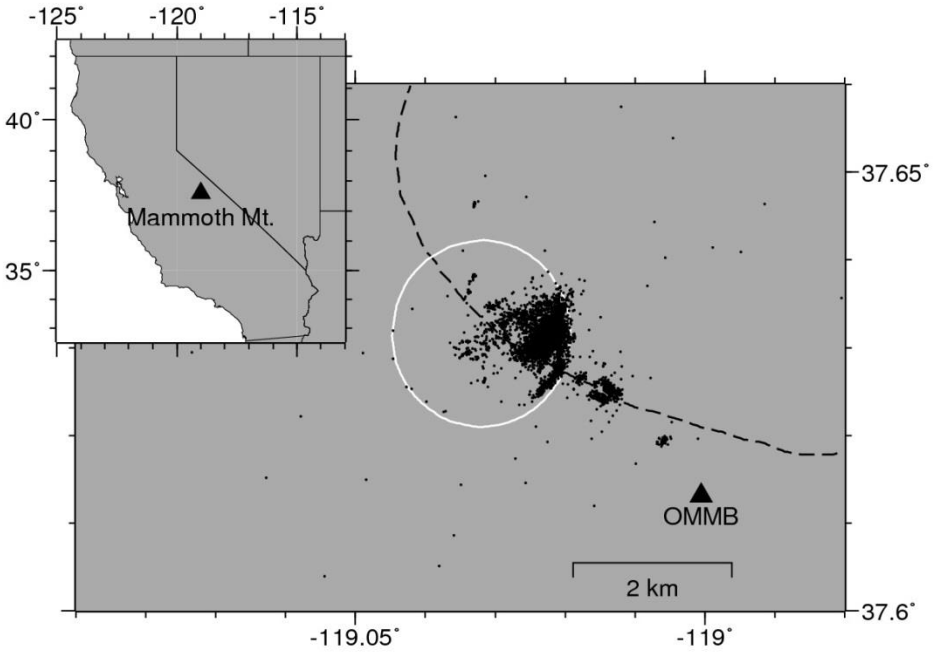

Figure 4.2. Map of Mammoth Mountain showing the NN OMMB station used in the RSD analysis that is compared with the February 2014 swarm described by Shelly et al. (2015) (black dots). White circle shows the deep ring structure beneath Mammoth Mountain and dashed line shows the edge of Long Valley Caldera.

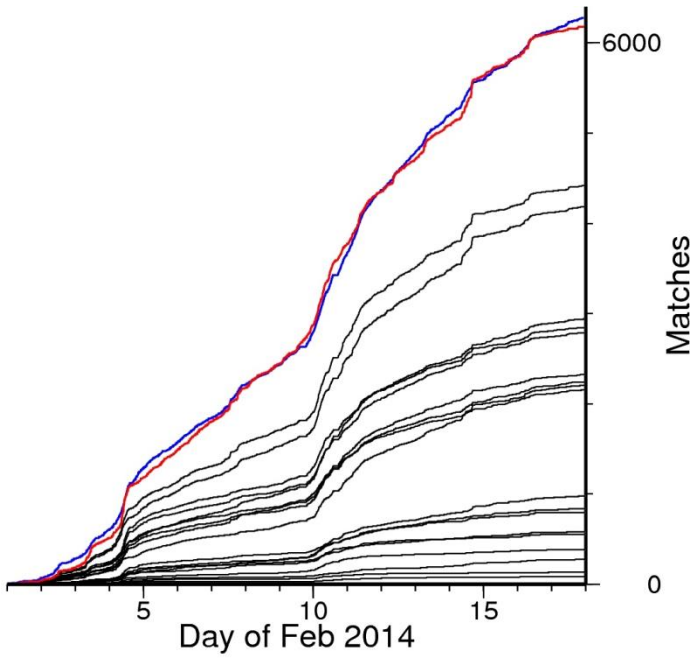

Figure 4.3. Cumulative number of events detected using the 18 stacked subfamilies identified by RSD in a cross-correlation routine for station OMMB near Mammoth Mountain shown as black lines. The catalog identified by large-scale template matching (Shelly et al., 2015) and the total unique events identified by RSD are shown as red and blue lines, respectively.

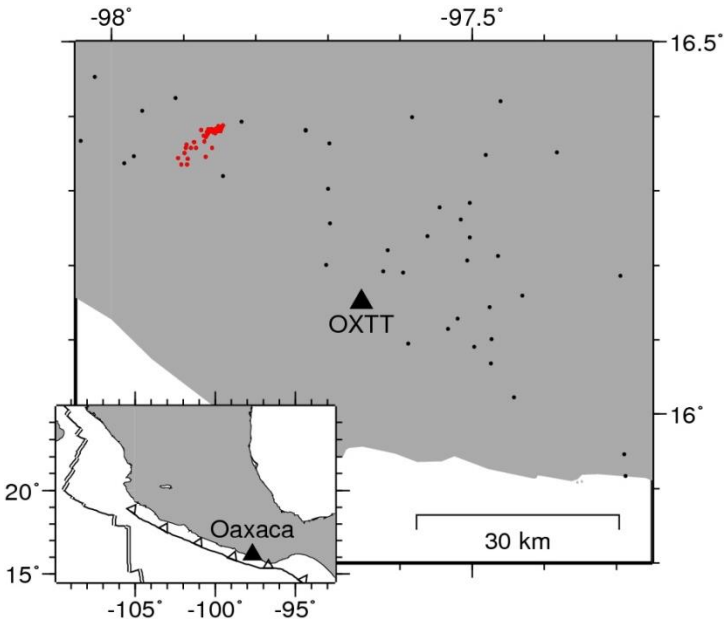

Figure 4.4. Map of Oaxaca, Mexico, showing the MU OXTT station used in the RSD analysis relative to the earthquakes (dots) identified by Fasola et al. (in press). The July 2006 swarm is highlighed in red.

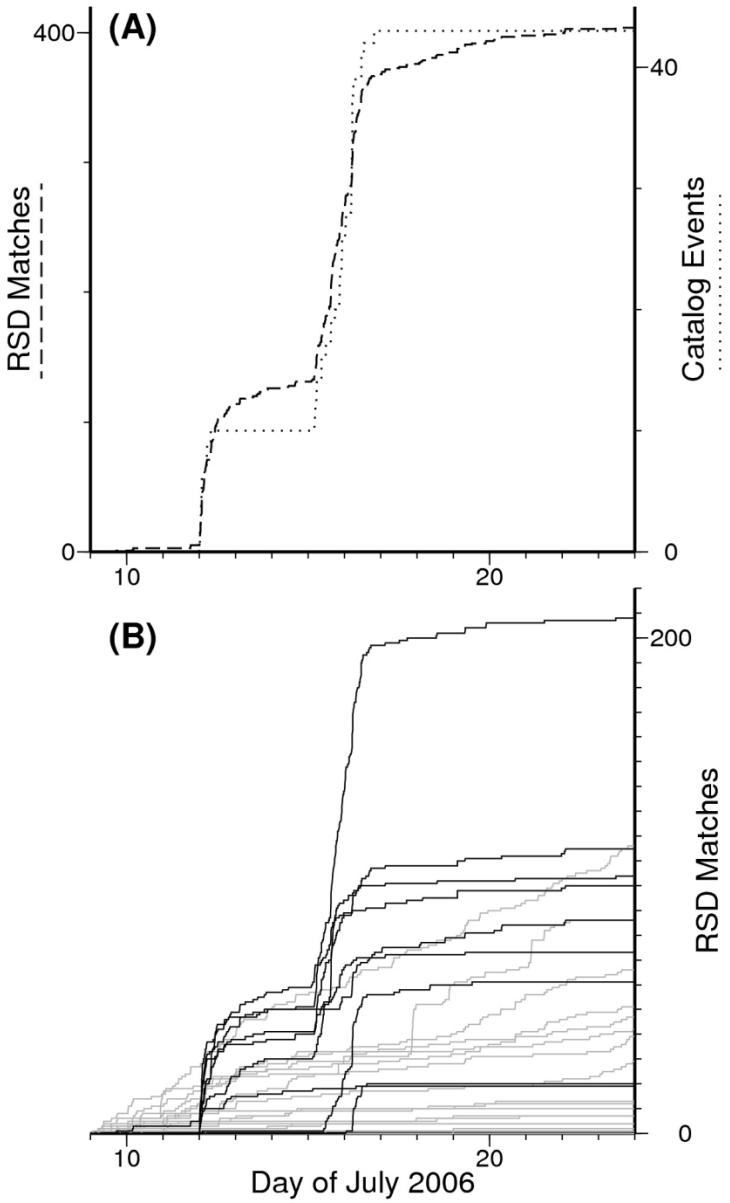

Figure 4.5. (**A**) Earthquakes identified by RSD (dashed line) relative to the earthquakes identified by Fasola et al. (2015) in the July 2006 swarm (dotted line). (**B**) Cumulative number of events detected using the 33 stacked subfamilies identified by RSD in a cross-correlation routine for station OXTT in Oaxaca, Mexico. Black lines denote subfamilies were determined to have matched with earthquake signals while the subfamilies represented by gray lines primarily matched with noise or had too few members. For example waveforms, see Supporting Information.

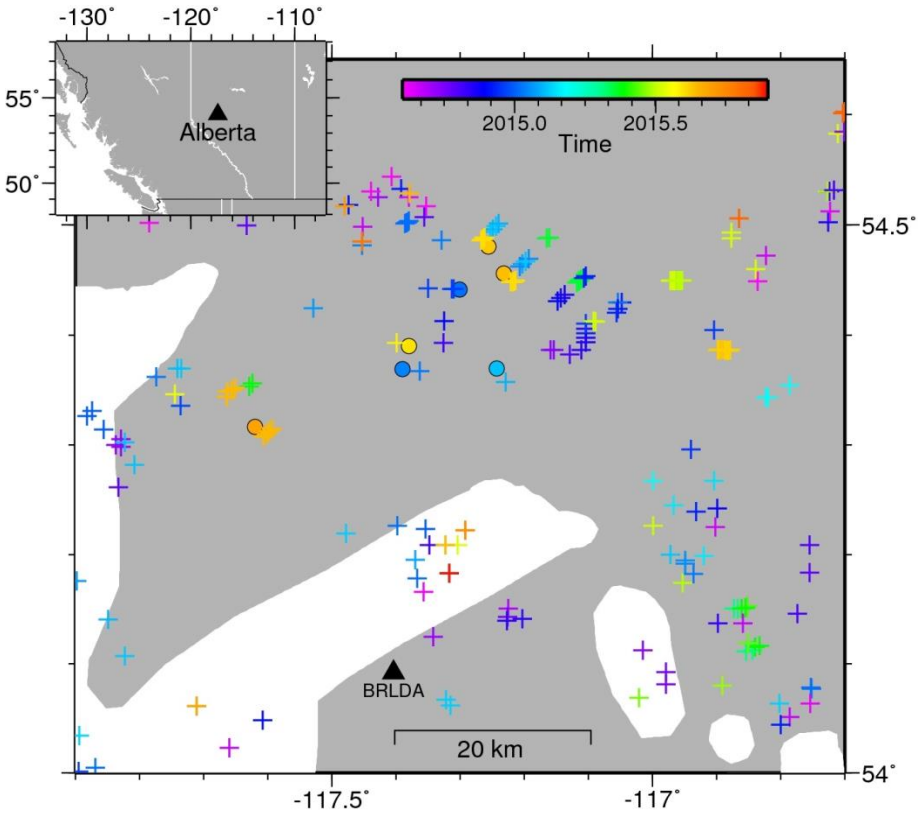

Figure 4.6. Map of the Kaybob region of Central Alberta, Canada. Crosses show unconventional wells of the Duvernay shale play colored by time of hydraulic fracturing, restricted to the time range of seismic analysis. Circles colored by time show epicenters determined in this study for sequences with large enough seismicity to be located with the regional network. Triangle shows the seismic station for which RSD was performed. Leduc reef formation that cuts through the Duvernay is shown in white (Switzer et al., 2008).

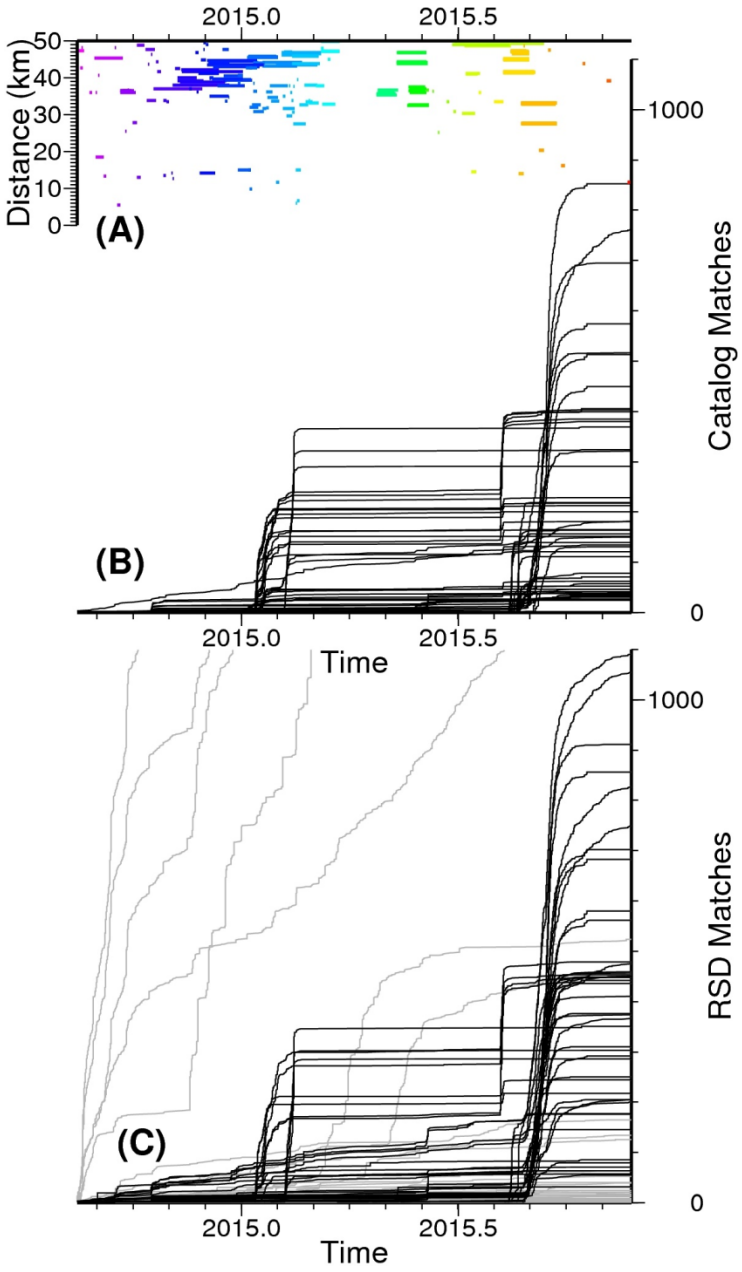

Figure 4.7. Cumulative detections using the catalog and signals detected by RSD in the Kaybob region of Central Alberta, Canada. (**A**) Length of lines denote duration of hydraulic fracturing operations in Alberta, Canada, with distance from station BRLDA. Cumulative number of events detected with a template matching routine using (**B**) 57 cataloged earthquakes and (**C**) 88 stacked subfamilies created by RSD. In (**B**) and (**C**), black lines denote subfamilies that matched with earthquakes while the subfamilies represented by gray lines matched with noise. For example waveforms, see Supporting Information.

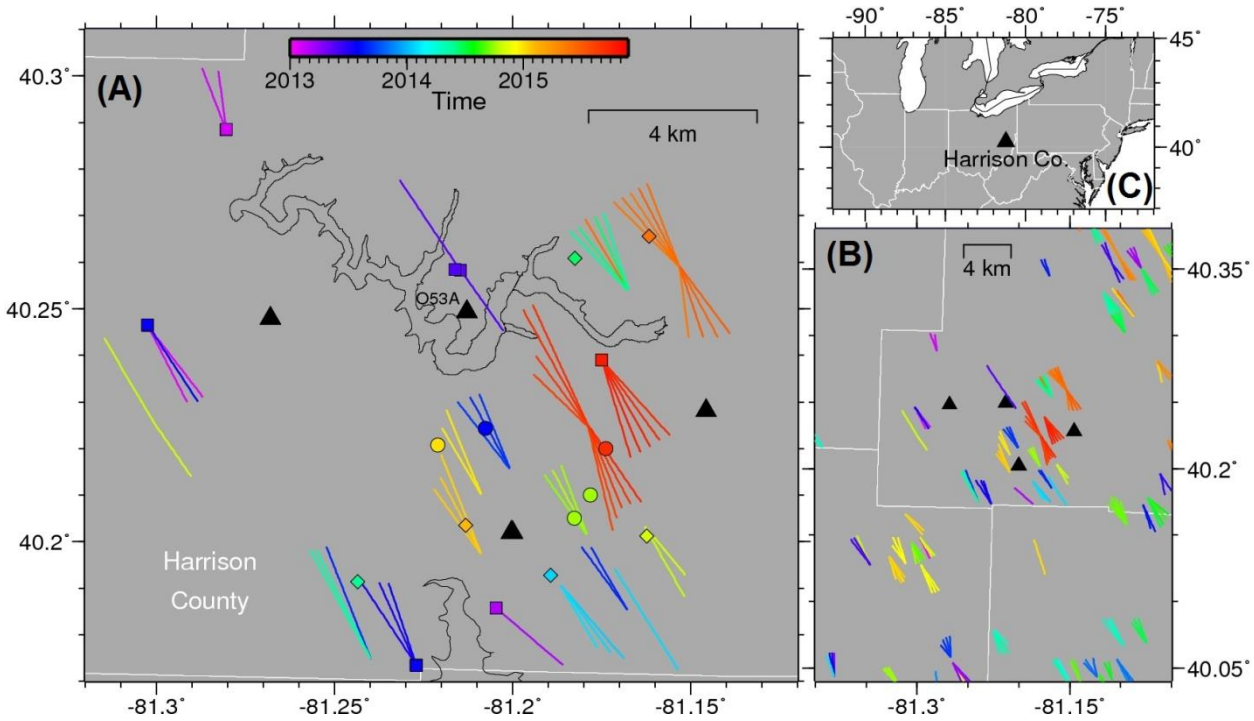

Figure 4.8. Map of the Harrison County, Ohio, study region. Lines show unconventional well head and toe, colored by time of hydraulic fracturing, restricted to the time range of seismic analysis. Triangles show local seismic stations. (**A**) Symbols are also colored by time and show locations of large (>750 events, circles) and small (diamonds) earthquake sequences. Squares identify wells stimulated before the local network was installed but correlate temporally with seismic activity with locations consistent with S-P times recorded by O53A. (**B**) Hydraulic fracturing in the surrounding region, illustrating the 2 wells south of our main study region (H: Horseshoe; K: Kirkwood) that also show evidence of seismic activity. (**C**) Broader regional map showing the location of Harrison County, Ohio.

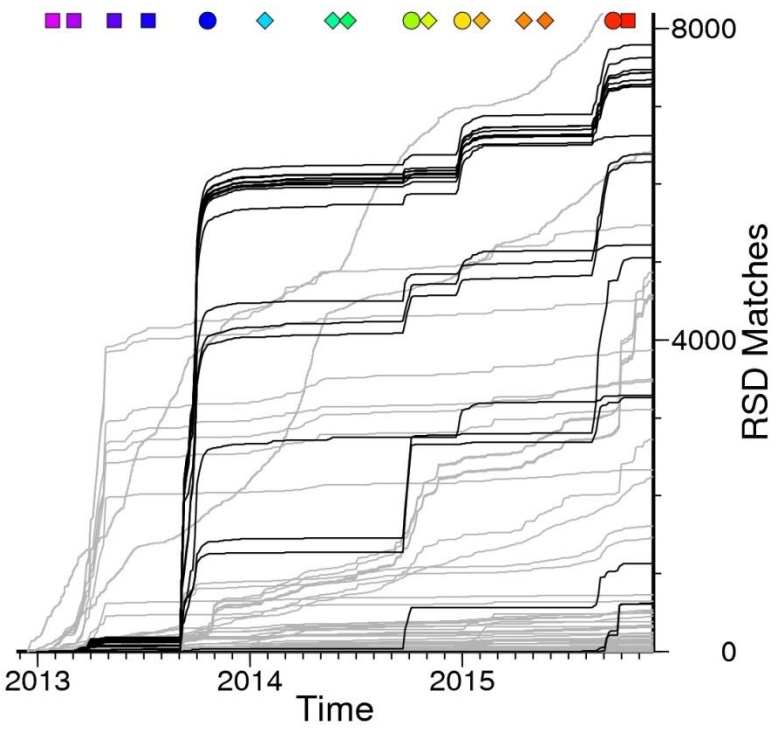

Figure 4.9. Cumulative number of events detected using the 85 stacked subfamilies identified by RSD in a cross-correlation routine for station O53A in Harrison County, Ohio. Black lines denote subfamilies with more than 600 members that primarily matched with earthquakes while the subfamilies represented by gray lines primarily matched with noise or had too few members. Colored symbols are consistent with Figures 2 & 4. For example waveforms, see Supporting Information.

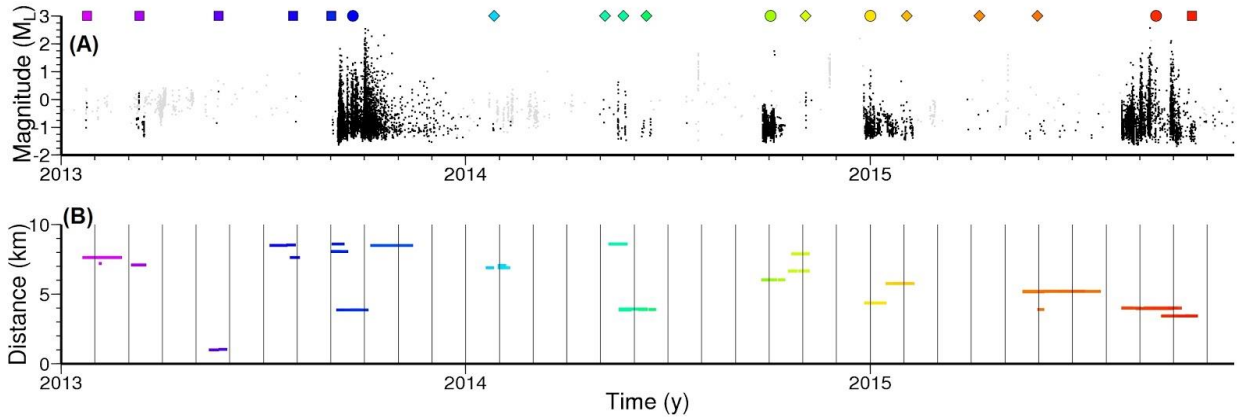

Figure 4.10. Temporal relationship between seismicity and hydraulic fracturing in Harrison County, Ohio. (**A**) Magnitudes of seismic events detected using RSD and template matching (black dots) and spurious cultural signals determined by manual waveform inspection (gray dots). Colored symbols are consistent with Figures 2 & 3. (**B**) Distance between station O53A and the wellheads of nearby hydraulic fracturing operations. The length of lines denote the timing of the hydraulic fracturing operations. Note that Kirkwood (Skoumal et al., 2015c) and Horseshoe wells in in Belmont County are > 10 km away from O53A and are not shown.

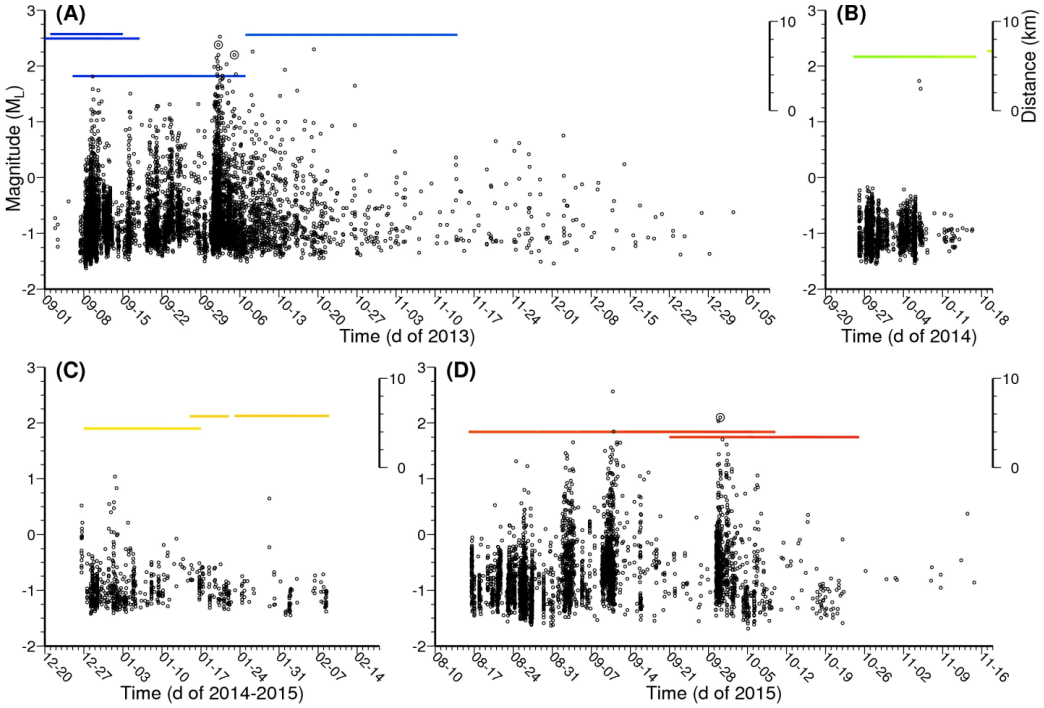

Figure 4.11. Magnitudes of the four primary induced sequences (black dots) in Harrison County, Ohio, identified using RSD sub-family stacks in a cross-correlation routine. Previously cataloged events are highlighted with circles. Colored lines denote timing of hydraulic fracturing operations (colors consistent with Figures 6-8).

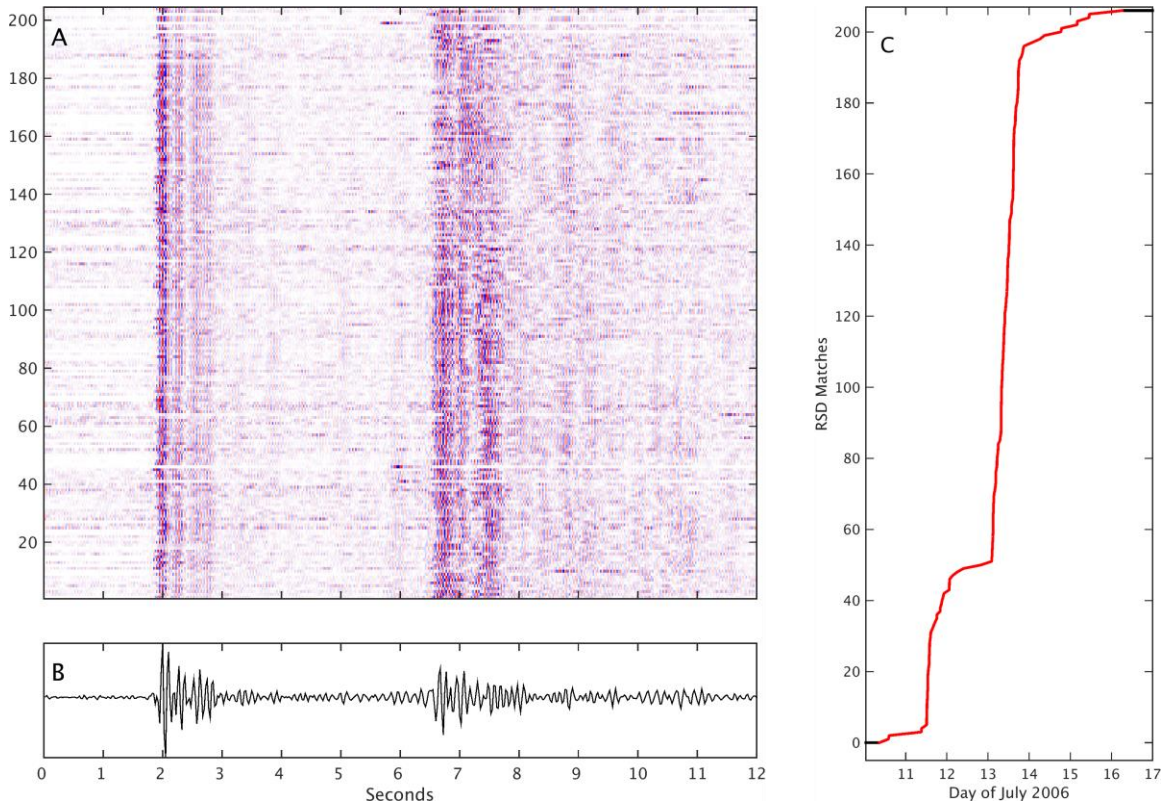

Figure 4.S1. (A) Example waveforms (MU OXTT BHZ) from the most productive family identified by RSD in Oaxaca, Mexico, bandpass filtered 5-15 Hz. (B) Normalized stack of the waveforms shown in (A). The waveform stack is not as clean in this case because it includes all matched events in the swarm. (C) Temporal pattern of the family. Waveforms from all matches (red line) are shown.

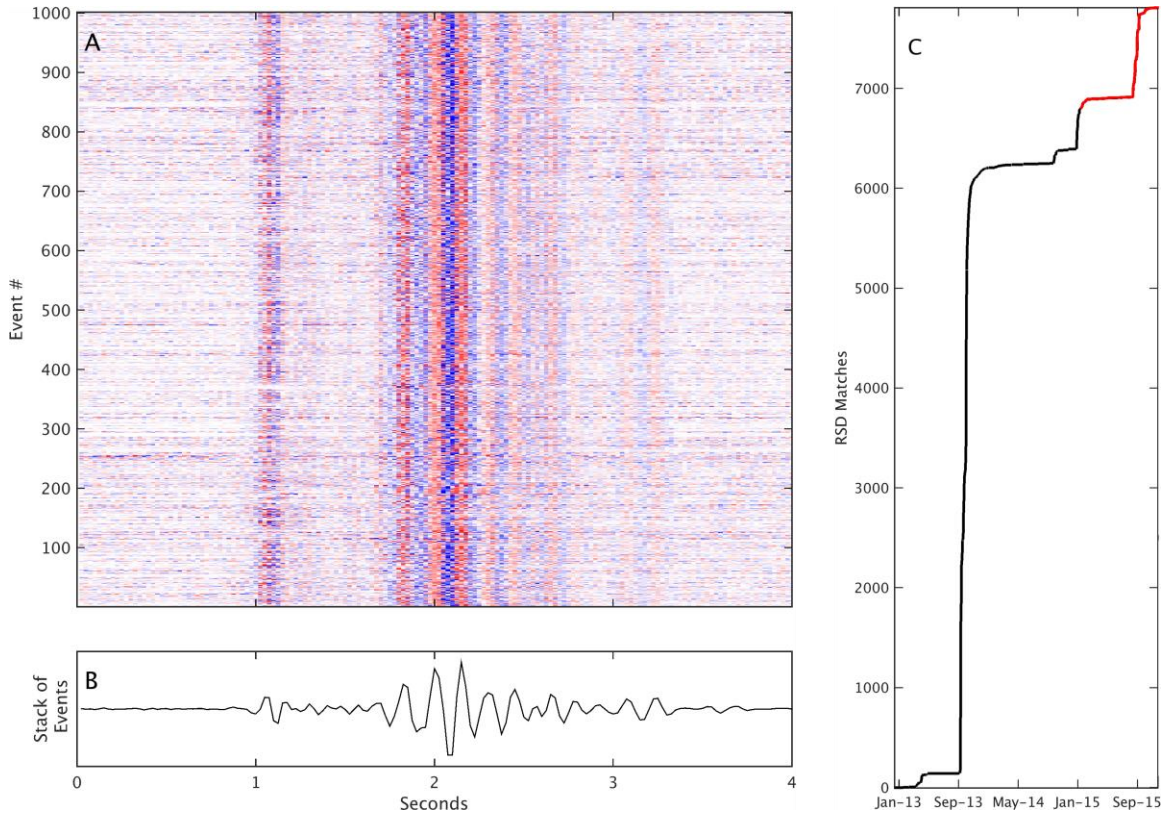

Figure 4.S2. (A) Example waveforms (TA O53A BHZ) from the most productive family identified by RSD in Harrison County, Ohio, bandpass filtered 5-15 Hz. (B) Normalized stack of the waveforms shown in (A). (C) Temporal pattern of the family. Waveforms from the last 1,000 matches (red line) are shown.

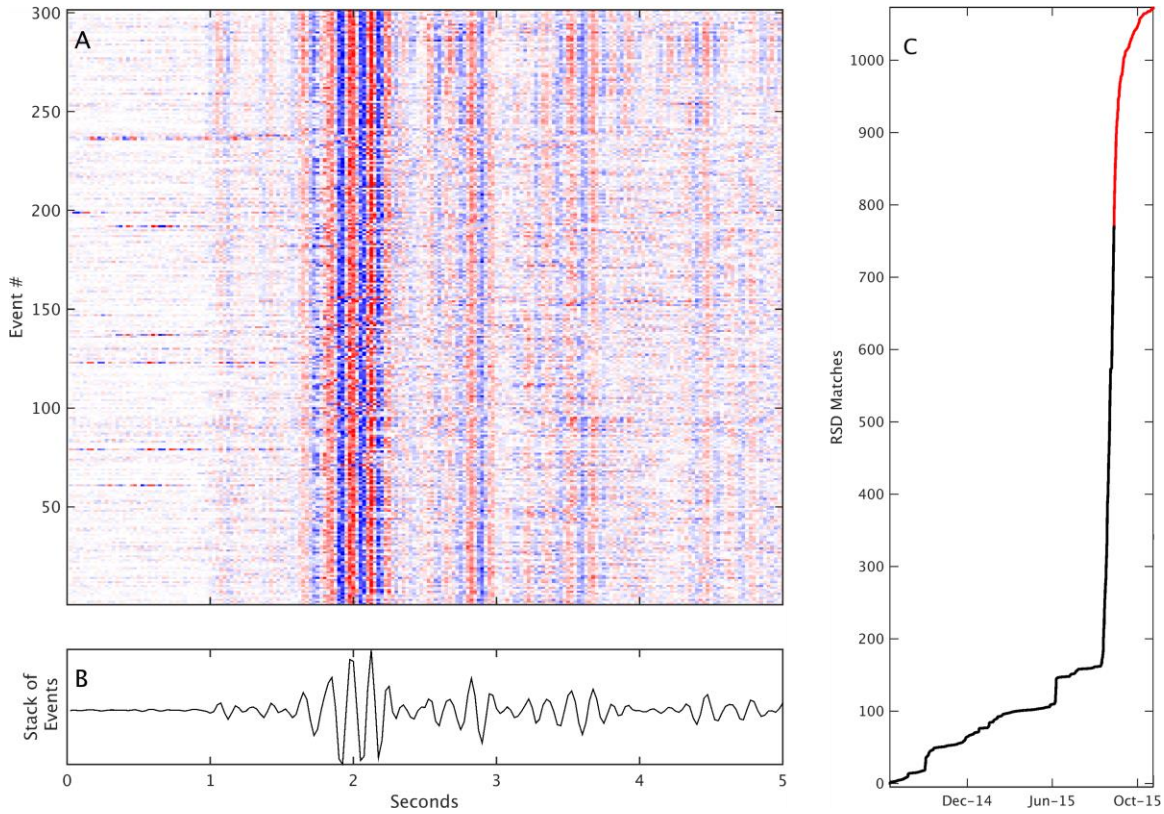

Figure 4.S3. (A) Example waveforms (RV BRDLA HHE) from the most productive family identified by RSD in Alberta, Canada, bandpass filtered 5-15 Hz. (B) Normalized stack of the waveforms shown in (A). (C) Temporal pattern of the family. Waveforms from the last 300 matches (red line) are shown.

Table 4.S1. Statigraphic 1D velocity model based on the Mobil KAYBOBS 6-12-61-20 Well sonic logs.

Depth (km)	Vp (km/s)	Vs (km/s)
0.000	3.292	1.903
1.217	3.605	2.084
1.905	3.928	2.271
2.293	5.721	3.307
3.096	4.486	2.593
3.355	5.945	3.436
4.000	6.200	3.584
10.000	6.400	3.715
40.000	8.100	4.682

CONCLUSIONS

Template matching and RSD algorithms have been demonstrated to be effective at detecting and characterizing earthquake swarms. These techniques can be applied on both a regional and local scale and be used to monitor for swarms and have the potential to be utilized in a near real-time manner. We have demonstrated the applicability of these algorithms to detect earthquake swarms in volcanic, subduction, and induced seismicity settings throughout North America. As more observations typically lead to improved interpretations, techniques like optimized template matching and RSD are important tools for the future understanding of earthquake swarms in a variety of settings.